In vitro enamel subsurface lesions : characterization and treatment

Rand Al-Obaidi

THÈSE POUR OBTENIR LE GRADE DE DOCTEUR DE L'UNIVERSITÉ DE MONTPELLIER

École doctorale : Sciences Chimiques et Biologiques pour la Santé

Unité de recherche EA 4203
Laboratoire de Bioingénierie et Nanosciences

In Vitro Enamel Subsurface Lesions: Characterization and Treatment

Présentée par Rand AL-OBAIDI

Le 12 septembre 2018

Sous la direction du Docteur Bruno Jacquot

Devant le jury composé de

M. Youssef HAIKEL, PU-PH, Université de Strasbourg	Président du jury
M. Guillaume PENEL, PU-PH, Université de Lille	Rapporteur
M. Bruno JACQUOT, MCU-PH, Université Aix-Marseille	Directeur
M. Fréderic CUISINIER, PU-PH, Université de Montpellier	Examinateur
M. Gérard ABOUDHARAM MCU-PH, Université Aix-Marseille	Examinateur

UNIVERSITÉ DE MONTPELLIER

Rand AL-OBAIDI

Laboratoire de Bioingénierie et Nanosciences, EA 4203

545, avenue du Professeur Jean-Louis Viala

34193 Montpellier Cedex 5, France

Lésions Carieuses de L'émail *in Vitro*: Caractérisation et Traitement

Mots clés:

Lésions de taches blanches

Émail dentaire humain

Reminéralisation

Optiques non-linéaires

Microscopie Raman confocale

Technique de nano-indentation

***In Vitro* Enamel Subsurface Lesions: Characterization and Treatment**

Key words:

White spot lesions

Human dental enamel

Remineralization

Confocal Raman microscopy

Nano-indentation technique

Nonlinear optical signals

RÉSUMÉ

Le concept de médecine préventive demande que les soins préventifs soient optimisés par une intervention précoce afin d'obtenir le bien-être des patients. Dans le cadre de ce modèle, appliqué par un nombre grandissant de pays, il est nécessaire de contrôler les facteurs de risque afin d'éviter les transitions vers l'état pathologique et de soigner la maladie à un stade plus précoce de son développement. Les soins de caries précoces, permis par une détection méticuleuse des caries, l'évaluation des lésions et le diagnostic, ainsi que les technologies modernes de prévention des caries, pourraient changer le visage de la pratique clinique de routine. Les dentistes doivent aider leurs patients à prévenir et contrôler les caries et à gérer leur santé bucco-dentaire (Kidd et al. 2008).

L'hypominéralisation de l'émail sous la surface sans formation de cavités représente la phase la plus précoce de formation de la carie. Quand elle devient cliniquement visible, elle est connue sous le nom de tache blanche. Cependant, en l'absence d'un traitement efficace, une cavitation peut se produire, ce qui augmente la nécessité d'un traitement réparateur invasif (Derks et al. 2004).

La prévalence incrémentielle de l'hypominéralisation légère à cause d'anomalies du développement sur les surfaces dentaires constitue un défi pour la détection et la prévention des caries. Ces taches blanches ont une prévalence estimée à 24% (Gorelick et al. 1982).

Cette prévalence est plus forte chez les patients atteint de maladie orthodontiques plusieurs années après le traitement (Gorelick et al. 1982; Hadler-Olsen et al. 2011). Par conséquent, la détection précoce et un traitement rapide et efficace; représentent les principaux enjeux de la dentisterie mini-invasive pour les années à venir. Ainsi, cela nécessite l'introduction de nouvelles technologies de diagnostic et de produits de soins dentaires efficaces pour répondre aux exigences actuelles. Ce type

de soins cliniques où l'intervention chirurgicale peut être totalement évitée est très important (Fejerskov and Nyvad 2003).

L'induction de lésions carieuses artificielles dans les tissus dentaires est un outil pertinent pour étudier les stratégies de détection, de prévention et de traitement des caries dentaires. Les modèles *in vitro* sont particulièrement bien adaptés aux expériences dont l'objectif est de tester un seul processus séparément. En effet, une situation plus complexe avec de nombreuses variables peut confondre les données. Différents systèmes de déminéralisation ont été développés dans le but de simuler les conditions du biofilm cariogène au cours du métabolisme du sucre. Le processus carieux *in vivo* prend beaucoup plus de temps que dans les modèles *in vitro*. Les cycles de pH sont devenus la méthode standard car ils permettent une meilleure simulation du processus carieux (Cate 1990). Ces modèles peuvent produire un continuum du processus de désintégration amélaire s'étendant des taches blanches presque indétectable aux cavités (Featherstone 1995).

Les méthodes précoces de détection des caries devraient compléter la prise de décision clinique, en soutenant la planification du traitement préventif en accord avec l'évaluation du risque carieux afin de prévenir la progression de la maladie. Les méthodes de diagnostic classiques, telles que l'observation visuelle et les radiographies dentaires de routine, ne permettent pas de détecter les taches blanches de l'émail sur n'importe quelle surface. Environ 30% à 40% des minéraux doivent être perdus avant qu'une petite lésion carieuse de l'émail puisse être détectée par radiographie (White 2004). Cette déminéralisation destructive de l'émail peut prendre 9 mois ou plus à apparaître (Lang et al. 1987), ce qui augmente la nécessité d'un traitement invasif.

Récemment, diverses techniques ont été explorées pour répondre au besoin d'outils diagnostiques hautement sensibles qui aident à la surveillance des caries et aide à la prise de décision et aux

processus de planification du traitement. Ces études de validation sont essentielles pour déterminer l'utilité clinique des nouvelles technologies avant leur mise en œuvre en pratique clinique.

Le nouveau rôle du dentiste est de fournir des soins dentaires basés sur : le maintien de la santé; la détection précoce et la surveillance; contrôler les agents causaux; l'utilisation d'agents pharmacologiques appropriés ainsi qu'une intervention minimale. Pour ces raisons, notre étude a été conçue pour atteindre les objectifs suivants :

I. Définir un modèle *in vitro* efficace pouvant provoquer des lésions carieuses uniformes et reproductibles confinées à la surface de l'émail et présenter une ressemblance histologique avec les lésions débutantes naturellement développées dans une période de temps beaucoup plus courte.
II. Explorer et valider la spécificité et la sensibilité de la microscopie confocale Raman et de la microscopie multiphotonique dans la détection précoce des caries afin de développer des modalités d'imagerie efficaces et mini-invasives essentielles pour étudier une variété de pathologies en dentisterie et prévenir les progrès de la maladie.
III. Examiner les changements affectant les propriétés mécaniques de l'émail humain après l'induction de la carie en utilisant une technique de nano-indentation et corréler ces changements aux variations de composition chimique de l'émail.
IV. Tester et comparer l'efficacité des systèmes de reminéralisation disponibles en ce qui concerne le traitement non- invasif des lésions carieuses initiales avec des ions calcium et phosphate bio-disponibles.

Pour réaliser les objectifs de cette étude qui est de renforcer l'idiome des soins minimalement invasifs, nous avons identifié un modèle de carie artificielle qui permet de provoquer des lésions sous la surface. Ceci est utilisé dans les études de profil pour valider les nouvelles technologies

d'évaluation des caries et examiner les produits de soins dentaires récemment commercialisés. En outre, nous avons cherché à évaluer les performances des méthodes de détection des caries de haute sensibilité dans le but de les utiliser ensuite en soins courants et à tester les technologies les plus récentes de prévention des caries. Ces objectifs représentent les concepts de base de la dentisterie moderne pour conseiller et aider les patients à prévenir la progression des caries.

Un modèle de cycle de pH modifié a été utilisé pour imiter les conditions intra-buccales qui conduisent à la formation de lésions de type tache blanche, dans un court laps de temps.

Des techniques optiques non invasives, comme la microscopie Raman confocale et la microscopie multiphotonique, ont été utilisées dans cette étude pour détecter de petits changements dans la composition chimique de l'émail in vitro.

De plus, la technique de nano-indentation a été appliquée pour étudier les changements dans les propriétés mécaniques de l'émail et les relier à ceux affectant sa composition chimique après l'induction des caries, afin d'ajouter de la spécificité chimique-mécanique aux informations sur les lésions sous-surface de l'émail.

Les résultats obtenus démontrent un grand potentiel pour les techniques examinées dans l'imagerie de la relation structure / caractéristique dans les tissus dentaires, fournissant une base importante pour des applications potentiellement intéressantes dans le diagnostic clinique de différentes pathologies dentaires.

Pour résoudre le problème du traitement des lésions primitives sans intervention chirurgicale, l'efficacité de la crème GC Tooth Mousse et du dentifrice contenant de la nano-hydroxyapatite «KAREX» dans l'amélioration de la reminéralisation de l'émail déminéralisé par la localisation du phosphate de calcium amorphe à la surface de la dent a été inspectée. L'étude a indiqué le manque de

preuves fiables soutenant l'efficacité des agents reminéralisants dans le traitement des taches blanches. En outre, la perméabilité de la couche superficielle de l'émail ainsi que la composition des matériaux pourraient représenter des facteurs principaux dans le développement de nouvelles technologies de reminéralisation. Ce travail doit être poursuivi par d'autres études in-vitro et par des études cliniques.

La première étude vise donc à comparer deux modèles basés sur des cycles de pH pour tester leurs efficacités dans la reproduction des lésions de tache blanche, dans un court laps de temps. La microscopie Raman confocale a été utilisée dans cette étude pour détecter de petits changements dans la composition chimique de l'émail *in vitro*. 12 prémolaires humaines saines ont été soumises à deux modèles. Le premier modèle (A) est décrit par Featherstone (Featherstone et al. 1986) . Le deuxième modèle (B) est dérivé du modèle A pour prendre moins de temps. Les dents ont été soumises à 7, 8 et 14 cycles respectivement et chaque cycle a duré 24 heures.

Les dents avec des taches blanches naturelles formées en bouche ont été utilisées comme un contrôle positif. Tous les échantillons ont été inspectés avec la caméra Soprolife et par microscopie Raman pour détecter de petits changements dans l'apparence et dans la structure de l'émail. Les changements dans la couleur naturelle de la dent tout au long du traitement ont été enregistrés avec un appareil photo. Les images montrant les variations de composition du phosphate ont été construites à partir de l'intensité du pic de phosphate correspondant à la vibration ν_1 (960 cm^{-1}). La profondeur des lésions de l'émail a été mesurée sur ces images. Le protocole A induit une légère modification de l'aspect de l'émail après 8 cycles. Alors que le protocole B produit une profonde lésion sous la surface après seulement 7 cycles. Ce dernier modèle prend moins de temps produit des lésions sous la surface de façon reproductible, sur une période relativement courte. Il faut sept cycles pour créer une tache

blanche comportant une couche de surface intacte caractéristique. La microscopie Raman en raison de sa sensibilité et sa résolution spatiale pourrait être considérée comme la méthode de référence pour les analyses chimiques des tissus minéralisés en particulier pour l'émail dentaire.

Apres avoir défini le modèle de cyclique de pH, nous avons développé notre travail en utilisant la technique de nano-indentation accompagné de la microscopie Raman confocale pour étudier les changements des propriétés mécaniques et pour essayer de les relier aux modifications chimiques. 20 prémolaires humaines saines ont été soumises à notre modèle cyclique (Al-Obaidi et al. 2018) pour provoquer des lésions sous la surface de l'émail *in vitro*. En outre, 2 dents avec des taches blanches naturelles ont été utilisées comme des références. Tous les spécimens ont été étudiés par microscopie Raman confocale. La technique de nanoindentation a été utilisée pour mesurer la dureté et le module d'Young de l'émail. Les images de concentration de phosphate ont montrées la présence d'une couche d'émail intacte en surface associé à une déplétion sévère de phosphate dans le corps de la lésion. Dans tous les groupes examinés, les propriétés mécaniques de l'émail ont diminué dans la zone de la lésion. En combinant les deux techniques nous avons pu associer les propriétés mécaniques de l'émail à sa composition en phosphate.

Actuellement, les technologies de détection de caries les plus avancées; sont celles basés sur la spectroscopie de fluorescence. Nous avons exploré les capacités de la microscopie multiphotonique pour évaluer son intérêt dans la détection précoce des caries. Les mesures sur 14 dents humaines ont été faites (après avoir provoqué des lésions sous la surface de l'émail *in vitro*) en associant la microscopie Raman confocale et la microscopie multi-photonique (MMP). En microscopie Raman l'intensité du pic de phosphate à 960 cm^{-1}, le rapport organique / minéral à (2931/430 cm^{-1}) ont été les deux paramètres chimiques suivi. En microscopie multiphotonique nous avons suivi génération de seconde harmonique (SHG) et la fluorescence à deux photons (2PEF); Nous avons étudiés des

sites d'émail endommagés et non-endommagés. Le rapport organique/minéral est plus élevé dans l'émail déminéralisé alors que l'intensité du phosphate dans la même zone est plus faible. La microscopie multi-photonique montre un décalage vers le rouge évident du spectre de fluorescence à deux photons de l'émail carié par rapport à celui de l'émail sain associé à l'apparition du pic de SHG dans la même zone. En comparant les images de 2PEF avec les motifs structuraux observés par microscopie Raman confocal une similitude morphologique est assez évidente. La conclusion principale est que l'intensité de 2PEF augmente avec la progression des caries, de ce fait cette intensité de 2PEF reflète les changements dans la composition chimique de l'émail c'est-à-dire la perte du phosphate. Ces résultats exposent également le rôle fondamental de la matrice organique de l'émail et nous indique que son intégrité est très important pour la réparation de l'émail.

Ces découvertes peuvent constituer une base pour des applications intéressantes dans le diagnostic clinique des pathologies dentaires. D'autres travaux sont nécessaires pour amener ces outils à l'application clinique afin de diagnostiquer les lésions carieuses au stade le plus précoce de leur développement.

Le diagnostic précoce des taches blanches doit permettre de mettre en œuvre un traitement préventif ou un traitement correcteur le moins invasif possible. Nous avons choisi dans notre travail de thèse de nous intéresser aux nouveaux traitements de reminéralisation de l'émail. L'efficacité de la crème GC Tooth Mousse (CPP-ACP), contenant du phosphate de calcium amorphe, en tant qu'agent reminéralisant a été proposé (Reynolds 1998). Récemment, le dentifrice «KAREX» contenant de la nano-hydroxyapatite (nHA) a été diffusé comme un produit de soins dentaires adapté à la rénovation des tissus dentaires. Dans la présente étude notre modèle de tache blanche artificielle a été utilisé pour comparer l'effet réparateur des deux produits. Chaque échantillon a été traité avec l'agent reminéralisant respectif pendant 5 min toutes les 24h pendant 21 jours, à l'aide d'applicateur en

coton. Les dents ont été scannées par microscopie Raman confocale pour fournir des cartes de concentration de phosphate en utilisant l'intensité du pic de phosphate à 960 cm $^{-1}$. La largeur à mi-hauteur de ce pic a été calculée à pour évaluer l'effet des agents de reminéralisation sur la structure. A la fin des traitements, une différence significative a été observée en ce qui concerne la hausse de phosphate dans le corps des lésions traitées par le dentifrice contenant de la nHA par rapport celle traitées par le CPP-ACP. Aucune différence significative entre les deux traitements en ce qui concerne la cristallinité de l'émail n'a été observée. L'étude a montré le manque de fiabilité de CPP-ACP et souligné l'activité de la nano apatite dans la reminéralisation des taches blanches. La perméabilité de la couche de surface de l'émail ainsi que la consistance des pattes pourraient sont peut être deux facteurs limtant la reminéralisation de la lésion sous la surface. D'autres études sur les molécules biomimétiques impliquées dans le calcium, la stabilisation du phosphate et la nucléation pourraient apporter d'autres améliorations dans le développement de nouvelles techniques de reminéralisation.

Conclusion : Notre travail de thèse a permis d'identifier de nouvelles techniques d'imagerie de l'émail dentaire, fournissant une caractérisation détaillée de ses composants organiques et inorganiques afin de pouvoir dans le futur aider à la détection précoce des caries.

La comparaison d'un système de caries de l'émail *in vitro* avec un modèle existant a montré que le système modifié présentait une alternative adéquate à ce dernier, en produisant rapidement des lésions sous la surface de l'émail; qui répondent à l'ensemble des critères de lésions carieuses naturelles.

Nous avons montré que les propriétés chimiques des particules de nano-hydroxyapatite jouent un rôle important dans la reminéralisation des lésions carieuses précoces par rapport au potentiel limité des phosphopeptides de caséine associés au phosphate de calcium. L'imagerie multiphotonique

utilisée dans cette recherche a démontré le rôle fondamental de la matrice organique dans l'intégrité de l'émail. Ceci doit être pris en compte pour optimiser les nouveaux produits dentaires reminéralisants.

Dans le futur nous souhaitons poursuivre nos efforts pour développer de nouveaux produits de reminénéralisation de l'émail utilisant de nouvelles protéines ou des nouveaux peptides extraits des coquillages. Le nouveau produit devra être de consistance fluide pour pénétrer en profondeur à l'intérieur de l'émail pour diffuser leurs principes actifs et compenser la perte de composition de l'émail. Notre modèle de carie *in vivo* et la spécificité chimique de la microscopie confocale Raman nous permettrons certainement de parvenir à notre but.

BIBLIOGRAPHIE

Al-Obaidi R, Salehi H, Desoutter A, Bonnet L, Etienne P, Terrer E, Jacquot B, Levallois B, Tassery H, Cuisinier F. 2018. Chemical & nano-mechanical study of artificial human enamel subsurface lesions. Scientific reports. 8(1):4047.

Cate JT. 1990. In vitro studies on the effects of fluoride on de-and remineralization. Journal of dental research. 69(2_suppl):614-619.

Derks A, Katsaros C, Frencken J, Van't Hof M, Kuijpers-Jagtman A. 2004. Caries-inhibiting effect of preventive measures during orthodontic treatment with fixed appliances. Caries research. 38(5):413-420.

Featherstone J, O'reilly M, Shariati M, Brugler S. 1986. Enhancement of remineralization in vitro and in vivo. Factors relating to demineralisation and remineralisation of the teeth. IRL Press. Oxford and Washington.

Featherstone JD. 1995. Clinical aspects of de/remineralization of teeth. International Association for Dental Research.

Fejerskov O, Nyvad B. 2003. Is dental caries an infectious disease? Diagnostic and treatment consequences for the practitioner. Nordic dentistry 2003 yearbook. Quintessence Publishing Co, Ltd. p. 141-152.

Gorelick L, Geiger AM, Gwinnett AJ. 1982. Incidence of white spot formation after bonding and banding. American journal of orthodontics. 81(2):93-98.

Hadler-Olsen S, Sandvik K, El-Agroudi MA, Øgaard B. 2011. The incidence of caries and white spot lesions in orthodontically treated adolescents with a comprehensive caries prophylactic regimen—a prospective study. The European Journal of Orthodontics. 34(5):633-639.

Kidd EA, Nyvad B, Espelid I. 2008. Caries control for the individual patient. Dental caries. Blackwell Publishing Ltd. p. 487-504.

Lang NP, Hotz PR, Gusberti FA, Joss A. 1987. Longitudinal clinical and microbiological study on the relationship between infection with streptococcus mutans and the development of caries in humans. Molecular Oral Microbiology. 2(1):39-47.

Reynolds EC. 1998. Anticariogenic complexes of amorphous calcium phosphate stabilized by casein phosphopeptides: A review. Special Care in Dentistry. 18(1):8-16.

White S. 2004. Benign tumor of jaw. Oral radiology Principles and interpretation.410-458.

SUMMARY

White spot lesion is the subsurface hypomineralization of enamel indicating the 1st stage of dental caries development. Early detection of incipient dental caries before it reaches the stage of cavitation offers an opportunity for effective dental care. Our aim was to strengthen the idiom of minimally invasive care through identifying an *in vitro* caries model with respect to its potential to induce subsurface lesions used in profile studies for validation of new caries assessment technologies and examination of recently marketed dental care products. In addition, we aimed to assess the performance of highly sensitive caries detection methods before employment in the dental clinic as well as testing recent caries prevention technologies. These objectives are representing the principle concepts of modern dentistry to counsel and assist patients in preventing caries progression.

A modified pH cycling model was used to mimic the intra-oral conditions that lead to white spot lesion formation in a short time. Non-invasive optical techniques including confocal Raman microscopy and multiphoton microscopy were used in this study to detect small changes in the chemical composition of enamel *in vitro*. Furthermore, nano-indentation technique was applied to investigate changes in the mechanical properties of enamel and link them to those affecting its chemical composition after caries induction to add chemico-mechanical specificity in providing important information about subsurface lesions in enamel. The obtained results demonstrate a great potential of the examined techniques in imaging the structure/feature relationship in dental tissues; providing an important basis for potentially valuable applications in the clinical diagnosis of different tooth pathological conditions.

To address the problem of treating primitive lesions without surgical intervention; the efficiency of GC Tooth Mousse cream (CPP-ACP) and nano-hydroxyapatite containing dentifrice “KAREX” in the enhancement of remineralization of demineralized enamel through localizing amorphous calcium phosphate at the tooth surface was inspected. The study indicated lack of reliable evidences supporting the effectiveness of remineralizing agents in WSLs treatment. Besides that, enamel surface layer permeability along with material consistency might represent principle factors in developing novel remineralizing technologies. Within the limitations of this study, further laboratory studies together with clinical research are therefore required to increase the available knowledge on this prevalent subject.

TABLE OF CONTENTS

ACHKNOWLEDGEMENTS

Foremost, I am eternally grateful for the Government of Iraq who made this project possible and supported me to improve my skills and promote my career. Concurrently, my special thanks are extended to the French government and to CAMPUS France organization for allowing me to achieve my goals.

I would like to express my sincere gratitude to my research advisor ***Prof. Fréderic Cuisinier*** for his continuous support to my Ph.D study and research, for his patient guidance, enthusiastic encouragement, immense knowledge and useful critique of this work. His guidance helped me in all the time of research and writing of this thesis. I could not have imagined having a better advisor and mentor for my Ph.D study.

Besides my advisor, I would like to thank the rest of my thesis committee: Prof. Penel and Prof. Haikel for their encouragement, insightful comments, and profuse questions.

I would like to express my heartfelt gratitude to Dr. Hamideh Salehi, for the stimulating discussions, for the long working days we were working together before deadlines, and for all the fun we have had in the last three years.

I must express my very profound gratitude to Mr. Alban Desoutter for providing me with unfailing support and continuous encouragement throughout my years of study and through the process of researching and writing this thesis.

I would like to express my very great appreciation to Prof. Hervé Tassery, Prof. Bernard Levallois and Dr. Veronique Montero for their valuable help and constructive suggestions during the planning and development of this research work. Their willingness to give their time so generously has been very much appreciated.

My sincere thanks also go to: Prof. Csilla Gergely, Dr. Thierry Cloitre & Prof. Pascal Etienne, for offering me the opportunity in their institutions and leading me working on diverse exciting projects.

I would also like to acknowledge Dr. Bruno Jacquot for his contribution.
I love to thank Mr. Laurent Bonnet and Mr. Frederic Fernandez for their valuable and unconditional technical support on this project.

I would like to thank my fellow doctoral students for their feedback, cooperation and of course friendship. In addition, I would like to express my gratitude to the staff of LBN for the last minute favors.

I would like to thank my friends for accepting nothing less than excellence from me.

Last but not least, nobody has been more important to me in the pursuit of this project than the members of my family. I would like to thank my family: ***my late Father who taught me the meaning of life***, ***my wonderful Mother the origin of my success*****,** my loving and supportive fiancé, ***Ali***, and my brother and sister for supporting me spiritually throughout writing this thesis and my life in general.

PUBLICATIONS

- Chemical & Nano-mechanical Study of Artificial Human Enamel Subsurface Lesions.

Al-Obaidi, R, Salehi, H, Desoutter, A, Bonnet, L, Etienne, P, Terrer, E, Jacquot, B, Levallois, B, Tassery, H, Cuisinier, FJG. Journal of Scientific reports, vol 8, Issue 1, pages 4047, ISSN 2045-2322.

LIST OF ABBREVIATIONS

PO_4^{3-}	Phosphate
Ca^{2+}	Calcium
$CaCl_2$	Calcium Chloride
CH_3COOH	Acetic acid
KCl	Potassium Chloride
KH_2PO_4	Monopotassium Phosphate
$Ca(NO_3)_2$	Calcium nitrate
ICDAS	International Caries Detection and Assessment System
LUT	Look-up table
ν	Nu
C	Cycle
H	Hardness
E	Young's modulus
NI	Nano-indentation technique
Ap	Projected surface
S	Slope
F	Maximum force
β	Geometrical constant
ν	Poisson's coefficient
Pd	Penetration depth
DEJ	dentin-enamel junction
KMCA	K-mean cluster analysis
NL	Natural lesion
WSL	White spot lesion
L	Lesion
ISL	Intact surface layer
TMR	Transverse microradiography
CO_3^{2-}	Carbonate ion
CHA	B-type carbonated hydroxyapatite

$Ca_{10}(PO_4)_6(OH)_2$	Hydroxyapatite crystals (HACs)
$Ca_5(PO_4)_3OH$	Hydroxyapatite (HA)
CPP	Casein phosphopeptides
$Ca(NO_3)_2•4(H_2O)$	Calcium nitrate tetrahydrate
$NaC_2H_6AsO_2•3H_2O$	Sodium cacodylate
SL	Subsurface lesion
NWSL	Natural white spot lesion
LED	Light-emitting diode
ACP	Amorphous calcium phosphate
nHA	Nano-hydroxyapatite
KAREX	nHA containing-dentifrice
CPP-ACP	GC Tooth Mousse
Na_3PO_4	Sodium phosphate
NaCl	Sodium chloride
KCl	Potassium chloride
$CaCl_2$	Calcium chloride
$MgCl_2$	Magnesium chloride
H_2SO_4	Sulphuric acid
$NaHCO_3$	Sodium carbonate
FWHM	Full-width at half-maximum
I_i	Initial phosphate intensity
I_f	Final phosphate intensity
D	Difference between Ii and I_f
D^-	Mean of D for each experimental group
$\bar{I}_i$	Mean of I_i for each experimental group
CI	Rate of change in the intensity
H_3PO_4	Phosphoric acid
AF	Auto-fluorescence
2PEF	Two-photon excitation fluorescence
SHG	Second harmonic generation

MPM	Multi-photon microscopy
H^+	Hydrogen
F^-	Fluoride
$Ca_{10}(PO_4)_6 F_2$	Fluoroapatite crystal

Chapter1
Introduction

1.1 INTRODUCTION

The concept of 'wellness management' is already the state of the art in some communities and is increasingly prominent in several countries' health care systems. This reflects both an attempt to ensure that preventive care is optimized by early intervention and an understanding of many patients' increasing desire to optimize and maintain health, rather than to suffer from a disease and its consequences. Under this model of care, one needs to pro-actively modify risk factors to avoid the transitions to the diseased state, or to catch the disease at an earlier stage in its development.

Non-operative caries care supported by meticulous caries detection, lesion assessment and diagnosis, together with modern caries prevention technologies, should change the face of routine clinical practice. Dentists can and should help their patients control caries preventively and manage their oral health (Kidd et al. 2008).

Subsurface enamel hypomineralization without cavity formation represents the early phase of caries formation. When it becomes clinically visible; it's known as white spot lesion (WSL). However, with the absence of effective treatment, cavitation may occur thereby increasing the necessity of invasive restorative treatment (Derks et al. 2004).

The incremental prevalence of mild hypomineralization due to developmental defects on tooth surfaces poses a challenge for caries detection and prevention. WSL exemplifies the most frequent cause responsible for white opaque areas in enamel, with an estimated prevalence of 24% (Gorelick et al. 1982). This proportion arises significantly in orthodontic patients; presenting a serious health problem lasting several years after treatment (Gorelick et al. 1982; Hadler-Olsen et al. 2011; Lucchese and Gherlone 2012). Therefore, primary and secondary caries prevention regimens which require early detection and prompt, effective treatment; represent the principle goals of minimally invasive dentistry in the coming years. Thus, this necessitates the introduction of powerful diagnostic

technologies and effective dental care products to meet the current requirements. In more and more patients, this type of clinical care where operative intervention could be entirely avoided, is very attractive (Fejerskov and Nyvad 2003).

The induction of artificial carious lesions in dental enamel is an important tool to investigate strategies for the detection, prevention and treatment of dental caries. In vitro models are particularly well suited to experiments whose objective is to test a single process separately, where a more complex situation with many variables may confound the data. Different demineralizing systems have been developed in an attempt to simulate the conditions of cariogenic biofilm during sugar metabolism. Caries process *in vivo* takes much longer than in *in vitro* models. Therefore, much can be learned about processes involved in a relatively shorter period of time. Chemical pH cycling models have become a powerful mean for many caries researchers applying *in vitro* techniques, as they provide better simulation of the caries process for both mechanistic studies and for profile studies designed to test novel dental care products (Cate 1990; White 1995). Suffice to say that these models can produce a continuum of the dental decay process with end results ranging from an almost undetectable WSL to cavity formation (Featherstone 1995; Ten Cate and Mundorff-Shrestha 1995).

Over and above, early caries detection methods should be an adjunct to clinical decision making, supporting preventive treatment planning in conjunction with caries risk assessment to prevent disease progression. Conventional diagnostic methods, such as visual observation and routine dental radiographs cannot detect enamel white-spot lesions on any surface. About 30% to 40% of minerals must be lost before an early enamel carious lesion becomes radiographically detectable (White 2004). This destructive enamel demineralization can take 9 months or longer to appear (Lang et al. 1987), thus increasing the necessity of invasive treatment.

Recently, various techniques have been explored to address the need for highly sensitive diagnostic tools that aid in caries monitoring and assisting in decision making and treatment planning processes. These validation studies are essential to determine the clinical utility of novel technologies before implementation in clinical practice.

The new dentist's role is providing dental care based on: health maintenance; early detection and monitoring; controlling causal agents; use of appropriate pharmacological agents, and minimal intervention. In view of these reasons, our study was designed to come upon the following objectives:

i. Define an effective *in vitro* model that can induce uniform, reproducible caries lesions confined to enamel surface and bear a histological resemblance to the naturally developed incipient lesions in a much shorter period of time.
ii. Explore and validate the specificity and sensibility of confocal Raman microscopy and multiphoton microscopy in early caries detection in order to develop effective and minimally invasive imaging modalities vital for investigating a variety of pathological conditions in dentistry and preventing disease progress.
iii. Examine the changes affecting the mechanical properties of human enamel after caries induction through the use of nano-indentation technique and correlate these changes to the variations in its chemical composition.
iv. Test and compare the efficacy of available remineralization systems in regard to non-invasive management of non-cavitated caries lesions with bioavailable calcium & phosphate ions.

1.2 BIOMINERALIZED TISSUES

Bones and teeth are composite structures consisting of inorganic mineral phase, organic phase, and cells which control the initial production of mineralized tissues. Osteoblasts control the mineralization of bone while odontoblasts and ameloblasts regulate the mineralization process of dentin and enamel respectively (Kawasaki et al. 2009). Biomineralized tissues protect the internal organs and perform different mechanical functions.

Calcium phosphate (CaP) salts are the major biomineral constituents of vertebrate bone and tooth (Batchelar et al. 2006; Sato 2007). Thus, they represent an important source of the key regulatory inorganic ions such as calcium, magnesium, and phosphate (McKee et al. 2005).

Enamel, dentin and cementum are the main components of the tooth. Enamel is the most mineralized of all biological tissues, with a density much greater than the dentine upon which it sits. Since enamel structure is the main subject of this research, therefore, a more detailed explanation of its composition, hypomineralization and remineralization processes are included below.

1.1.1 Dental enamel

Human dental enamel is a heterogeneous structure; its composition is varying markedly from the outer surface to inner layer and also from one region of the tooth to another. This unique mineralized substance is composed of 94% by weight minerals (Weatherell 1975), (2-3%) water, proteins and lipids comprise around 3% of organic material in enamel that surrounds the mineral crystals (Curzon MEJ 1983; Eastoe 1960; Odutuga and Prout 1974).

Enamel is organized into rod like structures (enamel prisms) composed of numerous hydroxyapatite crystals (HACs), arranged in a hexagonal elongated configuration. HACs are composed of calcium, phosphate and hydroxyl groups Ca_{10} $(PO4)_6(OH)_2$. These prisms begin at the dentino-enamel

junction (DEJ) and end at the outer enamel surface (Cuisinier et al. 1992). The enamel prisms are interlocked with each other in a keyhole configuration, resulting in alteration of the heads and tails of prisms. Each prism is enclosed inside a sheath rich in organic components which determines the permeability of enamel (Featherstone and Lussi 2006; Hicks et al. 2005).

1.2.2 Demineralization-Remineralization dynamic balance *in vivo*

Knowledge of mineralization processes and mechanisms in teeth is important for the prevention and treatment of dental diseases, ranging from superficial white spot lesions to dental caries formation. Remineralization is studied and described as the repair of established lesions. Such lesions have developed due to prolonged exposure to acid attack. Even though, it may be filled up with calcium phosphates when external conditions support mineral deposition from saliva or plaque fluid to plug small enamel defects formed during the demineralization episodes (Cuisinier and Voegel 1994). The relative magnitudes of demineralization and remineralization determine whether a tooth surface remains sound or a caries lesion develops. The remineralization process can help in preventing or limiting future tissue loss when the mineral precipitating in the lesion is less soluble than the original tissue (Ten Cate 2008).

Saliva and saliva-like remineralizing solutions are known to be supersaturated solutions with respect to calcium and phosphate ions in hydroxyapatites (solid-solution equilibrium in which no spontaneous precipitation occurs). However, supersaturated solutions contain only small amounts of dissolved minerals.

Release of bacterial acids leads to decrease in pH value in the acquired pellicle film which has a solubilizing effect on enamel. The equilibrium is rapidly lost and the medium becomes under-saturated with respect to enamel due to mineral precipitation in form of crystals. The buffering effect

of saliva neutralizes acids, raises pH value and increases back the concentration of free ions (Fig 1). Hence, the medium becomes supersaturated and new minerals can deposit on the enamel surface. If fluoride is present fluorapatite can form, which has a much lower solubility than the original enamel hydroxyl apatite (Featherstone and Lussi 2006).

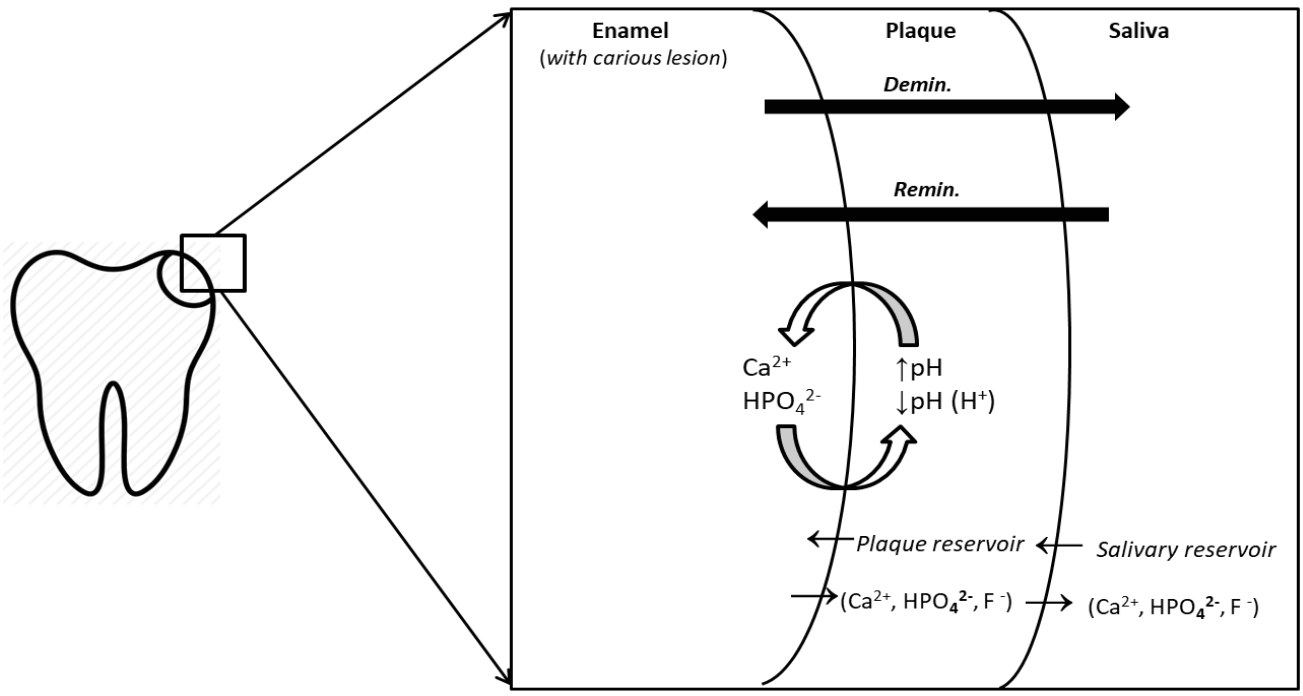

Figure 1. A diagram illustrates the reversible de/remineralization phases**.** Bacterial acid attacks the tooth surface, namely lowering the pH at the enamel surface, resulting in minerals dissolution. When saliva flows over the affected area; the pH rises to 7.0. If fluoride is present, together with salivary reservoir, the softened surface could be repaired.

1.2.3 Enamel white spot lesion (WSL)

An early caries lesion in enamel is observed clinically as a white opaque spot. Hollander (Hollander 1935) was among the first who observed this phenomenon but he thought that a photographic artifact was behind it.

The lesion area is slightly softer than the surrounding sound enamel. It becomes snow-white in color which becomes evident following dryness with air blowing (Larsen 1986b). The caries process necessitates repeated episodes of prolonged exposure to acidic conditions with intervening periods of remineralization. The development of clinically detectable white spot lesions (WSLs) occurs when the dynamic equilibrium is tilted towards demineralization (Anderson 2001; Fejerskov 1997; Silverstone et al. 1988). The early enamel lesion is characterized by four distinct histological zones. Two zones of demineralization are present: the translucent zone forming the advance front of the lesion and the body of the lesion representing the bulk of the lesion and situated beneath the overlying intact enamel surface layer. The later zone; together with the dark zone (laid superficial to the translucent zone) represent the zones of remineralization (Silverstone 1983; Silverstone et al. 1988).

1.2.4 Etiology of white spot lesion (WSL)

WSL is a multifocal disease that could affect teeth before eruption giving rise to what is called pre-eruptive WSL. This kind of WSL concerns non-orthodontic patients as in case of fluorosis which occurs due to enamel hypomineralization caused by excessive incorporation of fluorides during its formation (Fejerskov et al. 1974). In addition to traumatic hypomineralization which is a WSL that affects permanent teeth due to periodontal trauma of deciduous teeth (Arx 1993). Another kind of pre-eruptive WSL is the molar-incisor hypomineralization (MIH). In this case; enamel

hypomineralization begins at the dentino-enamel junction (DEJ) instead of starting at the outermost layer of enamel (Martinović et al. 2015).

In patients who underwent treatment with fixed orthodontic appliances, post-eruptive WSLs (most frequently seen in the dental clinic), are often seen under loose bands, around the periphery of the bracket base, and in areas that are difficult to access with a toothbrush (Bishara and Ostby 2008). Fixed orthodontic appliances induce a rapid increase in the bulk of dental plaque which has a lower pH than biofilm in non-orthodontic patients (Chatterjee and Kleinberg 1979; Gwinnett and Ceen 1979). The plaque-retentive properties of the fixed appliance predispose the patient to an increased cariogenic risk. To add to that, there is a rapid shift in the composition of bacterial flora of the microbial biofilm in patients receiving orthodontic treatment represented by elevated levels of acidogenic bacteria, such as *S. mutans*. If these bacteria have an adequate supply of fermentable carbohydrates; acid by-products will be produced, reducing the plaque pH. As the pH falls below the threshold necessary for remineralization, enamel demineralization occurs (Øgaard et al. 1988).

1.3 DETECTION OF INCIPIENT CARIES LESION

Conventional diagnostic methods are not reliable for pre-cavitation lesions detection. In addition, these clinical methods are unable to detect changes in caries development and do not possess neither the sensitivity nor the specificity to account for the dynamic process of de/remineralization (Scully 2000). Thus, more advanced diagnostic tools are required to identify early non-cavitated carious lesions and to monitor their activity as well as severity. Early caries detection can potentially increase the probability of conservative treatment centered on tooth preservation rather than restoration. Several methods addressing the need for powerful diagnostic tools with improved

sensitivity and specificity have been investigated (Hall and Girkin 2004; Stookey and González-Cabezas 2001), even though, their employment in the dental office is still limited.

1.3.1Nano-indentation technique

The method was developed in 1992 to measure the hardness and elastic modulus by instrumented indentation techniques and has widely been utilized in the characterization of mechanical behavior of materials at small scales (Oliver 1992; Oliver and Pharr 1992).

The mechanical characteristics of a material are determined from indentation load–displacement data obtained during one cycle of loading and unloading. The system was originally intended for application with sharp, geometrically self-similar indenters like the Berkovich triangular pyramid. A schematic representation of a typical data set obtained with a Berkovich indenter is presented in Fig. 2, where the parameter P designates the applied load or force and h denominates the penetration depth or displacement of the indenter relative to the initial non-deformed surface. For modeling purposes, deformation during loading is assumed to be both elastic and plastic in nature as the permanent hardness impression forms. During unloading curve, it is assumed that only the elastic displacements are recovered. Therefore, this method does not apply to the materials in which plasticity reverses during unloading.

This curve has two distinct parts: the first part (AB) is the loading curve corresponding to the penetration of the indenter inside the material. At point (B); the indenter reaches its maximum load representing the maximum depression of the point. (BC) is the unloading or discharge curve which corresponds to the withdrawal of the indenter. At point (C), h_f is the final depth representing the permanent depth of penetration when the indenter is fully unloaded. The tangent contacts the discharge curve at the maximum point of load (P_{max}), S is the contact or elastic stiffness between the

indenter and the sample that could be measured from tangent line since this contact is considered purely elastic during the discharge phase. The accuracy of hardness and elastic modulus measurements depend inherently on how well these parameters can be measured experimentally (Pharr and Bolshakov 2002).

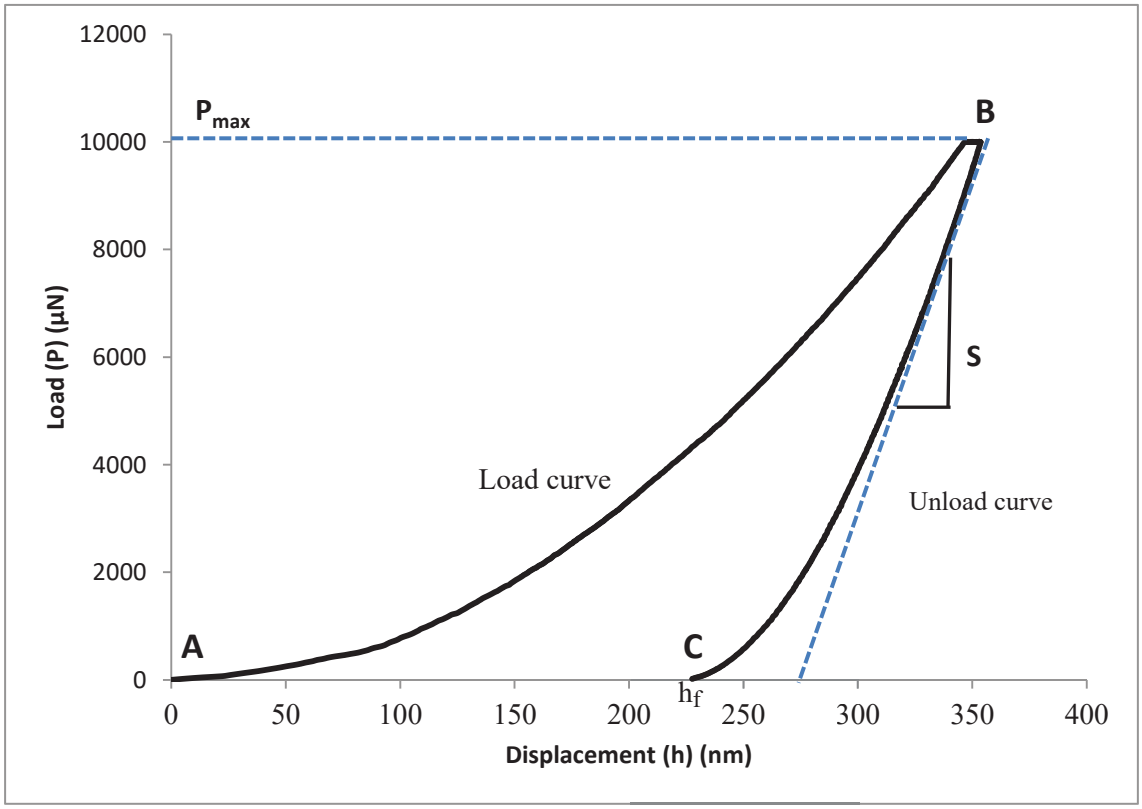

Figure 2. Schematic illustration of nano-indentation load–displacement curve showing important measured parameters

1.3.2 Confocal Raman Microscopy

Confocal Raman microscopy is an extremely useful multispectral technique that permits nondestructive, spatially resolved measurements deep within transparent samples simply by focusing the laser beam at the point of interest. Moving the laser focus allows generation of one-dimensional (1D) depth profiles, and 2D and 3D (volumetric) images (Everall 2009).

Raman spectroscopy is a vibrational molecular spectroscopy (Herzberg 1945)**,** used to obtain information about the structure and properties of molecules from their vibrational transitions (Ferrar and Nakamoto 1994; Grasselli and Bulkin 1991)**.**

In the 1920s, Raman noticed that light incident on a variety of surfaces is sometimes scattered with wavelengths different from the incident light. Elastic scattering and inelastic scattering take place when an incident visible light interacts with molecules inside a sample. Elastic scattering occurs when the scattered light has the same energy (and thus same wavelength) as the incident light; this process is termed Rayleigh scattering (Fig. 3A). The inelastic scattering (Raman scattering) happens when the energy of the scattered photon is different from the incident light. The difference in energy in case of Raman diffusion occurs because the molecule changes its vibrational state during the scattering process. The molecule that scatters the incident light can either end up in a higher vibrational state in which case the scattered photon is red shifted compared to the incident light. This type of light scattering is termed “Raman Stokes scattering”, in reference to the red-shift of the scattered photon (Fig. 3B). Alternatively, the molecule can end up in an energy state lower than its initial state via the emission of a blue-shifted photon (Raman anti-Stokes scattering). Anti-Stokes scattering requires the molecule to start out in a vibrationally excited state (Fig. 3C) (Lewis and Edwards 2001; Oheim et al. 2006). Some of the main Raman bands on tissues are at ~1450 band which is attributed to amide I and amide III stretching modes and the ~2931 cm^{-1} band is assigned to

the bending and stretching modes of CH groups of lipids and proteins. The ones at ~960, ~443, ~1051 and ~588 cm^{-1} are attributed to phosphate group in hydroxyapatie (Lopes et al. 2007).

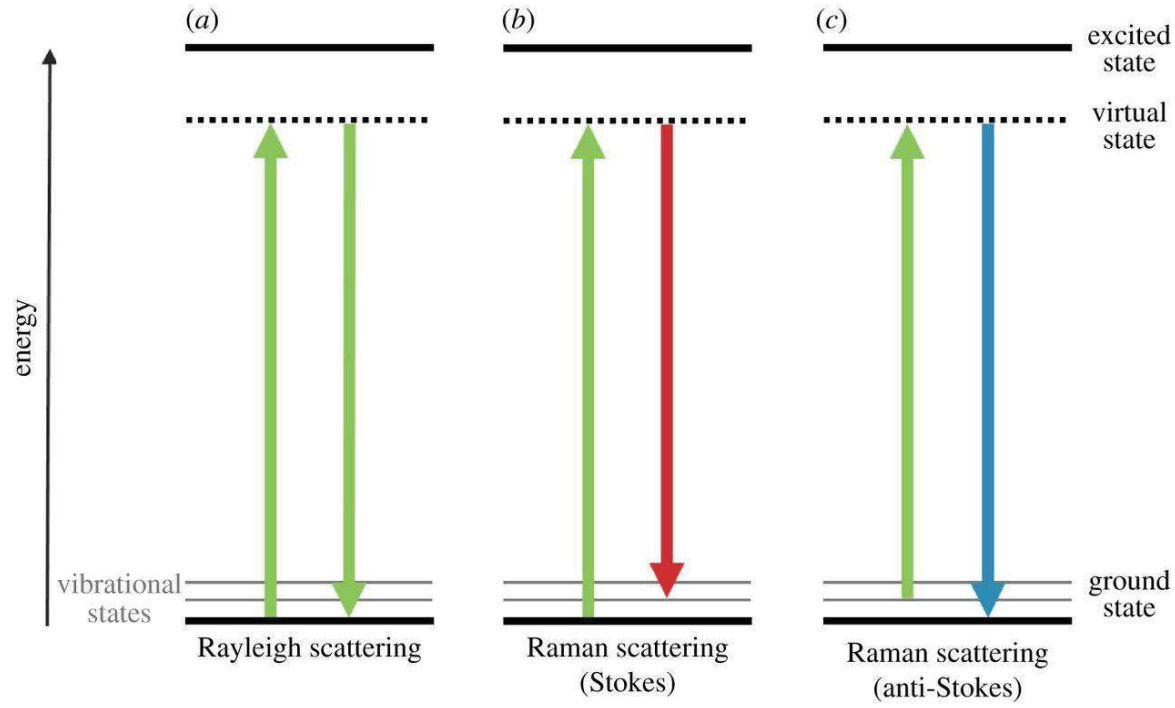

Figure 3. (A) Rayleigh scattering (B) Raman Stokes scattering (C) Raman anti-Stokes scattering Incident beams are shown in green lines while the detected signals are shown in green, red and blue lines respectively.

1.3.3Autofluorescence of biomineralized tissues

The mode of excitation is absorption of photons, which brings the absorbing species into an excited electronic state. The emission of photons accompanying de-excitation is then called fluorescence, which is one of the possible physical effects resulting from interaction of light with the matter. The emitted light has a longer wavelength, and therefore lower energy, than the absorbed radiation. Fluorescent materials would cease to glow immediately upon removal of the excitation source. Hence, it is not a persistent phenomenon (Valeur and Berberan-Santos 2012). The naturally occurring auto-fluorescence of cells and tissues is based on the presence of endogenous fluorohores such as amino acids, porphyrins..etc (Koenig and Schneckenburger 1994). Presently, the most advanced caries detection methods available; are those based on fluorescence spectroscopy. Among these methods; the nonlinear multiphoton microscopy which has been used in this study.

Multiphoton microscopy (MPM) is a powerful tool for imaging deep tissues and has many advantages over conventional single-photon microscopy with respect to biological applications. The large separation in wavelength between excitation and emitted fluorescence provides a good signal to noise ratio without sacrificing the fluorescence signal. It is a powerful technique for 3D imaging because the biological materials are transparent to infrared frequencies and can be excited to penetration depths inaccessible to one photon confocal microscopy. MPM is based on the nonlinear optical response of a medium, that is, the process that involves more than one photon interacting simultaneously with a molecule. The probability of the near-simultaneous absorption of two photons is extremely low. Therefore a high flux of excitation photons is typically required, usually from a femtosecond pulsed laser. MPM uses pulsed infrared light to excite fluorophores within the specimen being observed. The fluorophore absorbs the energy from two long-wavelength photons which must arrive simultaneously in order to excite the sample to a higher energy state, from which

it can decay, emitting a fluorescence signal. The longer wavelength, hence, low energy excitation lasers (wavelength is ranging from 760 to 900 nm) of multiphoton microscopes are well-suited to use in imaging live cells as they cause less photo-bleaching damage than short-wavelength lasers, so cells might be observed for longer periods with fewer toxic effects (Denk et al. 1990).

Multiphoton microscopy has become an important research tool for noninvasive imaging of thick specimens with cellular resolution using two-photon excitation fluorescence (2PEF) and second harmonic generation (SHG) signals which are produced only at the focal point causing less sample photo-damage and enabling sectional imaging (Gibson et al. 2011).

Two-photon excitation fluorescence (2PEF) is very similar to the traditional fluorescence, except that two photons of a lower energy are simultaneously absorbed to excite a fluorophore (Fig. 4A). Dental enamel has a strong 2PEF signal that can clearly reveal the structures of the enamel rods relying on auto-fluorescence properties of enamel (Cloitre et al. 2013; Gibson et al. 2011).

Second harmonic generation (SHG) is a nonlinear process that can only occur when light interacts with non-centrosymmetric molecular structures like collagen fibrils in dentin. These molecules can simultaneously scatter two lower-energy photons as a single photon of twice the energy (Fig. 4B) (Gibson et al. 2011). SHG provides useful information on the structure and optical properties of the inspected specimen.

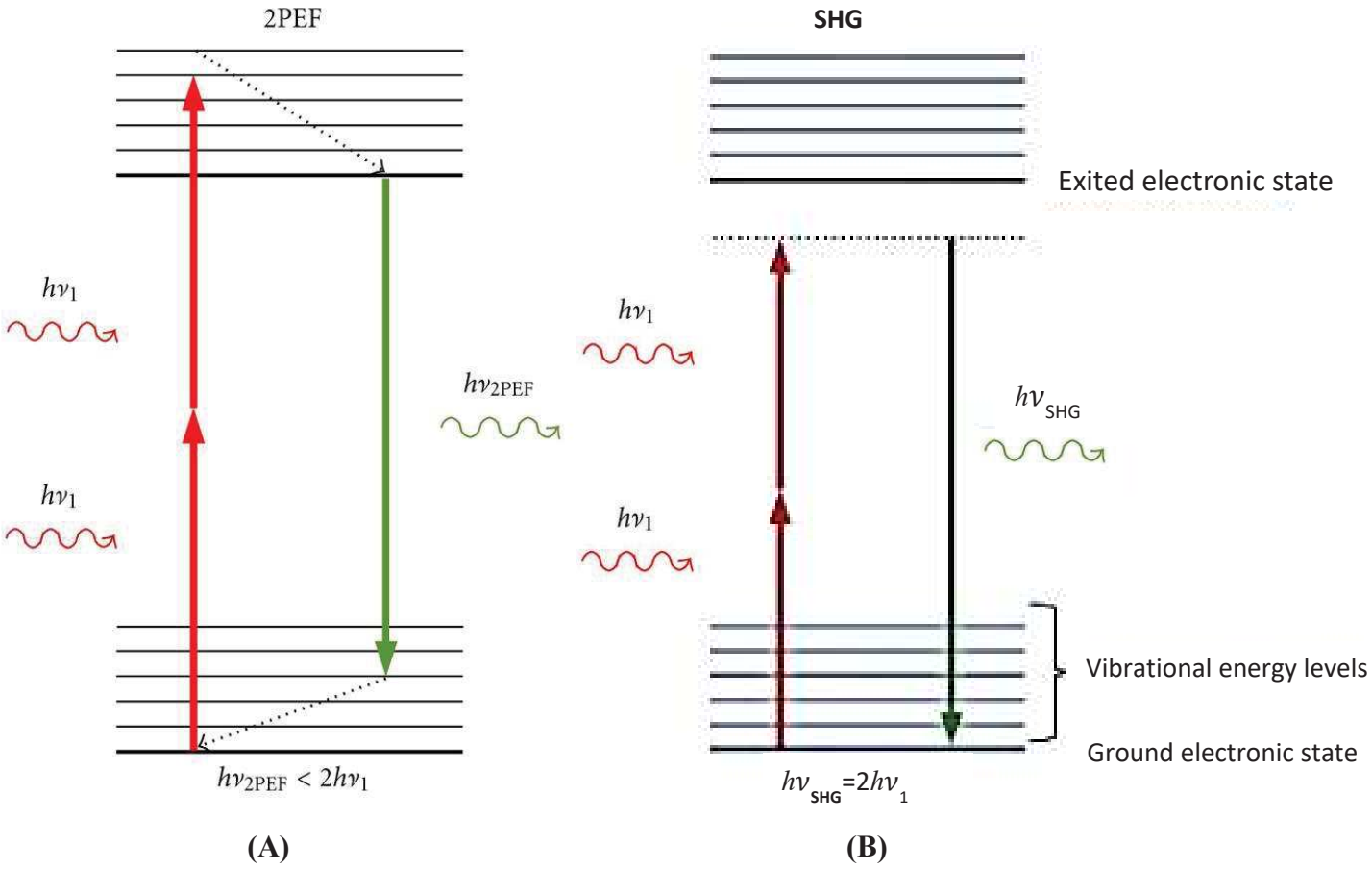

Figure 4. Jablonski diagram showing the interaction of multiple infrared photons with the electronic and vibrational energy levels of a molecule. (A) In two-photon excitation fluorescence (2PEF), the molecule absorbs two infrared photons that stimulate it to the excited electronic state. After non-radiant relaxation to a lower vibrational level, the molecule emits a lower energy (red-shifted) photon. (B) In second harmonic generation (SHG), two infrared photons are instantaneously up converted to a single photon of twice the energy.

REFERENCES:

Anderson M. 2001. Current concepts of dental caries and its prevention. Operative Dentistry.11-18.

Arx T. 1993. Developmental disturbances of permanent teeth following trauma to the primary dentition. Australian dental journal. 38(1):1-10.

Batchelar DL, Davidson M, Dabrowski W, Cunningham IA. 2006. Bone-composition imaging using coherent-scatter computed tomography: Assessing bone health beyond bone mineral density. Medical physics. 33(4):904-915.

Bishara SE, Ostby AW. 2008. White spot lesions: Formation, prevention, and treatment. Seminars in Orthodontics. 14(3):174-182.

Cate JT. 1990. In vitro studies on the effects of fluoride on de-and remineralization. Journal of dental research. 69(2_suppl):614-619.

Chatterjee R, Kleinberg I. 1979. Effect of orthodontic band placement on the chemical composition of human incisor tooth plaque. Archives of oral biology. 24(2):97-100.

Cloitre T, Panayotov IV, Tassery H, Gergely C, Levallois B, Cuisinier FJ. 2013. Multiphoton imaging of the dentine-enamel junction. Journal of biophotonics. 6(4):330-337.

Cuisinier F, Steuer P, Senger B, Voegel J, Frank R. 1992. Human amelogenesis i: High resolution electron microscopy study of ribbon-like crystals. Calcified tissue international. 51(4):259-268.

Cuisinier F, Voegel J. 1994. Early mineralization stages in different calcified systems: A hrem analysis. Curr Top Crystal Growth Res. 1:229-243.

Curzon MEJ FJ. 1983. Chemical composition of enamel. (ed) LE, editor.

Denk W, Strickler JH, Webb WW. 1990. Two-photon laser scanning fluorescence microscopy. Science. 248(4951):73-76.

Derks A, Katsaros C, Frencken J, Van't Hof M, Kuijpers-Jagtman A. 2004. Caries-inhibiting effect of preventive measures during orthodontic treatment with fixed appliances. Caries research. 38(5):413-420.

Eastoe J. 1960. Organic matrix of tooth enamel. Nature. 187(4735):411.

Everall NJ. 2009. Confocal raman microscopy: Performance, pitfalls, and best practice. Applied spectroscopy. 63(9):245A-262A.

Featherstone J, Lussi A. 2006. Understanding the chemistry of dental erosion. Dental erosion. Karger Publishers. p. 66-76.

Featherstone JD. 1995. Clinical aspects of de/remineralization of teeth. International Association for Dental Research.

Fejerskov O. 1997. Concepts of dental caries and their consequences for understanding the disease. Community dentistry and oral epidemiology. 25(1):5-12.

Fejerskov O, Johnson N, Silverstone L. 1974. The ultrastructure of fluorosed human dental enamel. European journal of oral sciences. 82(5):357-372.

Fejerskov O, Nyvad B. 2003. Is dental caries an infectious disease? Diagnostic and treatment consequences for the practitioner. Nordic dentistry 2003 yearbook. Quintessence Publishing Co, Ltd. p. 141-152.

Ferrar J, Nakamoto K. 1994. Introductory raman spectroscopy. Acad. Press, inc. Harcourt Brace and Comp., Publishers, Boston–San Diego–NY–London–Sudney–Tokio–Toronto.

Gibson EA, Masihzadeh O, Lei TC, Ammar DA, Kahook MY. 2011. Multiphoton microscopy for ophthalmic imaging. Journal of ophthalmology. 2011.

Gorelick L, Geiger AM, Gwinnett AJ. 1982. Incidence of white spot formation after bonding and banding. American journal of orthodontics. 81(2):93-98.

Grasselli JG, Bulkin BJ. 1991. Analytical raman spectroscopy. Wiley.

Gwinnett AJ, Ceen RF. 1979. Plaque distribution on bonded brackets: A scanning microscope study. American journal of orthodontics. 75(6):667-677.

Hadler-Olsen S, Sandvik K, El-Agroudi MA, Øgaard B. 2011. The incidence of caries and white spot lesions in orthodontically treated adolescents with a comprehensive caries prophylactic regimen—a prospective study. The European Journal of Orthodontics. 34(5):633-639.

Herzberg G. 1945. Infrared and raman spectra of polyatomic molecules. D. Van Nostrand Company.; New York.

Hicks J, Garcia-Godoy F, Flaitz C. 2005. Biological factors in dental caries enamel structure and the caries process in the dynamic process of demineralization and remineralization (part 2). Journal of clinical pediatric dentistry. 28(2):119-124.

Hollander F. 1935. The apparent radiopaque surface layer of the enamel. Dent Cosmos. 77:1187-1197.

Kawasaki K, Buchanan AV, Weiss KM. 2009. Biomineralization in humans: Making the hard choices in life. Annual review of genetics. 43:119-142.

Kidd EA, Nyvad B, Espelid I. 2008. Caries control for the individual patient. Dental caries. Blackwell Publishing Ltd. p. 487-504.

Koenig K, Schneckenburger H. 1994. Laser-induced autofluorescence for medical diagnosis. Journal of fluorescence. 4(1):17-40.

Lang NP, Hotz PR, Gusberti FA, Joss A. 1987. Longitudinal clinical and microbiological study on the relationship between infection with streptococcus mutans and the development of caries in humans. Molecular Oral Microbiology. 2(1):39-47.

Larsen M. 1986. The nature of early caries lesions in enamel. Journal of dental research. 65(7):1030.

Lewis IR, Edwards H. 2001. Handbook of raman spectroscopy: From the research laboratory to the process line. CRC Press.

Lopes CB, Pacheco M, Silveira Jr L, Duarte J, Cangussu MCT, Pinheiro A. 2007. The effect of the association of nir laser therapy bmps, and guided bone regeneration on tibial fractures treated with wire osteosynthesis: Raman spectroscopy study. Journal of Photochemistry and Photobiology B: Biology. 89(2-3):125-130.

Lucchese A, Gherlone E. 2012. Prevalence of white-spot lesions before and during orthodontic treatment with fixed appliances. European journal of orthodontics. 35(5):664-668.

Martinović BT, Ivanović M, Milosavljević Z, Mladenović R. 2015. Identifying basic chemical elements of hypomineralized enamel in first permanent molars. Vojnosanitetski pregled. 72(10).

McKee M, Addison W, Kaartinen M. 2005. Hierarchies of extracellular matrix and mineral organization in bone of the craniofacial complex and skeleton. Cells Tissues Organs. 181(3-4):176-188.

Odutuga A, Prout R. 1974. Lipid analysis of human enamel and dentine. Archives of oral biology. 19(8):729-731.

Øgaard B, Rølla G, Arends J. 1988. Orthodontic appliances and enamel demineralization: Part 1. Lesion development. American journal of orthodontics and dentofacial orthopedics. 94(1):68-73.

Oheim M, Michael DJ, Geisbauer M, Madsen D, Chow RH. 2006. Principles of two-photon excitation fluorescence microscopy and other nonlinear imaging approaches. Advanced drug delivery reviews. 58(7):788-808.

Oliver W. 1992. Wc oliver and gm pharr, j. Mater. Res. 7, 1564 (1992). J Mater Res. 7:1564.

Oliver WC, Pharr GM. 1992. An improved technique for determining hardness and elastic modulus using load and displacement sensing indentation experiments. Journal of materials research. 7(6):1564-1583.

Pharr G, Bolshakov A. 2002. Understanding nanoindentation unloading curves. Journal of materials research. 17(10):2660-2671.

Sato K. 2007. Mechanism of hydroxyapatite mineralization in biological systems. Journal of the Ceramic Society of Japan. 115(1338):124-130.

Silverstone L. 1983. Remineralization and enamel caries: New concepts. Dental Update. 10(4):261-273.

Silverstone L, Hicks M, Featherstone M. 1988. Dynamic factors affecting lesion initiation and progression in human dental enamel. Part i. The dynamic nature of enamel caries. Quintessence international (Berlin, Germany: 1985). 19(10):683.

Ten Cate J. 2008. Remineralization of deep enamel dentine caries lesions. Australian dental journal. 53(3):281-285.

Ten Cate J, Mundorff-Shrestha S. 1995. Working group report 1: Laboratory models for caries (in vitro and animal models). Advances in dental research. 9(3):332-334.

Valeur B, Berberan-Santos MN. 2012. Molecular fluorescence: Principles and applications. John Wiley & Sons.

Weatherell J. 1975. Composition of dental enamel. British medical bulletin. 31(2):115-119.

White D. 1995. The application of in vitro models to research on demineralization and remineralization of the teeth. Advances in dental research. 9(3):175-193.

White S. 2004. Benign tumor of jaw. Oral radiology Principles and interpretation.410-458.

LIST OF FIGURES

Chapter 2

First Article

Enamel Subsurface Lesions: Formation and Assessment in vitro.

ABSTRACT

This study aims to compare two pH-cycling models used to induce subsurface lesion (SL) with a less demineralized surface layer, besides, developing new technologies for assessing them through demonstrating the performance of confocal Raman microscopy in WSL detection. 12 sound premolars were subjected to two models (A & B) to induce (SLs). Teeth had in vivo formed white lesions were used as a positive control. All specimens were inspected by Soprolife camera and Raman microscopy to detect small changes in the appearance and structure of enamel. Changes in the tooth natural color throughout the treatment were recorded via the camera. Phosphate maps with their spectra constructed from phosphate peak at 960 cm^{-1} are shown here. Depth of different lesions was measured based on phosphate peak intensity variations. Protocol B is reliable to reproduce SLs in a relatively short period. Both protocols have intrinsic limitations as they could not completely simulate the complex intraoral conditions leading to WSL formation with respect to lesion depth and preservation of intact surface layer (ISL). Raman microscopy could be considered the gold standard for hard tissue mineralization analyses.

Keywords: White spot lesion (WSL), pH cycling model, Raman microscopy.

2.1 INTRODUCTION

Dental caries is a multifactorial disease resulting from a dynamic disparity present in the oral cavity in alternating periods of dissolution and mineral loss (Featherstone et al. 1979). White spot lesions (WSLs) represent an early stage of caries formation where subsurface enamel demineralization takes place. WSL formation can be reconstituted in the laboratory through the use of chemical systems in a relatively short period (Larsen 1974). pH cycling model is a chemical system involves exposition of dental enamel to combinations of de/ remineralization phases planned to mimic the dynamics of mineral loss and gain involved in caries formation. The resulted lesions help in supporting the possible mechanisms of caries prevention and/or remineralization in addition to better planning of clinical trials (White 1995).

Soprolife light-induced fluorescence assessor system (Acteon, La Ciotat, France) is newly released apparatus for detection and assessment of incipient dental caries, based on imaging and auto-fluorescence detection of dental tissues (Tassery et al. 2013).

Raman microscopy is a non-invasive spectroscopic method with minimal specimen preparation that provides detailed information about the biochemistry and molecular structure of mineralized tissues. Its high spatial resolution (300 nm), makes it a novel optical approach for analyzing calcified tissue components and detecting early changes in its composition (Slimani et al. 2017).
The incremental prevalence of mild hypomineralization due to developmental defects on tooth surfaces poses a challenge for caries detection and prevention. pH-cycling models enable the development of subsurface lesions in a relatively short periods which representing up to 6 to 12 months of clinical lesion progression. The present study was designed to compare two chemical

models with respect to their potential to induce artificial caries confined to enamel surface and demonstrate their ability to mimic the intra-oral conditions that lead to WSL formation. In addition, it anticipates developing new technology for assessing subsurface lesions through demonstrating the performance of Raman microscopy in incipient caries detection.

2.2 MATERIALS & METHODS

Sound premolars collected with informed consent from all subjects and approval of the local ethical research committee (process No. 2017-2907) before being used in this research.

4 premolars had *in vivo* formed WSLs were used as reference (positive control). 12 sound teeth were randomly divided into 3 groups which were exposed to two pH cycling models; A & B respectively. Teeth were undergone 7, 8 and 14 cycles respectively. Each cycle lasted 24h. Different numbers of cycles were used to produce artificial early caries lesions with various ranges of lesion depths to measure the representative characteristics of early caries lesions, such as fluorescence loss, color changes and amount of mineral loss by the intraoral camera and the confocal microscopy.

The first model (A) is described by Featherstone (Featherstone et al. 1986) has held for 14 days. The demineralizing solution is composed of 2.0 mM $Ca(NO_3)_2 \cdot 4H_2O$), 2.0 mM KH_2PO_4, 75.0 mM CH_3COOH, at pH = 4.4). Remineralizing solution composition is 1.5 mM $Ca(NO_3)_2 \cdot 4H_2O$), 0.9 mM KH_2PO_4, 130 mM KCl, 20 mM $NaC_2H_6AsO_2 \cdot 3H_2O$, at pH = 7.

Second model (B) (Al-Obaidi et al. 2018) uses a demineralizing solution (0.075 M L^{-1} CH_3COOH, 1.0 mM $CaCl_2$, 2.0 mM KH_2PO_4, at pH= 4.3). The remineralizing solution contains

(150 mM KCl, 1.5 mM $Ca(NO_3)$, 0.9 mM KH_2PO_4, at pH = 7). All chemical products were supplied by Sigma-Aldrich, France.

Each tooth was immersed in 20 ml of demineralizing solution for 6 hours. Then it was removed and rinsed with running water before being immersed in 20 ml of remineralizing solution for 18 hours. The temperature maintained at 37 ◦C. Teeth were sectioned longitudinally into two halves to have cross sections of teeth which then were embedded in self-curing acrylic resin, having the cross sectioned surface of samples facing the surface that is to be polished later.

2.2.1 Soprolife Camera:

The camera can be used to capture high resolution images of caries lesions, which will extremely facilitate clinical assessments (Pitts 2004). All teeth were filmed with it pre- and post-intervention in order to detect changes in enamel surface appearance. The camera provides anatomical images in (daylight mode) and fluorescent images in (diagnostic mode). The light is provided by 4 blue-light LEDs of wavelength 450 nm.

2.2.2 Raman microscopy:

Raman spectra were recorded using a Witec Confocal Raman Microscope System alpha 300R (Witec, Ulm, Germany). Excitation is assured by a frequency doubled Nd: YAG laser (Newport, Evry, France) at 532nm. Enamel chemical mapping was started at the outer surface and ending before dentin enamel junction (DEJ). The phosphate (PO_4^{3-}) ion has four vibrational modes. The peak at 960 cm^{-1} is assigned to ν_1 vibration peak of the phosphate group in enamel which was selected as the inner standard to observe changes in the intensity of the strongest peak at 960 cm

$^{-1}$. Using an indicative look-up table (LUT), yellow and dark brown hues indicate maximum and minimum phosphate intensity in a chosen area.

Overall mean and standard deviation (SD) of lesion depth were calculated. Statistical analysis was performed using One Way ANOVA Analysis of Variance. All statistical procedures were performed at over all significant level of $\alpha = 0.05$ with SigmaPlot 11.0 (Systat Software; Inc., USA).

2.3 RESULTS

Image pairs were recorded using the intraoral camera as an additional method for visual inspection (Fig.1A, B, C, D). A & B represent images in daylight mode before intervention. C& D represent images exhibiting changes in enamel surface appearance after 8 cycles-protocol A and 7 cycles- protocol B consecutively. Mean of depth of artificial lesions was measured and compared to that of natural lesions based on phosphate peak intensity variations in each dental section. A statistically significant difference ($p<0.05$) in depth value was found between positive control group and 8 cycles-B. The difference was significant between 7 & 8 cycle lesions (protocol B) as well. A non-significant difference ($p>0.05$) was detected between other groups (Fig.1 E).

Phosphate maps with their corresponding spectra presented in (Fig. 2A, B, C, D, E) are constructed from phosphate peak intensity at 960 cm^{-1}. All examined samples exhibited an important phosphate signal at outer enamel surface which indicates the presence of ISL. Then, there was a severe depletion in PO_4^{3-} peak in the area corresponding to body of the lesion. At a greater distance inside the enamel; the intensity meets that of sound enamel indicating end of the lesion.

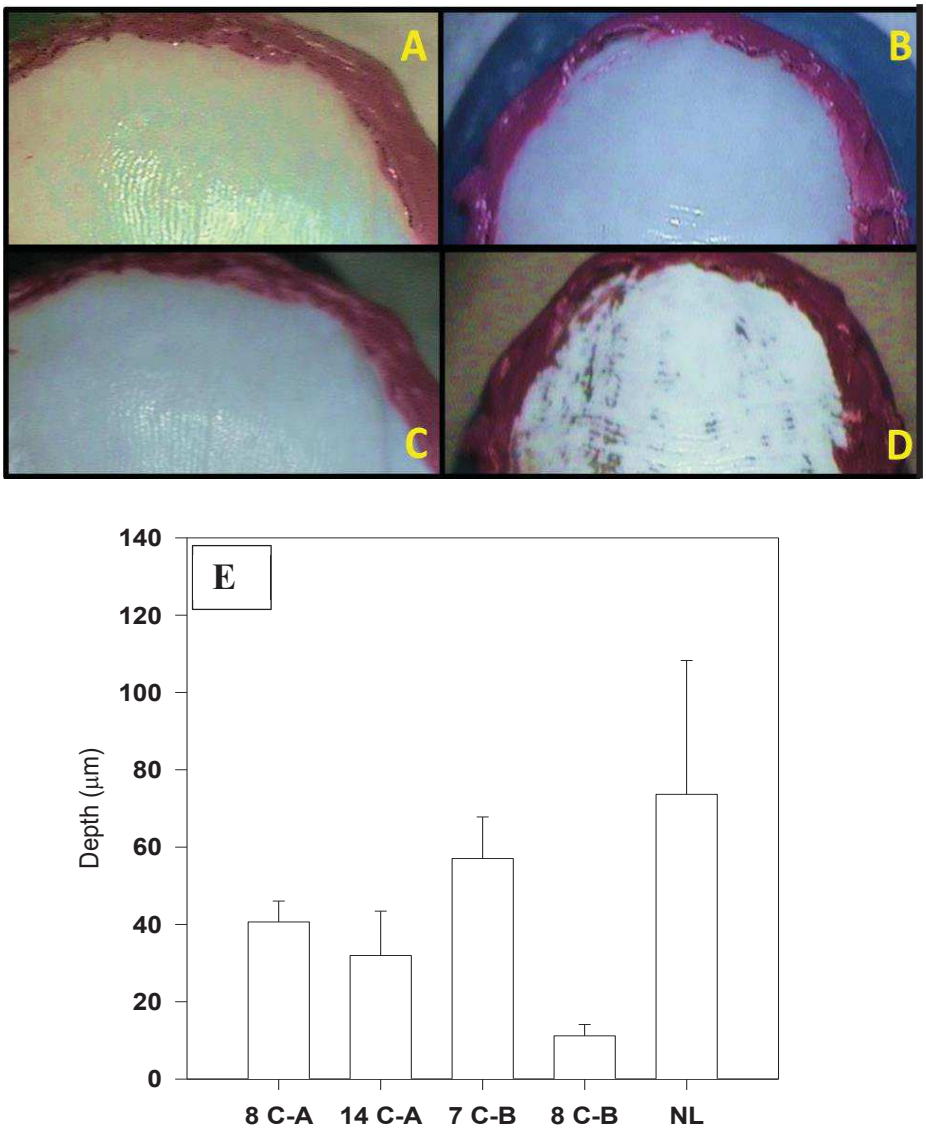

Fig. 1 Anatomical images in daylight mode made by intraoral camera. (A & B) Teeth before cycling. (C) Image after 8 cycles- Protocol A. (D) Image after 7 cycles- Protocol B. (E) Depth of different lesions based on PO_4^{3-} intensity, produced by: Protocol A after 8 cycles (8C-A), on the same group, test has continued till 14 cycles (14C-A). Protocol B after 7cycles (7C-B) and after 8 cycles (8C-B). (NL) Natural Lesion. (C) Cycle. SD values are represented by error bars.

2.4 DISCUSSION

This paper aims to compare two pH-cycling models, focusing on their strengths, limitations and the period required to induce subsurface lesion. The Chemical composition of subsurface lesions was described using Raman microscopy which can detect very small changes by identifying variations in phosphate intensity that reflects the amount of mineral content in the target zone (Mohanty et al. 2013). Data analysis of each acquired scan which is comprised of tenth thousands of spectra; was used to reconstruct different detailed images.

Natural WSLs are formed in complex intraoral conditions due to imbalance between pathological factors that cause demineralization and protective factors that drive to remineralization. De/remineralization phases occur in the mouth several times every day as a dynamic process that takes much longer than in the laboratory models (Featherstone 2004b). Therefore, WSLs are more sophisticated than *in vitro* subsurface lesions (SLs) in respect to chemical composition of enamel and lesion depth due to the presence of saliva and plaque *in vivo.* WSLs are quite variable; ISL is almost present due to strong possibility of remineralization from the oral environment. While the amount of mineral loss from the subsurface lesion is completely inconstant (Featherstone 2004b).

Subsurface lesion produced by protocol A after 8 cycles was invisible after inspection with the camera (Fig.1C) even after prolonged dryness due to humble demineralization and thus small changes in the chemical composition of enamel represented by PO_4^{3-} peak intensity (Fig.2A). After 14 cycles; changes became more evident with the formation of pronounced subsurface lesion accompanied by undermining of ISL (Fig.2B). However, protocol B was able to induce first changes in enamel appearance after merely 3 cycles. Extremely white enamel became evident after only 7 cycles (Fig.1D) along with chemical map showing a deep lesion with intense

decrease in phosphate amount in lesion body and presence of ISL (Fig.2 C). A distinct dissolution of the outer surface was encountered after 8 cycles (Fig.2 D).

When light enters sound enamel which is a low light scattering material, it travels an average distance of 0.1 mm before being scattered (Angmar-Månsson and Ten Bosch 1987). When minerals are lost from enamel due to demineralization, they will be partly replaced by water which leads to increase differences in refractive index (RI) between sound and demineralized enamel leading to greater scattering at the enamel/ air interface (Wang et al. 1999). When the lesion is dried, the water is replaced by air and the average refractive index declines even more, leading to an even whiter lesion. Besides that, whiteness of the initial lesions is an optical phenomenon, resulted from increased voids within the enamel crystalline structure (Angmar-Månsson and Ten Bosch 1987; Torres et al. 2011). Thus, changes in enamel appearance could be detected only when distinct subsurface lesion is developed owing to interior opacity and surface scattering effect (Årtun and Thylstrup 1989). Chemical protocols have limitations regarding lesion depth and ISL conservation due to the difficulty to completely simulate the complex intraoral conditions that leading to WSL development (White 1992). Protocol A induced slight change in enamel appearance after 8 cycles. Whereas, protocol B produced deep subsurface lesion after only 7 cycles. The latter model is less time consuming and reliable to reproduce SLs *in vitro* in a relatively short period as long as it is limited to seven cycles to ensure the presence of ISL which represents the characteristic feature of these lesions that complicates their non-invasive treatment. These subsurface lesions are essential in profile studies for rapid and low-cost testing of developing and recently marketed remineralizing dental products (White 1995).

Moreover, Raman microscopy could be considered as the gold standard for hard tissue mineralization analyses. Further work is required to present this tool to clinical application to perceive carious lesions at an early stage of development.

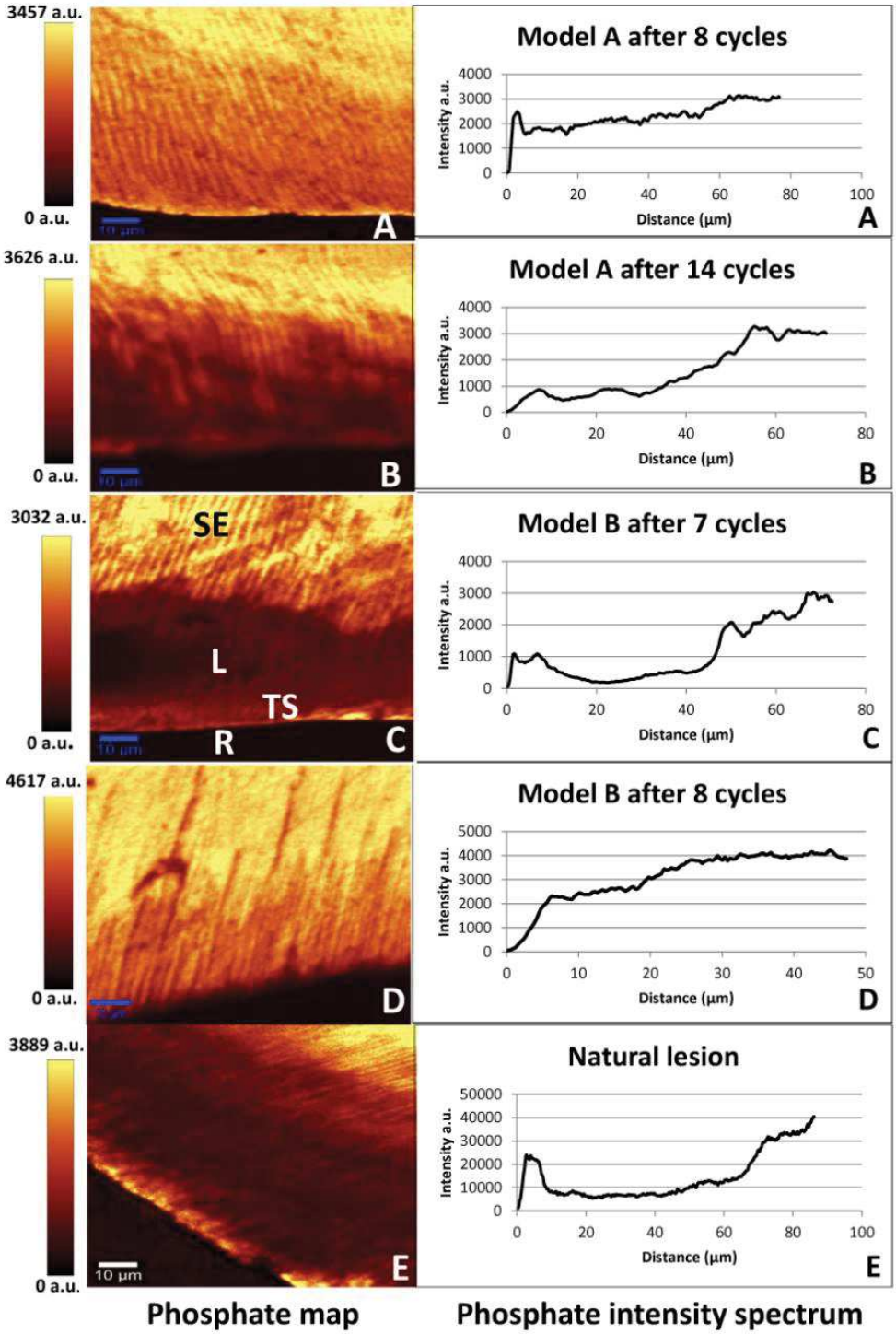

Fig. 2 Phosphate maps with their correspondent spectra constructed from phosphate peak at 960 cm^{-1}. (A & B) demonstrating lesions produced by protocol A after 8 and 14 cycles. (C & D) Protocol B after 7 and 8 cycles. (E) Natural lesion. Individual LUTs on the left. (Following symbols fixed on image (C) are valid for all images: **SE**; sound enamel, **L**; lesion, **TS**; tooth surface, **R**; resin.

REFERENCES

Featherstone J, Duncan J, Cutress T (1979) A mechanism for dental caries based on chemical processes and diffusion phenomena during in-vitro caries simulation on human tooth enamel. Archives of oral biology 24, 101-12.

Larsen MJ (1974) Chemically induced in vitro lesions in dental enamel. European journal of oral sciences 82, 496-509.

White D (1995) The application of in vitro models to research on demineralization and remineralization of the teeth. Advances in dental research 9, 175-93.

Tassery H, Levallois B, Terrer E, Manton D, Otsuki M et al. (2013) Use of new minimum intervention dentistry technologies in caries management. Australian dental journal 58, 40-59.

Slimani A, Nouioua F, Desoutter A, Levallois B, Cuisinier FJG et al. (2017) Confocal Raman mapping of collagen cross-link and crystallinity of human dentin-enamel junction. J Biomed Opt 22, 1-8.

Featherstone J, O'reilly M, Shariati M, Brugler S (1986) Enhancement of remineralization in vitro and in vivo. Factors relating to demineralisation and remineralisation of the teeth. IRL Press. Oxford and Washington.

Al-Obaidi R, Salehi H, Desoutter A, Bonnet L, Etienne P et al. (2018) Chemical & Nano-mechanical Study of Artificial Human Enamel Subsurface Lesions. Scientific reports 8, 4047.

Pitts N (2004) Are we ready to move from operative to non-operative/preventive treatment of dental caries in clinical practice? Caries research 38, 294-304.

Mohanty B, Dadlani D, Mahoney D, Mann AB (2013) Characterizing and identifying incipient carious lesions in dental enamel using micro-Raman spectroscopy. Caries research 47, 27-33.

Featherstone J (2004) The continuum of dental caries—evidence for a dynamic disease process. Journal of dental research 83, 39-42.

Angmar-Månsson B, Ten Bosch J (1987) Optical methods for the detection and quantification of caries. Advances in dental research 1, 14-20.

Wang X-J, Milner TE, de Boer JF, Zhang Y, Pashley DH, Nelson JS (1999) Characterization of dentin and enamel by use of optical coherence tomography. Applied Optics 38, 2092.

Torres CRG, Borges AB, Torres LMS, Gomes IS, de Oliveira RS (2011) Effect of caries infiltration technique and fluoride therapy on the colour masking of white spot lesions. Journal of dentistry 39, 202-7.

Årtun J, Thylstrup A (1989) A 3-year clinical and SEM study of surface changes of carious enamel lesions after inactivation. American journal of orthodontics and dentofacial orthopedics 95, 327-33.

White D. (1992) The comparative sensitivity of intra-oral, in vitro, and animal models in the'profile'evaluation of topical fluorides. Journal of dental research 71.

Chapter 3

Second Article

Chemical & Nano-mechanical Study of Artificial Human Enamel Subsurface Lesions.

ABSTRACT

White lesions represent an early phase of caries formation. 20 human sound premolars were subjected to pH cycling procedure to induce subsurface lesions (SLs) *in vitro*. In addition, 2 teeth with naturally developed white spot lesions (WSLs) were used as references. All specimens characterized by confocal Raman microscopy being used for the first time in examining white & subsurface lesions, providing a high resolution chemical and morphological map based on phosphate peak intensity alterations at 960 cm^{-1}. Nanoindentation technique was used to measure Hardness (H) and Young's modulus (E) of enamel. Phosphate map of examined samples exhibited presence of intact surface layer (ISL) followed by severe depletion in (PO_4^{3-}) peak in the area corresponding to the body of the lesion. In all examined groups, the mechanical properties of enamel were decreased in lesion area and found to be inversely related to penetration depth of indenter owing to enamel hierarchical structure. By combining the above two techniques, we linked mechanical properties of enamel to its chemical composition and ensured that the two methods are highly sensitive to detect small changes in enamel composition. Further work is required to bring these two excellent tools to clinical application to perceive carious lesions at an early stage of development.

Keywords: Raman microscopy, Crystallinity, KMCA (K-mean cluster analysis), nanoindentation (NI).

3.1 INTRODUCTION

Subsurface enamel demineralization is known as white spot lesions (WSLs); they represent the early stage of caries formation where affected surfaces seem to be intact upon gentle probing. However, with absence of effective treatment, cavitation may occur thereby increasing the necessity of invasive restorative treatments (Bergstrand and Twetman 2011; Derks et al. 2004).

The WSL presents itself as a milky white opacity on smooth surfaces of teeth (Summitt et al. 2006). By examining histological sections of WSL, four zones could be distinguished: relatively intact surface layer (ISL), body of the lesion, dark zone and translucent zone which represents the advanced front of the lesion (Gorelick et al. 1982).

The translucency of enamel is an optical phenomenon that depends on the size of intercrystalline spaces. In early stages, active caries requires air drying to be visible, as the dissolution process of crystals at outer enamel surface begins. Further enlargement of intercrystalline spaces results in white patch visible without dryness. The effect of dehydration on enamel translucency is resulting from replacement of water content around enamel prisms with air. In a heterogeneous system, like enamel prisms surrounded by a fluid medium, scattering occurs due to difference in refractive indices (RI) of the two involved components. As RI of enamel is approximately 1.65, while that of water is 1.33 and of air is 1.00. Hence, larger difference in RI values, produces greater scattering at the enamel/ air interface (Wang et al. 1999).

Every day, demineralization and remineralization occur in the mouth several times as an active process, with progression or reversal of dental caries being the end result. The process of dental caries can be modeled in the laboratory to produce the early manifestation of caries, namely, the subsurface lesions (SLs). The dynamic nature of the process has been modeled in numerous

laboratories by various pH cycling models (Featherstone 2004a; Ten Cate and Mundorff-Shrestha 1995) in an attempt to simulate intraoral conditions in which enamel is subjected to repeated sequences of de/remineralization periods. The advantage of those models is that much can be learned about the processes involved, in a shorter period of time.

Transverse microradiography (TMR) is an essential method to determine the amount of mineral gain or loss in subsurface carious lesions *in vitro*. In addition, it has become a standard method, by which other recently developed caries detection techniques are compared and validated (Hsu et al. 2008; Manesh et al. 2009). Though, preparing sections as thin as 100 μm that need to be very plane to ensure accuracy of the measurements; representing a major problem for this method. This fact makes this technique destructive and time consuming. Particularly, in case of enamel, probably because of its brittleness, this method was frequently found to yield irregular sections (Lo et al. 2010).

Per contra, Raman microscopy which is a non-invasive technique; requires minimal specimen preparation, less expensive in term of cost and allows for simultaneous characterization of organic and inorganic tooth phases (Salehi et al. 2013). The high spatial resolution (300 nm) makes it an excellent tool for analyzing human enamel components, enabling the detection of WSL at an early stage of development (Desoutter et al. 2014). Lesion depth measurements obtained from Raman scans; are based on phosphate peak intensity alterations which are closely related to its content in a given section (Akkus et al. 2016). This fact is even making the definition of the outer surface of a lesion easier when it is difficult to delineate it under TMR (Ten 1991).

Nanoindentation (NI) technique enables investigations of local mechanical properties under various loading regimes based on load displacement data of indentations on submicron scale. Using this technique to measure mechanical characteristics at multiple locations within the same enamel sample is appropriate because it can accurately measure the mechanical properties of very small volumes with fine spatial resolution and show high sensitivity to any change affecting their values (Alsayed et al. 2016; Dickinson et al. 2007)

Our approach of combining confocal Raman microscopy, being used for the first time in examining white and subsurface lesions, with nanoindentation technique will add chemico-mechanical specificity in providing important information about an artificial model of subsurface lesions in human teeth to facilitate the future investigations on the efficacy WSLs treatments.

3.2 MATERIALS & METHODS

3.2.1 pH cycling procedure:

(2) Premolars with naturally developed WSL (used as references for comparison purposes), in addition to (20) sound premolars (without any enamel developmental defects), were employed in this study. These teeth were extracted for orthodontic reasons and were used after obtaining approval of the local ethical research committee (process No. 2017-2907) and informed consent from all subjects. All procedures were carried out in accordance with relevant guidelines and regulations.

The number of teeth required in this study was calculated by using BiostaTGV site (iPLESP 2000). By comparing two means that were observed during our preliminary studies; we found that the minimum number of teeth in each group is 5 teeth per group.

Teeth washed with de-ionized water to remove any debris, stored in de-ionized water with 0.1% antimicrobial thymol and kept in the refrigerator at 4°C until use. Teeth were polished with non-fluoridated paste and further cleaned ultrasonically (Elfallah et al. 2015).

To create enamel subsurface lesions; 20 sound teeth were randomly divided into 4 groups which undergone 5, 6, 7 and 8 pH cycles respectively. Each cycle lasted 24h. Different numbers of cycles were used in order to produce SLs that resemble, as much as possible, the naturally developed white lesions which classified as score 1 and 2 according to ICDAS (Ismail et al. 2007) Teeth were subjected to pH cycling procedure; using a demineralizing solution (0.075 M/L acetic acid, 1.0 mM/L calcium chloride and 2.0 mM/L potassium phosphate, pH= 4.3) and a remineralizing solution (150 mM/L potassium chloride, 1.5 mM/L calcium nitrate, 0.9 mM/L potassium phosphate, pH = 7). All chemicals were supplied by Sigma-Aldrich, France.

The procedure includes the immersion of each tooth in 20 ml of demineralizing solution for 6 hours at 37 °C. Then it removed and rinsed with distilled water for 2 min. before immersion in 20 ml of remineralizing solution for 18 hours at 37 °C. Adhesive tape disk of 6mm diameter was cut and burnished on the buccal surface of each tooth. An acid resistant nail varnish was used to cover the whole surface of each tooth; the tape was removed leaving a window of 6 mm in diameter on buccal surface.

After the achievement of different number of cycles; teeth were divided longitudinally into two halves by using high speed diamond saw (Isomet 2000, Buehler, USA) to produce cross sections of teeth which then embedded in self-curing acrylic resin and keeping the cross sectioned surfaces exposed. The sections were polished by SiC papers #800, #1000 and #1200, followed by diamond pastes, using a polishing machine (Escil, France).

3.2.2 Raman microscopy:

Raman spectra are recorded using a Witec Confocal Raman Microscope System alpha 300R (Witec Inc., Ulm, Germany). Excitation in the confocal Raman microscopy is assured by a frequency doubled Nd: YAG laser (Newport, Evry, France) at a wavelength of 532nm. The incident laser beam is focused onto the sample through a ×20 NIKON objective (Nikon, Tokyo, Japan). Then Raman backscattered radiation mixed with Rayleigh scattered are passed through an edge filter to block the Rayleigh's. Acquisition time of a single spectrum was set to 0.05 s. Each spectrum corresponding to a spatial unit defined as a voxel ($300\ nm \times 300\ nm \times 1\ \mu m$). All data acquisition and processing were performed using Image Plus software from Witec.

Chemical mapping of dental enamel was carried out over cross sections of all specimens with naturally and artificially developed subsurface lesions. The phosphate (PO_4^{3-}) ion has four internal vibrational modes. We chose to observe changes in intensity of the strongest peak at 960 cm^{-1} which is attributed to ν_1 (PO_4^{3-}) symmetric stretching mode.

Using an indicative look-up table (LUT), red hues indicate highest phosphate intensities, CO_3^{2-}/PO_4^{3-} ratio and crystallinity rates while purple hues represent lowest value of previous variables in a chosen region. K-mean cluster analysis (KMCA) divides data into K mutually exclusive clusters which are compact and well-separated. Each cluster represents a zone depending upon the magnitude of its phosphate peak intensity. Four zones with pseudo color were distinguished (Salehi et al. 2013).

Crystallinity degree in enamel is determined by measuring changes in peaks ratio of symmetric mode of phosphate at 960 cm^{-1} over 950 cm^{-1} (Slimani et al. 2017).

Raman peak at 1070 cm^{-1} is assigned to B-type carbonated hydroxyapatite (CHA).The ratio of intensities of carbonate to phosphate at (1070/960 cm^{-1}) were calculated throughout the whole section of each sample in order to detect variations in carbonate content in different zones of each sample (Xu et al. 2009).

3.2.3 Nanoindentation technique:

A nanoindenter equipped with a Berkovich tip (CSM, Switzerland), was used to measure hardness (H) and Young's modulus (E) of enamel. Tests were made in lesion, intermediate and sound enamel areas respectively. Indentations with a maximum load of 10 mN were marked on the samples where nanoindentation test was performed. The distance between each 2 neighboring indentations was at least 10 μm. A load of 20 μN was set for all tests, and loading and unloading time was 270 s. At least; ten indentations were done on each zone of the examined enamel surface.

H and E variables of samples were obtained from load-displacement loading/unloading curves, using Oliver and Pharr method (Oliver and Pharr 2004), which is the most successful model for nanoindentation data analysis.

The hardness (H) is calculated at the maximum force according to the following relation:

$$H = \frac{F}{A_P} \quad \ldots\ldots (1)$$

Where F is the maximum force and A_p is the projected surface contact area between the indenter and the sample.

The Young's modulus (E) of the sample can be obtained using the slope (S) at the beginning of the unloading curve according to the following relations:

$$E^* = \frac{\sqrt{\pi}}{2\beta} \frac{S}{\sqrt{A_P}} \quad \ldots\ldots\ldots (2)$$

and $\frac{1}{E^*} = \frac{1-\nu^2}{E} + \frac{1-\nu_i^2}{E_i}$ ……. (3)

Where β is a geometrical constant depending upon the indenter shape (1.034 in our case), E_i (1070 GPa) and ν_I (0.07) are Young's modulus and Poisson's coefficient of diamond indenter respectively. ν is the Poisson's coefficient of the sample which equals to 0.3 for enamel (Haines 1968).

Overall mean and standard deviation (SD) for lesion depth (measured from Raman's data), penetration depth (Pd), H and E of different groups (data obtained from nanoindentation test) were calculated. Statistical analysis was performed using One Way ANOVA Analysis of Variance for all experimental groups, followed by multiple comparison procedures between each two pairs with Holm-Sidak method. All statistical procedures were performed at over all significant level of α = 0.05 with SigmaPlot version 11.0 (Systat Software, Inc., USA).

3.3 RESULTS

Depth of artificial subsurface lesions was measured and compared to that of natural lesion. Depth measurements were based on phosphate peak intensity alterations and found to increase linearly with gradual rise in number of cycles except for 8 cycles lesion, where a considerable loss of enamel layer has taken place. A statistically significant difference ($p < 0.05$) was found between all examined groups (Fig.1).

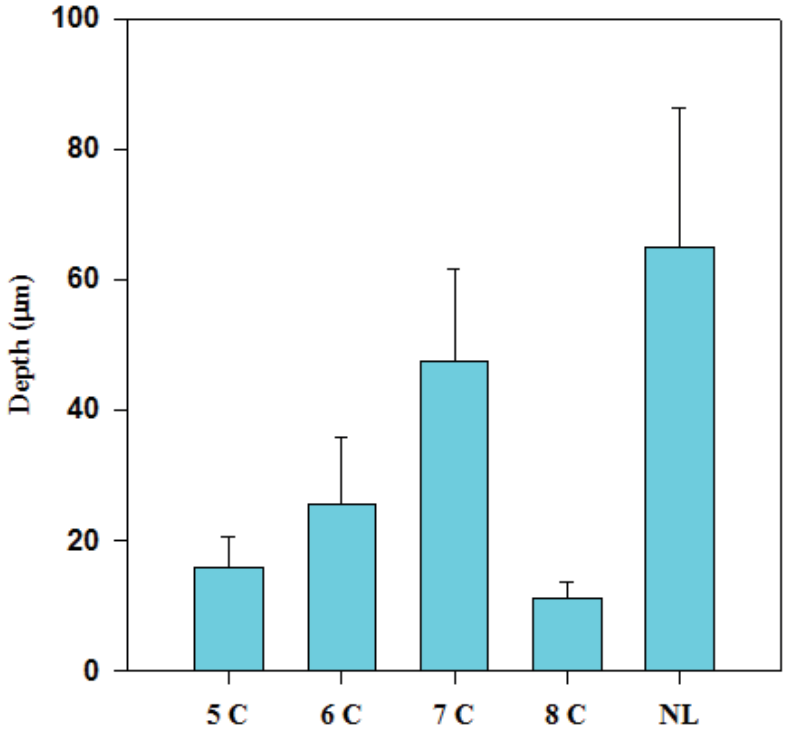

Figure 1. The relation between means of lesion depths determined by measuring variations in PO_4^{3-} peak intensity at 960 cm^{-1} & number of cycles (C). SD values are represented by error bars. (NL) natural lesion.

Raman acquisitions were carried out from outer enamel surface towards dentin-enamel junction (DEJ). Images constructed from phosphate peak intensity at 960 cm^{-1} are shown in (Fig. 2A, D, G, J). All examined samples exhibited phosphate signal at outer enamel surface which indicates the presence of ISL. A severe depletion in (PO_4^{3-}) peak in the area corresponding to body of the lesion. At greater distances into the enamel; phosphate peak intensity converges to that of sound enamel signaling the end of the lesion.

The reconstructed images of enamel crystallinity of all groups, almost exhibit a pattern similar to that of PO_4^{3-} images (Fig. 2C, F, I, L). Each pseudo color in these images; represents a special crystallinity value. Leveled color scale bars are designed to estimate the value of each color. Crystallinity decreases abruptly in lesion zone (blue). Thereafter; it starts to increase gradually in the intermediate zone (green, yellow hues) before it reaches to its maximum value in sound enamel (red area) beyond subsurface lesion.

Results of K-mean cluster analysis of data set of four clusters are shown in (Fig. 2B, E, H, K). Images constructed via KMCA demonstrating clusters with four distinguished colors: acrylic resin (green), sound enamel with two different intensities of phosphate (in turquoise zone, PO_4^{3-} intensity is stronger than that in blue zone) and demineralized lesion body (red).

Reconstructed images derived from CO_3^{2-}/PO_4^{3-} ratio (Fig. 3A, B, C, D) were used to analyze changes in enamel inorganic components in each zone of the lesion. They revealed an increase in CO_3^{2-}/PO_4^{3-} ratio in lesion zone in comparison to sound enamel zone.

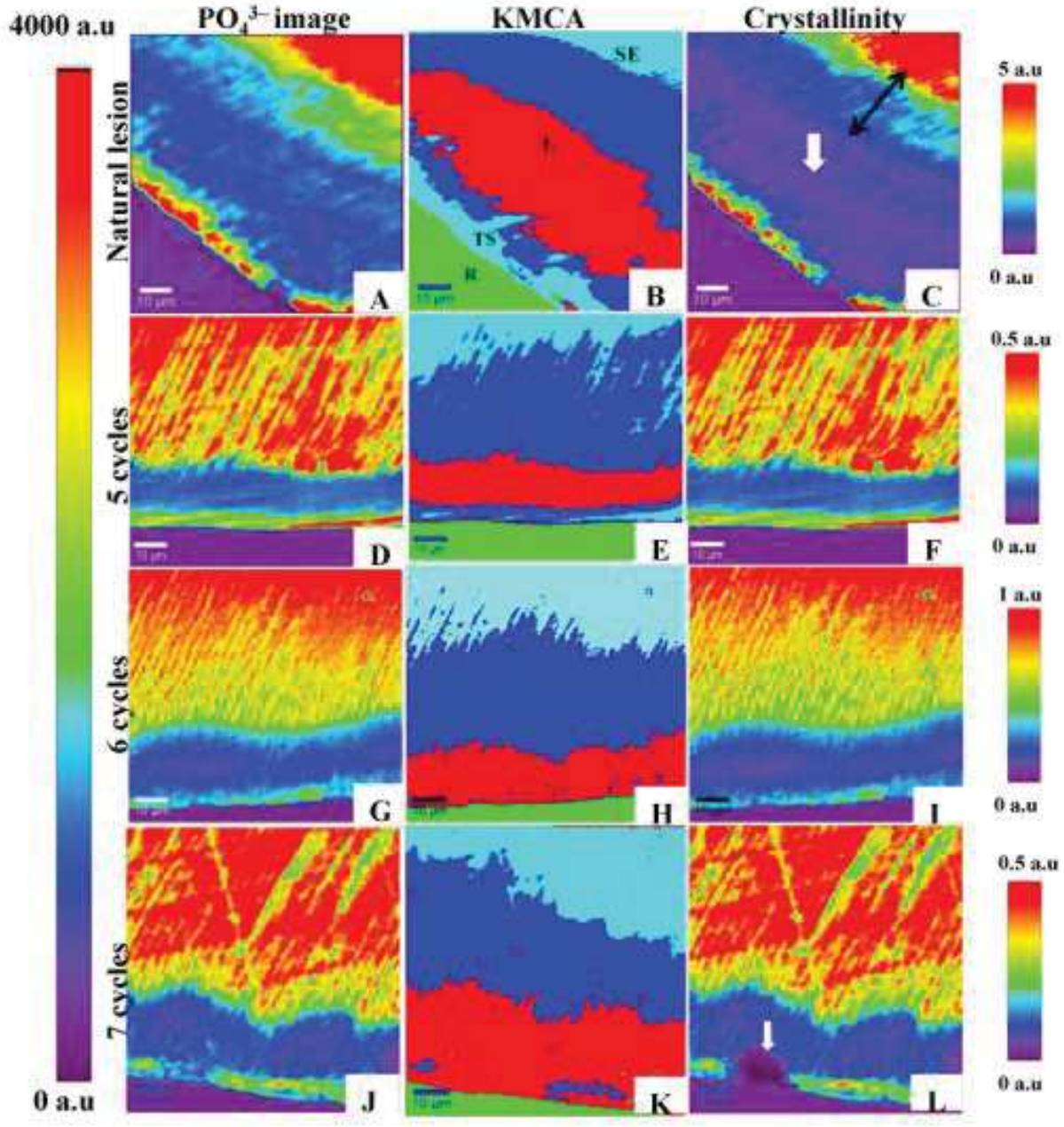

Figure 2. Natural lesion versus in-vitro lesions exposed to 5, 6 and 7 cycles. **(A, D, G & J)** images constructed from phosphate peak intensity at 960 cm^{-1}. Look-Up Table (LUT) on the left. **(B, E, H & K)** K-mean cluster analysis (KMCA) images, green zones are corresponding to embedding resin. **(C, F, I, & L)** images of crystallinity (phosphate peaks ratio at (960) over (950) cm^{-1}). Individual LUTs on the right. Purple zones are corresponding to embedding resin. Crystallinity images are almost following phosphate pattern in the 1st group of images, except for C and L images; where we can observe the presence of purple hues (white solid arrows) in lesion area which indicate total loss of crystallinity in lesion area. (Following symbols in image **B** are valid for all images: **SE**; sound enamel, **L**; lesion, **TS**; tooth surface, **R**; resin).

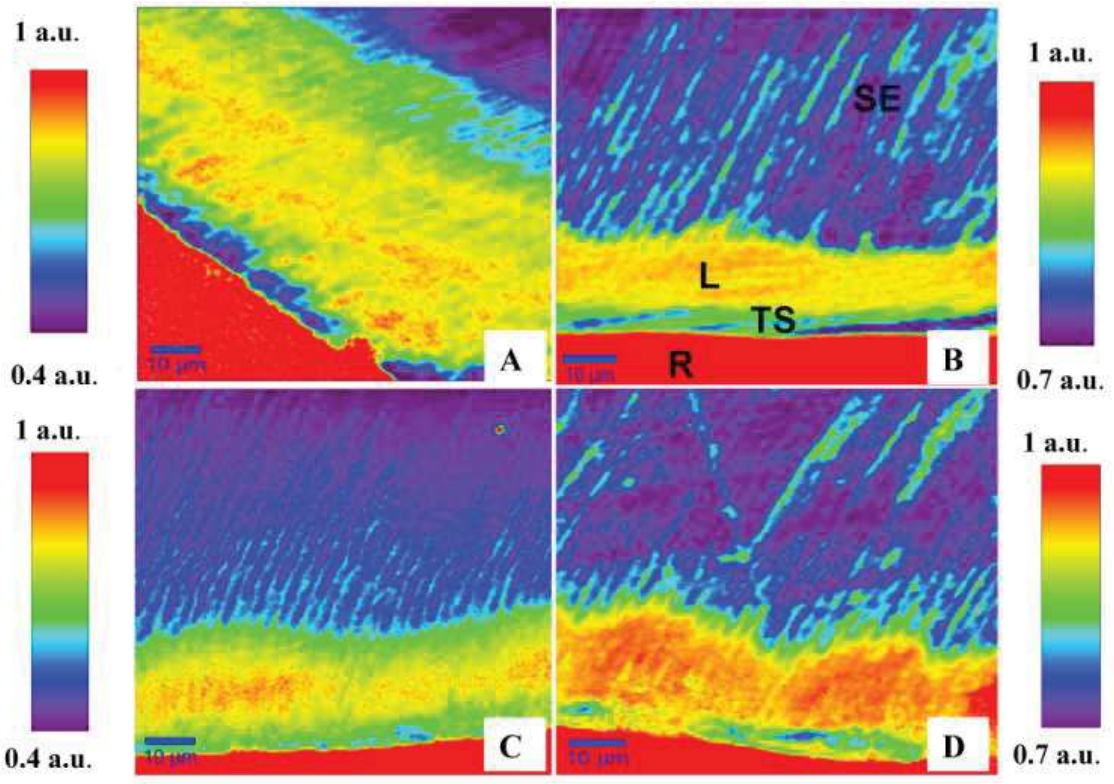

Figure 3. **(A)** Natural lesion versus in-vitro lesions **(B, C, D)** exposed to 5, 6 and 7 cycles respectively. Images constructed from CO_3^{2-}/PO_4^{3-} ratio at (1070 cm^{-1}) over (960 cm^{-1}). Individual LUTs on left & right where red hues indicate highest CO_3^{2-}/ PO_4^{3-} ratio and purple hues represent lowest values of the same ratio. (Following symbols in image B are valid for all images: **SE**; sound enamel, **L**; lesion, **TS**; tooth surface, **R**; resin).

Nanoindentation load-displacement curve is drawn from applied load versus depth profile (Fig. 4B). Curves were derived from different indentations made in three zones of enamel: unaffected enamel close to dentin, lesion area which is confined to enamel surface and intermediate zone which lies between the two areas to show differences in penetration depth of indenter tip.

H and E of enamel were determined in all zones of each group to measure intra-tooth variations. A reduction in two variables value was detected in lesion area in all examined groups (Fig. 4C, D). E rates display a positive relationship with those of H, except for the natural lesion (NL) where E value is smaller than expected. Difference was found to be significant ($p< 0.05$) by comparing E value of (NL) with those of other artificial lesions. While, the difference was found to be non-significant ($p> 0.05$) by comparing changes in rates of Pd and H of lesions (Table 1).

Tested area	Pd (µm) Mean ± SD	H (GPa) Mean ± SD	E (GPa) Mean ± SD
SE	**0.3 ± 0.01**	**4.5 ± 0.67**	**74.7 ± 3.3**
NWSL	**0.54 ± 0.09**	**1.26 ± 0.32**	**11.4 ± 5.2**
5 cycles lesion	**0.5 ± 0.08**	**1.58 ± 0.61**	**32.8 ± 9**
6 cycles lesion	**0.6 ± 0.24**	**1.1 ± 0.52**	**27.5 ± 8.2**
7 cycles lesion	**0.5 ± 0.2**	**2 ± 1.4**	**42.5 ± 18.4**

Table 1. Penetration depth (Pd), Hardness (H), elastic modulus (E) in lesion area of natural white spot lesion (N=2) & artificial lesions of 5, 6 & 7 cycles (N=5 in each group). Difference was found to be significant ($p < 0.05$ between E value of NL (natural lesion) & those of other artificial lesions, while non-significant differences ($p > 0.05$) were found between Pd and H values of all kinds of lesions.

3.4 DISCUSSION

Chemical composition and mechanical properties of WSLs and subsurface artificial lesions were described using Raman microscopy and nanoindentation techniques. Both techniques tested the same areas within each sample.

To our knowledge, confocal Raman microscopy has been used for the first time in this study to detect WSLs and experimentally induced subsurface lesions. It can provide a high resolution chemical and morphological map of an examined specimen, detecting even very small changes in its chemical composition. Data analysis of each acquired scan which is comprised of tenth thousands of single spectrums, is used to reconstruct different Raman detailed images. Transverse microradiography is a quantitative method depending on x-ray absorbance of an object and images reflect mineral concentration in mineralized tissue slices (de Jong and Ten Bosch 1985). Systematic and random errors represent the two sources of errors that could affect x-ray absorbance measurement. The crucial factor with regard to systematic errors is the beam inhomogeneity, while, film choice is the vital factor in respect to random errors (de Jong and Ten Bosch 1985). Moreover, artifacts result from inadequate section preparation as we mentioned before, may incorrectly be interpreted as additional demineralization in the lesion part of the specimen. Furthermore, TMR is usually applied, to determine overall changes in mineral content and not detailed structures of biological tissues (Damen et al. 1997). TMR resolution is dependent on X-ray detector resolution, i.e., silver grain diameter of radiographic film and on the microscope scanner used to read the film. High resolution microradiograph is with a pixel resolution of 2.15 μm (Can et al. 2008), comparing to a voxel size of ($300\,nm \times 300\,nm \times 1\,\mu m$) for confocal Raman microscopy. Hence, Raman microscopy could be considered as a

superior alternative for Raman spectroscopy and transverse microradiography (Desoutter et al. 2014).

The deepest subsurface lesion that we could produce *in vitro* is shallower than naturally developed one, in spite of lower concentrations of calcium, phosphate, and even lower pH values that have been used to induce a faster demineralization *in vitro.* Besides that, thickness of subsurface lesions reported by other studies (Mohanty et al. 2013; Moron et al. 2013) was greater than thickness of this study. However, there is less detailed information about these fabricated lesions, in particular, the evidences concerning the presence of ISL.

Enamel is composed of large number of hydroxyapatite crystals (HACs); represented by the chemical formula $Ca_{10}(PO4)_6(OH)_2$ with incorporation of many cations and anions in their lattice resulting in the formation of different kinds of apatite. The main substituent in biological apatite is carbonate ion (CO_3^{2-}) which substitutes the phosphate group (PO_4^{3-}) to form B-type CHA containing 4–6 wt % carbonate (Aoki 1991; Leventouri et al. 2001). Incorporation of carbonate into enamel increases its dissolution rate by interfering with crystal structure (Legeros et al. 1967). In particular, crystallinity, i.e., crystal size and perfection of apatite are of great importance, because small, more imperfect crystals due to presence of substituents, make them more susceptible to acid dissolution and caries progression (Pleshko et al. 1991). Therefore, reduced enamel crystallinity in lesion zone of our samples could be related to the increase in CO_3^{2-}/PO_4^{3-}ratio in the same zone (Pucéat et al. 2004; Simmer and Fincham 1995; Xu et al. 2012).

KMCA method assembles set of spectra of the same or close intensities in a well-recognized cluster (Salehi et al. 2013). High resolution images constructed by KMCA visibly reveal changes in enamel structure associated with number of cycles. As ISL becomes thinner, less mineralized

and more porous layer; thickness of demineralized area increases progressively with time, until the eighth cycle, where enamel surface dissolved. These results emphasize the fact that degree of enamel dissolution strengthens with repeated and prolonged variations in pH values.

Mechanical properties of enamel are inconstant and dependent on its chemical composition and structural organization. Enamel is anisotropic material where prisms are arranged in pattern perpendicular to their long axis, so that any variations in its prisms direction and composition may lead to differences in its mechanical properties (Radlanski et al. 2001).

Our results showed no significant difference between mechanical properties of intermediate zone and lesion area of NL (Fig. 4C, D) contrary to other artificial lesions. Simultaneously, we exclusively observed that crystallinity degree has obviously declined in intermediate zone of NL (Fig. 2C, double ended black arrow) which indicates an alteration in crystal size and shape and consequently reduced apatite perfection which constitutes the structural unit of enamel prisms. These modifications in enamel structure could help in explaining the reduced mechanical properties of intermediate zone of WSL.

Outer enamel layers are harder than inner layers which are close to DEJ, where enamel becomes less compact due to increase inter-prismatic voids and less mineralized due to decrease mineral density and increase organic matrix contents. This could explain the low H and E values for sound enamel in NWSL group (Fig. 4C, D), where indentations in this zone were made next to DEJ because of extensive depth of NWSL (> 60μm) (Cuy et al. 2002; He et al. 2010).

Table 1 demonstrates how the mechanical properties of enamel (hardness and elastic modulus) are inversely related to penetration depth of indenter owing to enamel hierarchical structure. Obtained average values of H ~ 4.5 GPa and E~ 74.7 GPa for sound enamel at 10 mN load are

consistent with values reported in previous study where E~ 80 GPa and H ~ 4 GPa (Chan et al. 2011).

Mechanical properties were considerably reduced in demineralized enamel compared to sound enamel as a result of inorganic substance loss (Table 1). Records obtained from the above two methods show similar changes across the lesion and represent a mechanism for linking mechanical properties of enamel to its composition which is in coincident with prior studies (Gallagher et al. 2010; Xu et al. 2012).

We can conclude that our protocol is reliable to reproduce subsurface lesions *in vitro* in a relatively short period as long as it is limited to seven cycles to ensure the presence of highly mineralized ISL which represents the characteristic feature of these lesions which complicates their clinical non-invasive treatment. These subsurface lesion models with methods of characterization, particularly confocal Raman microscopy, are typical to test the efficacy of new dental care products. Our work certifies that the two methods are highly sensitive to detect small changes in enamel composition. Further work is required to facilitate their use in the dental clinic to detect carious lesions at an early stage of development.

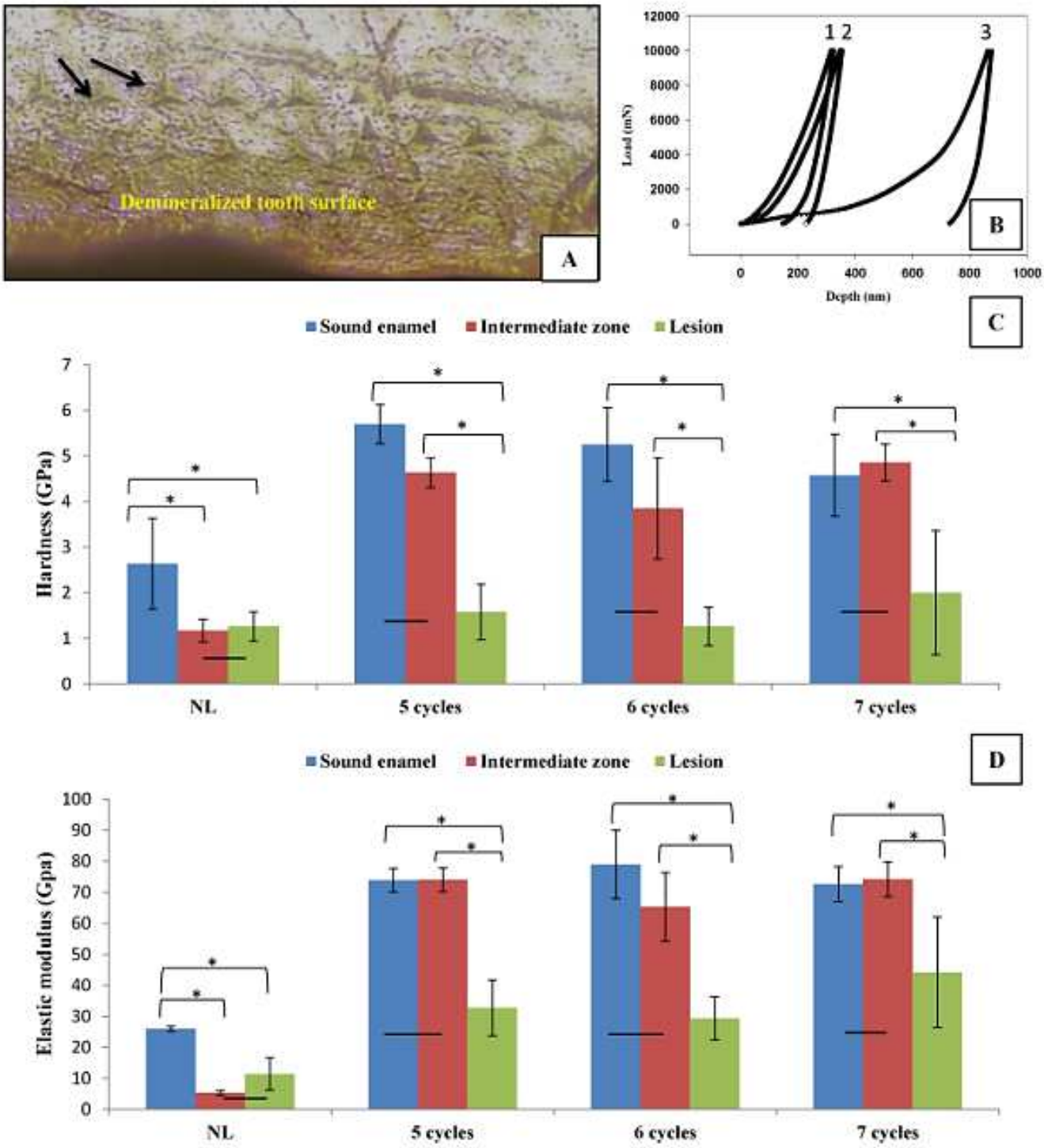

Figure 4. (A) Optical microscopic image of polished enamel surface with prints of Berkovich tip indenter in lesion zone. **(B)** A graph demonstrating the nanoindentation load-displacement curves in: **1**sound enamel, **2** intermediate zone & **3** lesion area. The difference in penetration depth (Pd) between the three zones is very obvious; indicating an inverse relationship between the reduction in hardness value and the increase in the depth of penetration. **(C & D)** bar graphs showing H and E mean values in all zones in: Natural lesion versus artificial lesions after 5, 6 and 7 cycles consecutively. Asterisk (*) shows a statistically significant difference ($p < 0.05$) between zones connected by bracket within each group. Horizontal bar indicates no significant difference ($p > 0.05$) among subgroups linked by it.

REFERENCES

Akkus A, Akkus A, Roperto R, Akkus O, Porto T, Teich S, Lang L. 2016. Evaluation of mineral content in healthy permanent human enamel by raman spectroscopy. Journal of clinical and experimental dentistry. 8(5):e546.

Alsayed EZ, Hariri I, Nakashima S, Shimada Y, Bakhsh TA, Tagami J, Sadr A. 2016. Effects of coating materials on nanoindentation hardness of enamel and adjacent areas. Dental Materials. 32(6):807-816.

Aoki H. 1991. Science and medical applications of hydroxyapatite. Ishiyaku Euroamerica.

Bergstrand F, Twetman S. 2011. A review on prevention and treatment of post-orthodontic white spot lesions–evidence-based methods and emerging technologies. The open dentistry journal. 5(1).

Chan YL, Ngan AH, King NM. 2011. Nano-scale structure and mechanical properties of the human dentine-enamel junction. Journal of the mechanical behavior of biomedical materials. 4(5):785-795.

Cuy JL, Mann AB, Livi KJ, Teaford MF, Weihs TP. 2002. Nanoindentation mapping of the mechanical properties of human molar tooth enamel. Archives of oral biology. 47(4):281-291.

Damen J, Exterkate R, Ten Cate J. 1997. Reproducibility of tmr for the determination of longitudinal mineral changes in dental hard tissues. Advances in dental research. 11(4):415-419.

De Jong EdJ, Ten Bosch J. 1985. Error analysis of the microradiographic determination of mineral content in mineralised tissue slices. Physics in medicine and biology. 30(10):1067.

Desoutter A, Salehi H, Slimani A, Marquet P, Jacquot B, Tassery H, Cuisinier FJG. 2014. Structure and chemical composition of the dentin-enamel junction analyzed by confocal raman microscopy. 8929:892907.

Derks A, Katsaros C, Frencken J, Van't Hof M, Kuijpers-Jagtman A. 2004. Caries-inhibiting effect of preventive measures during orthodontic treatment with fixed appliances. Caries research. 38(5):413-420.

Dickinson M, Wolf K, Mann A. 2007. Nanomechanical and chemical characterization of incipient in vitro carious lesions in human dental enamel. Archives of oral biology. 52(8):753-760.

Elfallah HM, Bertassoni LE, Charadram N, Rathsam C, Swain MV. 2015. Effect of tooth bleaching agents on protein content and mechanical properties of dental enamel. Acta biomaterialia. 20:120-128.

Featherstone J. 2004a. The continuum of dental caries—evidence for a dynamic disease process. Journal of dental research. 83(suppl 1):C39-C42.

Gallagher RR, Balooch M, Balooch G, Wilson RS, Marshall SJ, Marshall GW. 2010. Coupled nanomechanical and raman microspectroscopic investigation of human third molar dej. Journal of dental biomechanics. 2010.

Gorelick L, Geiger AM, Gwinnett AJ. 1982. Incidence of white spot formation after bonding and banding. American journal of orthodontics. 81(2):93-98.

Haines D. 1968. Physical properties of human tooth enamel and enamel sheath material under load. Journal of biomechanics. 1(2):117IN17119-17118IN22125.

He B, Huang S, Jing J, Hao Y. 2010. Measurement of hydroxyapatite density and knoop hardness in sound human enamel and a correlational analysis between them. Archives of oral biology. 55(2):134-141.

Hsu DJ, Darling CL, Lachica MM, Fried D. 2008. Nondestructive assessment of the inhibition of enamel demineralization by co2 laser treatment using polarization sensitive optical coherence tomography. Journal of biomedical optics. 13(5):054027-054027-054029.

Biostatgv. 2000. [accessed]. https://marne.u707.jussieu.fr/biostatgv.

Ismail A, Sohn W, Tellez M, Amaya A, Sen A, Hasson H, Pitts N. 2007. The international caries detection and assessment system (icdas): An integrated system for measuring dental caries. Community dentistry and oral epidemiology. 35(3):170-178.

Legeros RZ, Trautz OR, Legeros JP, Klein E, Shirra WP. 1967. Apatite crystallites: Effects of carbonate on morphology. Science. 155(3768):1409-1411.

Leventouri T, Chakoumakos B, Papanearchou N, Perdikatsis V. 2001. Comparison of crystal structure parameters of natural and synthetic apatites from neutron powder diffraction. Journal of materials research. 16(9):2600-2606.

Lo E, Zhi Q, Itthagarun A. 2010. Comparing two quantitative methods for studying remineralization of artificial caries. Journal of dentistry. 38(4):352-359.

Manesh SK, Darling CL, Fried D. 2009. Nondestructive assessment of dentin demineralization using polarization-sensitive optical coherence tomography after exposure to fluoride and laser irradiation. Journal of Biomedical Materials Research Part B: Applied Biomaterials. 90(2):802-812.

Mohanty B, Dadlani D, Mahoney D, Mann AB. 2013. Characterizing and identifying incipient carious lesions in dental enamel using micro-raman spectroscopy. Caries research. 47(1):27-33.

Moron BM, Comar LP, Wiegand A, Buchalla W, Yu H, Buzalaf MA, Magalhaes AC. 2013. Different protocols to produce artificial dentine carious lesions in vitro and in situ: Hardness and mineral content correlation. Caries research. 47(2):162-170.

Oliver WC, Pharr GM. 2004. Measurement of hardness and elastic modulus by instrumented indentation: Advances in understanding and refinements to methodology. Journal of materials research. 19(01):3-20.

Pleshko N, Boskey A, Mendelsohn R. 1991. Novel infrared spectroscopic method for the determination of crystallinity of hydroxyapatite minerals. Biophysical journal. 60(4):786-793.

Pucéat E, Reynard B, Lécuyer C. 2004. Can crystallinity be used to determine the degree of chemical alteration of biogenic apatites? Chemical Geology. 205(1):83-97.

Radlanski RJ, Renz H, Willersinn U, Cordis CA, Duschner H. 2001. Outline and arrangement of enamel rods in human deciduous and permanent enamel. 3d-reconstructions obtained from clsm and sem images based on serial ground sections. European journal of oral sciences. 109(6):409-414.

Rechmann P, Fried D, Desoutter A, Salehi H, Slimani A, Marquet P, Jacquot B, Tassery H, Cuisinier FJG. 2014. Structure and chemical composition of the dentin-enamel junction analyzed by confocal raman microscopy. 8929:892907.

Salehi H, Derely L, Vegh AG, Durand JC, Gergely C, Larroque C, Fauroux MA, Cuisinier FJG. 2013. Label-free detection of anticancer drug paclitaxel in living cells by confocal raman microscopy. Applied Physics Letters. 102(11):113701.

Simmer J, Fincham A. 1995. Molecular mechanisms of dental enamel formation. Critical Reviews in Oral Biology & Medicine. 6(2):84-108.

Slimani A, Nouioua F, Desoutter A, Levallois B, Cuisinier FJG, Tassery H, Terrer E, Salehi H. 2017. Confocal raman mapping of collagen cross-link and crystallinity of human dentin-enamel junction. J Biomed Opt. 22(8):1-8.

Summitt JB, Robbins JW, Hilton TJ, Schwartz RS. 2006. Fundamentals of operative dentistry: A contemporary approach. Quintessence Pub.

Ten BJ. 1991. A review of quantitative method for studies of mineral content of intra-oral incipient caries lesion. J Dent Res. 70:2-14.

Ten Cate J, Mundorff-Shrestha S. 1995. Working group report 1: Laboratory models for caries (in vitro and animal models). Advances in dental research. 9(3):332-334.

Wang X-J, Milner TE, de Boer JF, Zhang Y, Pashley DH, Nelson JS. 1999. Characterization of dentin and enamel by use of optical coherence tomography. Applied Optics. 38(10):2092.

Xu C, Reed R, Gorski JP, Wang Y, Walker MP. 2012. The distribution of carbonate in enamel and its correlation with structure and mechanical properties. Journal of materials science. 47(23):8035-8043.

Xu C, Yao X, Walker MP, Wang Y. 2009. Chemical/molecular structure of the dentin–enamel junction is dependent on the intratooth location. Calcified tissue international. 84(3):221.

Chapter 4

Third Article

Liaison between changes in chemical composition of enamel subsurface lesions and the emitted nonlinear optical signals.

ABSTRACT

Enamel can be regarded as a functionally graded natural biocomposite, which will require special attention using high-resolution characterization methods to fully appreciate the significance of such a structure. Measurements on 14 human teeth were made using two incident lights of different wavelengths; released by confocal Raman microscopy and multi-photon microscopy (MPM). Phosphate peak intensity at 960 cm^{-1} together with organic to mineral ratio at (2931/430 cm^{-1}) and nonlinear optical signals (SHG second harmonic generation and 2PEF two-photon excitation fluorescence) spectra; were recorded from the damaged and healthy enamel sites. Raman spectral maps showed that the higher the organic/mineral ratio in the demineralized enamel, the lower is the intensity of mineral component in the same zone. Moreover, MPM outcomes demonstrated an evident red shift of the fluorescence spectrum from carious enamel compared to that from sound enamel, in addition to the emergence of SHG peak from lesion zone of two specimens. These findings present another indication of carious lesion formation. By comparing 2PEF images with the structural motifs observed by confocal Raman imaging system; the morphological similarity of the acquired images is quite evident. The main conclusion is that 2PEF intensity increases with caries progression, thereby; any change in 2PEF intensity reflects changes in chemical composition of enamel. These findings may provide an important basis for potentially valuable applications in the clinical diagnosis of tooth pathological conditions. In addition, the outcomes expose the fundamental role of organic matrix in enamel integrity and reparation.

Keywords: non-invasive optical techniques, organic matrix, mineral components, auto-fluorescence (AF).

4.1 INTRODUCTION

Hydroxyapatite crystals (HACs) constitute about 96% of minerals in enamel (Brès et al. 1990). While the proteins and lipids comprise around 3% of organic material in enamel that surrounds the mineral crystals. However, the organic matrix plays a paramount role in enamel integrity (Curzon MEJ 1983; Eastoe 1960; Odutuga and Prout 1974).

Dental caries formation and progression happen due to an imbalance between de/remineralization periods in enamel. When demineralization proceeds; white spot lesion (WSL) develops, signaling changes in enamel chemical composition (Cury and Tenuta 2009). Improving the diagnostic ability of initial caries lesions; will improve the potential of treatment without surgical intervention. Therefore, the development of new diagnostic technologies with high sensitivity and high specificity became compulsory. Based on the light scattering and autofluorescence (AF) properties, spectroscopic and microscopic methods can have the potential to detect dental caries rather early (De Jong et al. 1995). Thus, the development of an effective, minimally invasive imaging modality is vital for investigating a variety of physiological phenomena and pathological conditions in dentistry.

Raman effect is resulted from the energy difference between the incoming excitation light and the scattered photons which is proportional to the vibrational energy of the molecules within the sample under study (Huminicki et al. 2010). Confocal Raman microscopy is a powerful technique that measures the inelastic scattering of incident light which is used to analyze the internal structure of mineralized tissues. The spatial resolution of Raman microscopy (300 nm) makes it a sensitive diagnostic tool appropriate for early caries detection (Slimani et al. 2017).

Fluorescence is a phenomenon by which an object is excited by a light of particular wavelength and then emits light at higher wavelength (De Jong et al. 1995). The molecules that can absorb photons and emit the energy as a photon with a red shifted wavelength known as fluoro or chromophores (Gibson et al. 2011) which are responsible for fluorescence in enamel (Stookey 2005). In dental research, Benedict (Benedict 1928) was one of the pioneers who described enamel fluorescence and thereafter proposed it as a method to detect dental caries (Benedict 1929). The source of two-photon excitation fluorescence (2PEF) in dental tissues may vary with diverse excitation mechanisms involved and concerning both organic and inorganic components (Bachmann et al. 2006; Björkman et al. 1991). Enamel rod or prism is the basic unit of enamel structure filled with inorganic HA crystals, bounded by a sheath rich in organic components, giving rise to the 2PEF. Whereas the inorganic crystalline regions inside the prisms reveal low or no fluorescence due to low organic content (Cloitre et al. 2013). Whereas dentin is a relatively elastic structure composed of collagen fibers (Bachmann et al. 2006) which generates strong SHG and 2PEF signals (Zipfel et al. 2003a; Zoumi et al. 2002b). Multi-photon microscopy (MPM) has become a preferred imaging modality in biological research (Denk et al. 1990; Zipfel et al. 2003b), providing a powerful means of visualizing dental tissues, in both healthy and carious conditions (Hall and Girkin 2004; Lin et al. 2011). MPM is a nonlinear imaging approach where fluorophores are excited by simultaneous absorption of two (or more) low-energy photons. 2PEF refers to the light emitted when a fluorophore absorbs two photons of equal wavelength arrive within a period of an attosecond (1×10^{-18} of second) and collaborate to excite the molecule (Oheim et al. 2006). Concurrently, these photons can also induce second harmonic generation (SHG) which is a coherent, nonlinear process that generates particularly strong signals when the molecules are well-ordered in non-centrosymmetric biological structures

(Zoumi et al. 2002a). The major advantage of MPM lies in its capability to create images simultaneously based on the fluorescence signals produced by the process of multiphoton excitation (2PEF) and second harmonic generation (SHG) (Zipfel et al. 2003a). Collecting 2PEF signals is considered to be a promising technique for tissue auto-fluorescence imaging that allows deeper sample penetration and reduced photodamage thanks to laser excitation feature that produces signal only at the focal point (Helmchen and Denk 2005; So et al. 2000).

The present research aims to correlate fluorescence-based results provided by multi-photon microscopy (MPM) with confocal Raman microscopy records regarding the phosphate level at 960 cm^{-1} and the organic matrix at ~2931 cm^{-1} in healthy and demineralized enamel of extracted human teeth.

4.2 MATERIALS & METHODS

14 sound premolars were extracted from patients aged between 13 to 14 years for orthodontic reasons. All teeth were collected with informed consent from all subjects and after approval of the local ethical research committee (process No. 2017-2907) before being used in this research. All procedures were carried out in accordance with relevant guidelines and regulations. The number of teeth required in this study was calculated by using BiostaTGV site (iPLESP 2000).

Teeth were washed with de-ionized water to remove any debris, stored in de-ionized water with 0.1% antimicrobial thymol and kept at 4°C until use. All teeth were exposed to pH cycling chemical model (Al-Obaidi et al. 2018) to create uniform, reproducible subsurface enamel lesions *in vitro*. Teeth were then sectioned longitudinally into two halves by using high speed diamond saw (Isomet 2000, Buehler, USA) to produce cross sections of teeth which then embedded in self-curing acrylic resin (GC, Japan), having the cross sectioned surface of the

samples facing the surface that is to be polished later. For further details see (Al-Obaidi et al. 2018).

4.2.1 Raman microscopy:

Witec Confocal Raman Microscope System alpha 300R (Witec, Ulm, Germany) was used to register Raman spectra. Excitation in the confocal Raman microscopy was assured by a frequency doubled Nd: YAG laser (Newport, Evry, France) that illuminated the inspected sample with a visible light of wavelength 532 nm. Raman spectra were attained using a ×20 objective with numerical aperture of 0.46 (Nikon, Tokyo, Japan) focused on the specimens. Then Raman backscattered radiation mixed with Rayleigh scattered light were passed through an edge filter to block the Rayleigh scattering. Exposure time of a single spectrum was set to 0.05 s. Each spectrum corresponding to a spatial unit is defined as a voxel ($300\,nm \times 300\,nm \times 1\,\mu m$). All data acquisition and processing were performed using Image Plus software from Witec inc (Salehi et al. 2013).

Raman linear mapping of dental enamel was attained from enamel cross section, starting at the outer enamel surface and ending in the inner enamel ahead of the dentin enamel junction (DEJ). Raman peak at 960 cm $^{-1}$ is assigned to ν_1 vibration mode of the phosphate group in enamel which was selected as the inner standard to observe changes in sum-intensity of the strongest PO_4^{3-} peak. The 2931cm^{-1} Raman band attributed to the C–H stretching/deformation of organic matrix in enamel, was related to the phosphate peak at (ν_2) 430 cm^{-1}. The later peak was chosen as the internal standard for the normalization adjustment and calculation of organic to mineral components ratio in the sound and carious enamel in order to evaluate the variances in the chemical composition of enamel (Reed et al. 2015a). Red and violet hues of an indicative look-

up table (LUT); designate the maximum and minimum phosphate intensities and organic/mineral ratio in a chosen area respectively (Salehi et al. 2013).

4.2.2 Multiphoton Microscopy (MPM)

For further investigations, each cross section was scanned by MPM to support the results provided by Raman microscopy. 2PEF images were registered with a custom-built multiphoton microscope based on a SliceScope upright microscope (MPSS-1000P) equipped with a Multiphoton Scan Head (MP-2000), both from Scientifica LTD. For sample excitation, we used a Spectra-Physics Tsunami Ti-Sapphire laser operated in pulsed mode, wavelength range, 760 to 900nm, typically 870 nm, repetition rate 80 MHz; pulse duration ~100 fs. The laser beam was focused on the sample by a Nikon CFI75 LWD-16x-W objective (NA 0.8, water immersion).

Images were created by laser raster scanning the sample. The fuorescence signal was epi-collected through the objective; separated from the backscattered laser light and SHG signal by the combination of a 735nm long pass dichroic mirror (87-065 Edmund Optics), a 750 nm short pass filter (FESH0750, Thor Labs), and a 475-nm long-pass filter (84-705, Edmund Optics); and then detected with a photomultiplier tube (R928P; Hamamatsu). The SHG signal was collected through a 1.4-NA oil-immersion condenser (U-AAC, Olympus), filtered by using a 482 nm long pass dichroic mirror (86-331, Edmund Optics) and a 447 nm high-performance band-pass filter (48-074, Edmund Optics) and then detected by a H7422P photomultiplier (Hamamatsu). The method enables acquisition of in-depth Z-stacks of 2-dimensional images of the sample based on their nonlinear optical response (SHG and 2PEF emission) when excited in the infrared domain. Recorded images were treated by Image J software (http://rsb.info.nih.gov/ij/; National Institutes of Health, Bethesda, MD, USA) through the use of green lookup table.

4.2.3 Nonlinear Optical Spectroscopy

2PEF and SHG spectra were obtained using a fiber coupled imaging spectrometer and a back-illuminated CCD (Acton SP215i and PIXIS 400B Excelon, Princeton Instruments). 2PEF signal was epi-collected and coupled via the optical fiber using achromatic lenses. The backscattered laser light was filtered out with the same 735nm long pass dichroic /750-nm short-pass filter combination.

4.2.4 Statistical analyses:

Phosphate intensity at 960 cm^{-1} together with ratio of intensities of two Raman peaks (2931 to 430 cm^{-1}) and nonlinear optical (SHG and 2PEF) spectra were gathered from the damaged and healthy enamel sites. Data were plotted and the mean and the standard deviation were calculated. Statistical analyses were performed using Kruskal-Wallis One Way ANOVA Analysis of Variance on Ranks for data that were not normally distributed. All statistical tests were made at over all significant level of $\alpha = 0.05$ with SigmaPlot version 11.0 (Systat Software, Inc., USA). Representative Raman spectra along with nonlinear optical spectra were enhanced (after baseline correction) by using (SpectraGryph- optical spectroscopy software, Version 1.2.7, 2017).

4.3 RESULTS

Phosphate map was mounted from phosphate peak intensity at 960 cm^{-1} is presented in (Fig. 1A). According to the adjacent (LUT); highest PO_4^{3-} peak intensity is demonstrated by sound unaffected enamel (region 1) which looks red in color. Whereas, an important decrease in PO_4^{3-} intensity is revealed by the subsurface lesion (region 2). The demineralized area is delineated by double ended black arrow in (Fig. 1A). Fig.1B shows a false image constructed from organic/mineral ratio at (2931/430 cm^{-1}) with a noticeable difference perceived between region 1 & 2. In accordance with the corresponding LUT; the red shade in region 2 confirms a marked increase in the amount of enamel organic matrix compared to the degraded blue shade observed in region 1. Representative Raman spectra from both regions are presented in (Fig. 1C). The two spectra vary significantly in respect to PO_4^{3-} peak intensity at two internal vibrational modes v_1 & v_2 consecutively. Moreover, the original peak at 2931cm^{-1} related to the C–H bond has shown up solely after collecting spectra from different demineralized enamel zones.

2PEF images with their corresponding nonlinear optical spectra generated by sound enamel (1) and subsurface lesion (2) regions are shown in (Fig.2 A, B, C). The green pseudo-color was used to designate auto-fluorescence of enamel. The characteristic enamel rods structure is clearly observed in the high-resolution 2PEF images in (Fig.2 A, B). The intensity contrast among regions 1 and 2 reveals the importance of organic matrix in enamel. In region 1, enamel prism sheaths (white arrows) revealed high fluorescence, whereas no fluorescence was detected from the prisms themselves. These observations were entirely overturned in region 2.

Dental enamel emitted broad 2PEF spectra from 400 to 700 nm. Maximum 2PEF intensity was localized at 520 nm. Site-specific spectral profiles from sound enamel and lesion area vary

slightly in terms of intensity as well as in the relatively strong shift of the carious enamel spectrum to the red (at about 650-750 nm) compared to the intact enamel spectrum (Fig.2 C).

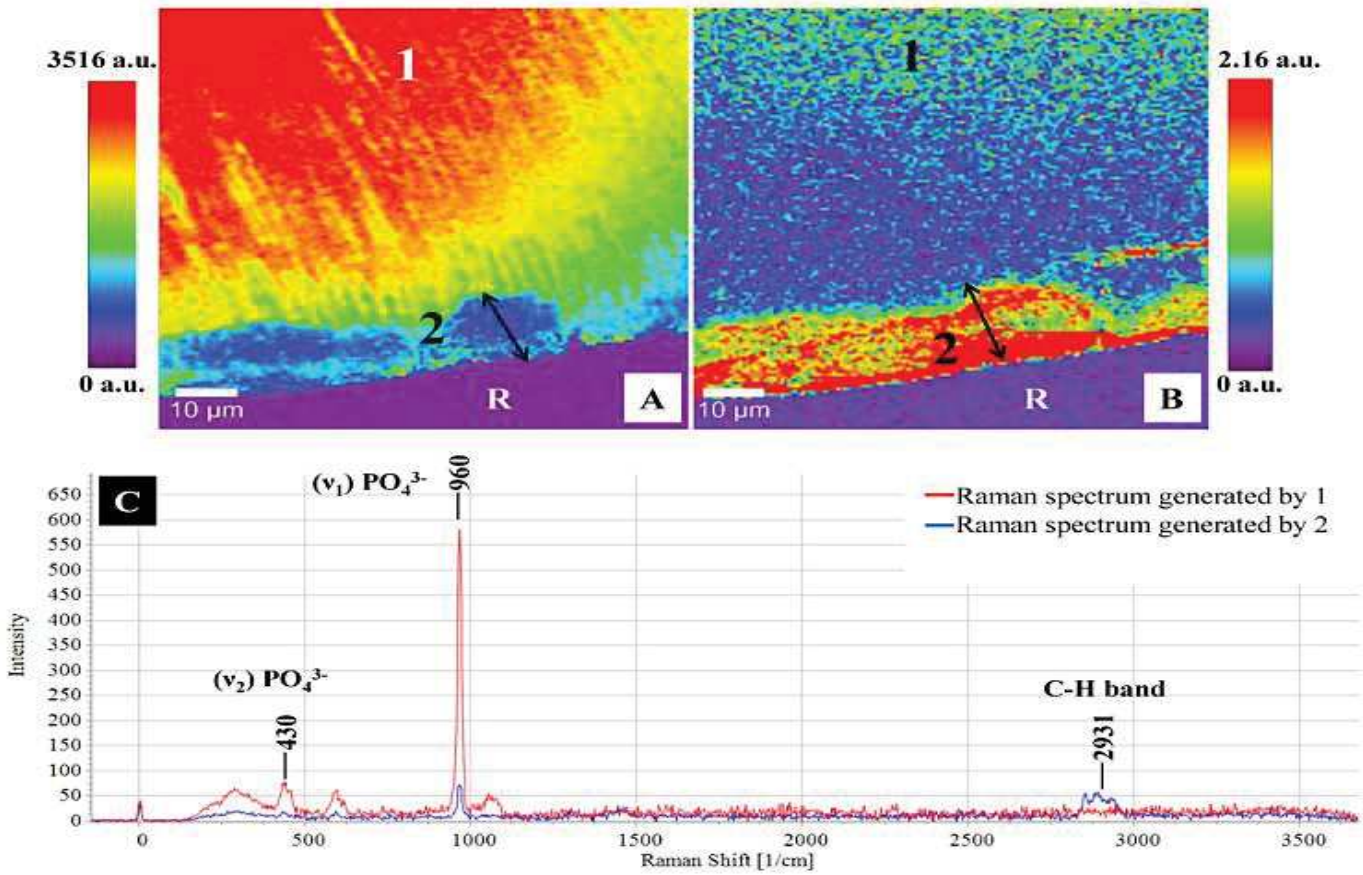

Figure 1. (**A**) Raman phosphate map built from phosphate peak intensity at 960 cm^{-1}. (**B**) Image constructed from organic to mineral ratio at (2931/430 cm^{-1}). Individual Look Up Tables (LUT) on both sides. Region 1: Sound enamel, Region 2: Lesion area, R: Resin. (**C**) Corresponding Raman spectra generated by region 1, 2 respectively.

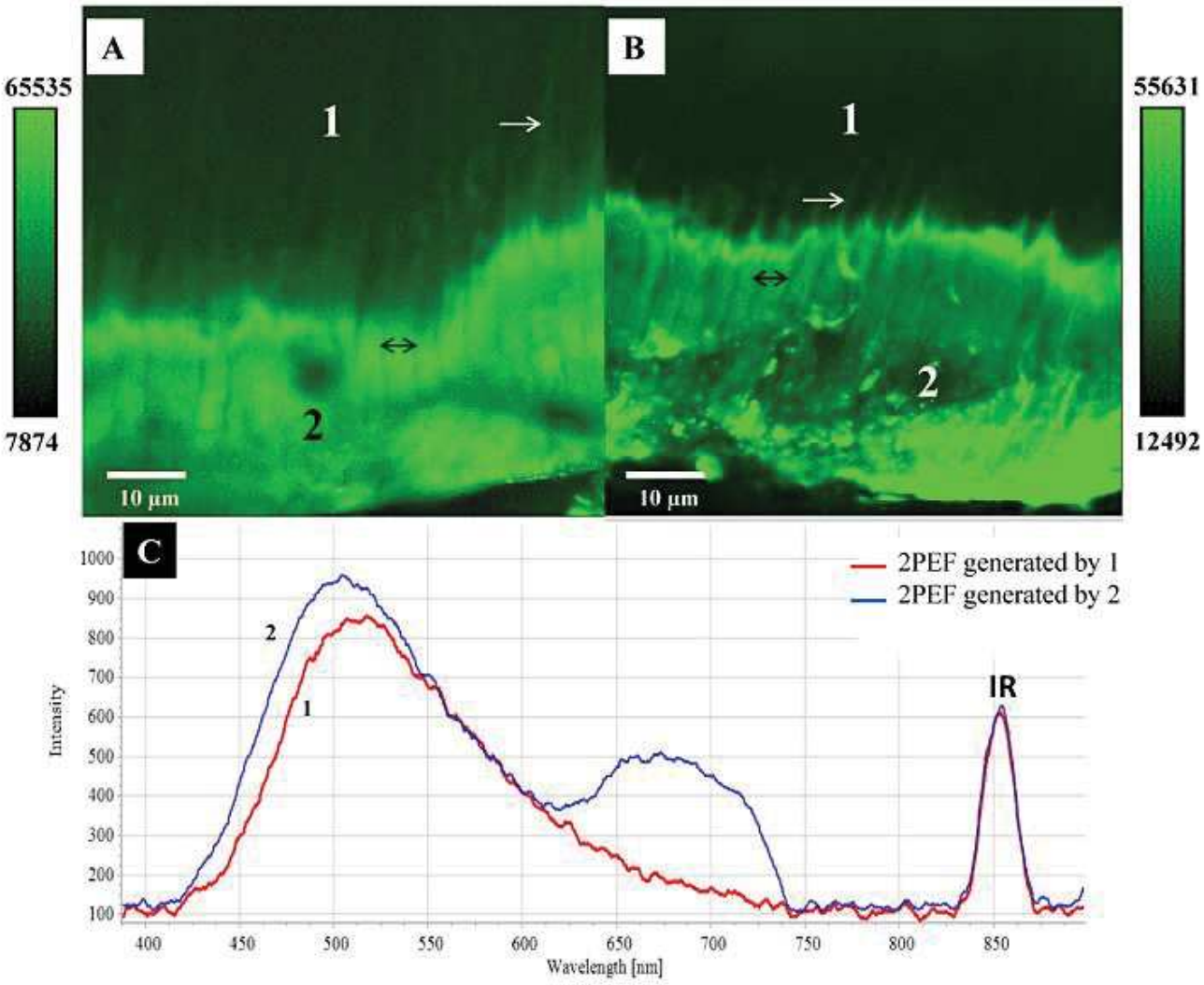

Figure 2. (**A & B**) 2PEF signal images; where region 1 belongs to sound enamel while region 2 belongs to lesion area. Subjective calibration bars on both sides. White arrows refer to enamel prism sheathes. Double ended black arrows delineate enamel rods. (**C**) Corresponding nonlinear optical spectra generated by region 1(red line-sound enamel), 2 (blue line-lesion area) respectively. IR: Infrared excitation laser.

Moreover, SHG peak at ~435 nm was exceptionally collected from lesion zone of two specimens as depicted in (Fig.3).

Fig.4B describes the alteration in organic/mineral ratio at (2931/430 cm^{-1}) in the selected regions. The ratio of the two intensities was calculated by incorporating the area under the peaks to analyze the variation in organic matrix composition of affected and unaffected enamel. This difference was found to be statistically significant. Recorded spectra were employed in terms of intensity as illustrated in (Fig.4 A, C, D). The graphs combine the obtained PO_4^{3-} intensity at 960 cm^{-1} and 2PEF signal intensity at 520 & 675 nm; produced by region 1 & 2 respectively. A significant difference has noticed regarding the PO_4^{3-} intensity at 960 cm^{-1} released by the two regions (Fig.4A). Slight increases in the intensity of 2PEF signal at 520 nm generated by region 2 was detected as compared to region 1. Though, the statistical difference was not significant (Fig.4C). However, the red shift of the fluorescence at 675 nm differs significantly in terms of intensity after comparing the two spectra emanated by the two regions (Fig.4D).

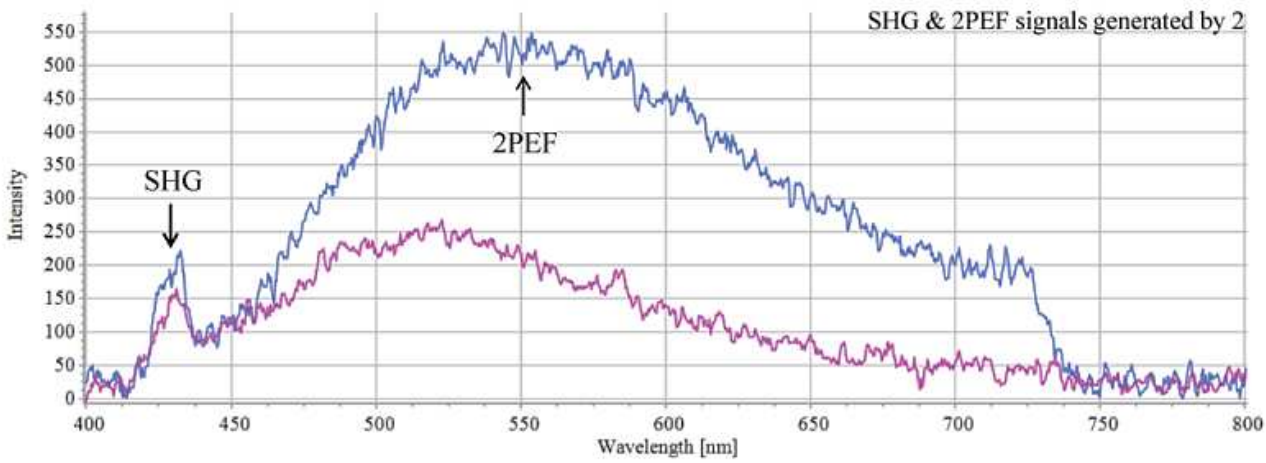

Figure 3. Nonlinear optical spectra generated by lesion zone (region 2). SHG peak at ~435 nm is evident, arising from broken 6/m point group symmetry due to the external strains in subsurface lesion area.

4.4 DISCUSSION

Confocal Raman microscopy and multiphoton microscopy are non-invasive optical techniques which are potentially useful in detecting tiny changes in the chemical composition of enamel in vitro. To date there are no studies outside our research group that investigate and demonstrate the combined performance of these methods in caries detection.

The Raman spectrum acquired from a dental section shows eminent vibrational bands related to the tooth structure. Among the main distinguished Raman bands of tissues is the one at 960 cm^{1} which is assigned to ν_1 (PO_4^{3-}) symmetric stretching mode. Since the phosphate peak intensity is linearly proportional to its amount within the inorganic crystals; perceptible alterations in its intensity can refer to the changes in the degree of enamel mineralization (Al-Obaidi et al. 2018;

Gilchrist et al. 2007; Hannig et al. 2005). In this study; phosphate peak exhibits greater intensity in sound enamel, confirming its higher mineral content compared to the lesion zone as demonstrated by (Fig.1A, C) and (Fig. 4A).

The CH group was previously employed to investigate the effect of laser and radiotherapy treatment on chemical composition of dental hard tissues (Liu and Hsu 2007; Reed et al. 2015b). As far as we know, this is the first work that shows how to exploit the CH stretch band to evaluate the consequence of enamel subsurface lesion development with respect to its organic matrix. Likewise, the presented work tries to correlate the changes affecting the enamel organic and inorganic components stimulated by caries progression through the use of characteristic vibrational bands.

Raman band at 2931 cm^{-1} observed just after acquiring a set of spectra from different lesions (Fig. 1C); is related to the bending and stretching modes of CH group of lipids and proteins (Lopes et al. 2007; Pinheiro et al. 2010). Accordingly, the observed alterations in mineral component of enamel at 960 cm^{-1} were accompanied by changes in the amount of organic matrix represented by the ratio of organic component at 2931 cm^{-1} to mineral at 430 cm^{-1}. Based on the Raman spectral maps; the higher the organic/mineral ratio in the outer part of enamel (looks alike red zone in Fig.1B); the lower is the intensity of mineral content in the same zone (blue area in Fig.1A). Earlier studies (He and Swain 2009; Wentrup-Byrne et al. 1997) invested the CH stretch band to inspect the distribution of organic components in an intact cross section of a human tooth. They localized a remarkable gradual compositional change through the enamel film, represented by increased organic contents of inner enamel nearby DEJ compared to the outer counterpart. Contrary to our findings where the organic/mineral ratio in the outer demineralized enamel was found to be significantly higher than that in the inner intact enamel

layer (Fig. 4B). This distinguished deleterious effect induced by caries formation, could help in identifying caries lesion early enough.

In this work, the fluorescence of demineralized tooth surface was correlated to the variation in its chemical composition which has been detected through the use of Raman microscopy. By comparing 2PEF images with the structural motifs observed by confocal Raman imaging system; the morphological similarity of the acquired images is quite evident.

2PEF images (Fig.2A, B) were made in the region of sound and diseased enamel. In region 1, the main 2PEF contrast comes from the prism sheaths rich in organic matrix rather than from inside-prism spaces evenly filled with inorganic HA crystals. Whereas 2PEF emanates from inside the prisms in region 2; where destructive caries lesion has induced changes in the chemical structure of enamel as well as intense crystals abnormality (Amjad et al. 1981; Huang et al. 2007). In consonance with the attached calibration bars that set the upper and lower limits with respect to fluorescence intensity; carious areas depicted by the 2PEF images comprise some semi-filled (deep green) and completely filled (bright green) prisms that could be related to the level of demineralization and subsequent optical inhomogeneity. These results are in accordance with earlier results communicated by Chen (Chen et al. 2008).

The 2PEF of enamel is an inherent fluorescence issued by intrinsic fluorophores (Stookey 2005) that could arise from decomposition of organic components from larger, longer-chained molecules into smaller, shorter chained molecules. Hence, the emergence of CH band at 2931 cm^{-1} in carious enamel spectrum (Fig.1C) as well as the increased organic/mineral ratio in the carious enamel part (Fig.4B); can stand behind the fluorescence of diseased enamel.

The evident red shift of the fluorescence spectrum from carious enamel, compared to that from sound enamel in (Fig.2 C); is another indication of carious lesion formation (Slimani et al. 2018; Sundström et al. 1985). Since there was an evident shift of the fluorescence (released by diseased enamel) to longer wavelengths, there was also a pronounced difference in the intensity of the fluorescence at 675nm (Fig. 4D). The red shift is probably large enough to allow the construction of a relatively simple opto-electrical system for its detection. As expected from earlier research with other types of UV-sources (Bjelkhagen 1982; Booij and Ten Bosch 1982); it is likewise possible that the incident light in the red or near infrared region becomes applicable for the detection of carious lesions due to the even red shift of the fluorescence from the regions with enamel caries, compared to that from non-carious enamel (Booij and Ten Bosch 1982). The outcomes of this research are consistent with results reported in previous studies (Mendes et al. 2004; Yokoyama et al. 2008) where they concluded that fluorescence intensity increases with caries progression. Another study showed that undamaged tooth structure exhibits little or no fluorescence while damaged tissue exhibits fluorescence proportional to the degree of caries severity (Lussi et al. 2004). However, our results are discordant with other studies (Alfano and Yao 1981; Ando et al. 2001), where teeth were illuminated with a blue light of wavelength 488nm. In these researches; damaged enamel generally exhibited less fluorescence and appeared darker than the healthy tissues. The nature or type of fluorescence is dependent on the wavelength of the incident light. Unlike shorter wavelengths; the infrared light is less susceptible to scattering and absorption by enamel than visible light (Denk et al. 1990; Lin et al. 2005). Therefore, changes in light absorption and scattering mode, could explain the discrepancy of the obtained results (Pretty and Ellwood 2013; Ten Bosch 1996).

Hydroxyapatite crystals in enamel belong to the 6/m point group symmetry. Thus, no SHG is anticipated to arise from ideal HA crystals (Boyd 1992; Jiang and Cao 2004; Lyubchanskii et al. 2000). However, the SHG can arise from the external strains around the cracks and from WSL areas that induce breakage of the 6/m point group symmetry (Chen et al. 2008; Ichim et al. 2007; Popowics et al. 2004). These studies are in agreement with our records demonstrated in (Fig.3).

4.5 IN CONCLUSION: The obtained results demonstrate a great potential for both techniques in imaging and elucidating the structure/feature relationship in dental tissues. Changes in 2PEF reflect changes in chemical composition of enamel; thereby simplifies quantification of subsurface lesions. Moreover, since non-invasive management of enamel subsurface lesions represents an essential goal of modern dentistry, the obtained results reveal the fundamental role of organic matrix that must be taking into account while developing remineralizing dental products based on calcium phosphate salts. With the limitations of this study, further laboratory studies together with clinical research are consequently required to increase the knowledge on this subject.

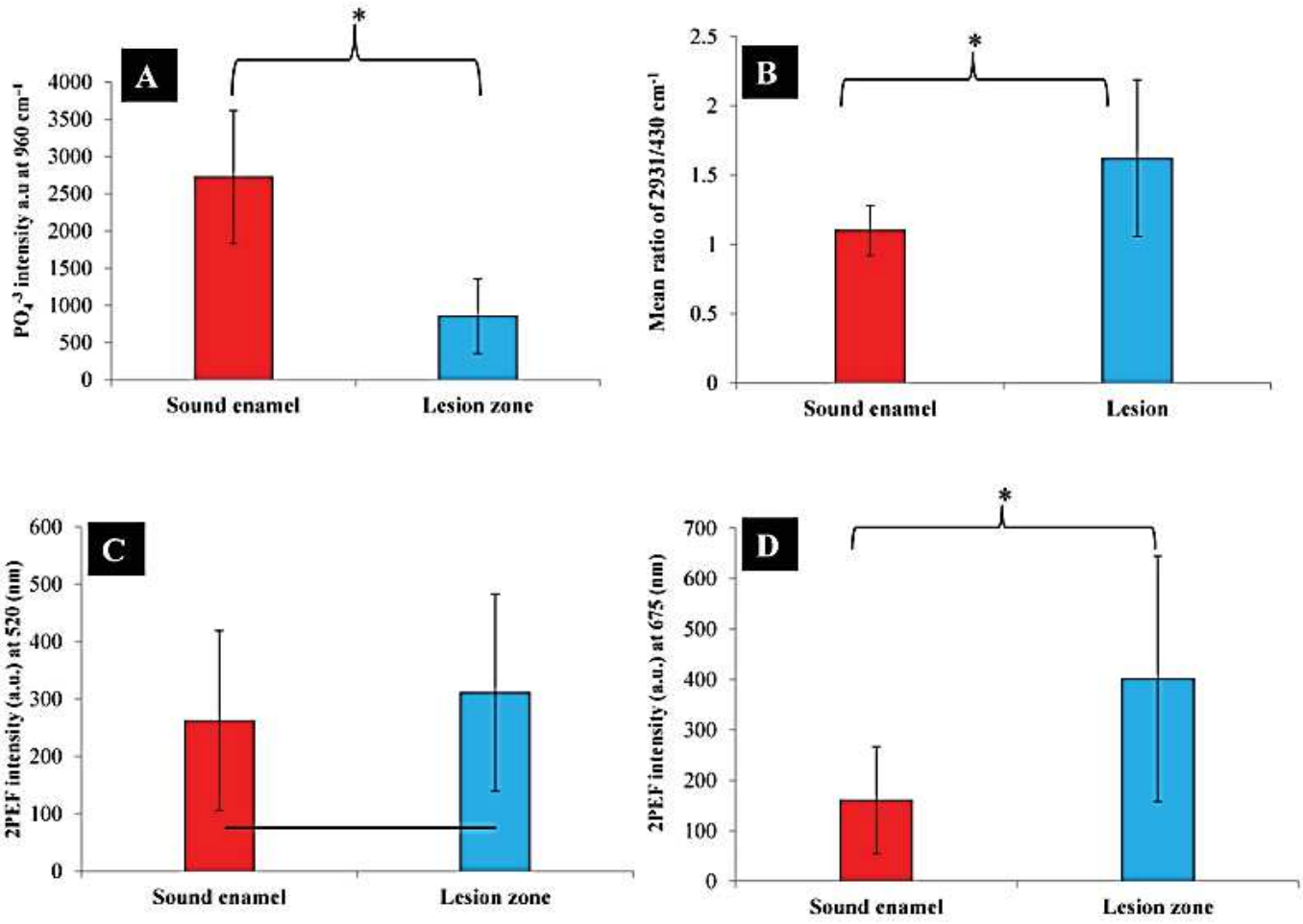

Figure 4. Raman spectra applied with reference to the peak intensity to show: (**A**) Variation in PO_4^{3-} intensity at 960 cm^{-1} & (**B**) Alteration in the ratio of two intensities at (2931/430 cm^{-1}) between sound and carious enamel. Nonlinear optical spectra measured by MPM, were employed in respect to 2PEF intensity at: (**C**) 520 nm and (**D**) at 675 nm to demonstrate the difference between healthy and carious enamel in terms of intrinsic fluorescence. Asterisk (*) recurrently indicates a significant difference ($p < 0.05$) between the two zones. Horizontal bar indicates no significant difference ($p > 0.05$) among the groups linked by it.

REFERENCES

Akkus A, Akkus A, Roperto R, Akkus O, Porto T, Teich S, Lang L. 2016. Evaluation of mineral content in healthy permanent human enamel by raman spectroscopy. Journal of clinical and experimental dentistry. 8(5):e546.

Al-Obaidi R, Salehi H, Desoutter A, Bonnet L, Etienne P, Terrer E, Jacquot B, Levallois B, Tassery H, Cuisinier F. 2018. Chemical & nano-mechanical study of artificial human enamel subsurface lesions. Scientific reports. 8(1):4047.

Alfano R, Yao S. 1981. Human teeth with and without dental caries studied by visible luminescent spectroscopy. Journal of dental research. 60(2):120-122.

Alsayed EZ, Hariri I, Nakashima S, Shimada Y, Bakhsh TA, Tagami J, Sadr A. 2016. Effects of coating materials on nanoindentation hardness of enamel and adjacent areas. Dental Materials. 32(6):807-816.

Amjad Z, Koutsoukos P, Nancollas G. 1981. The mineralization of enamel surfaces. A constant composition kinetics study. Journal of dental research. 60(10):1783-1792.

Anderson M. 2001. Current concepts of dental caries and its prevention. Operative Dentistry.11-18.

Andersson A, Sköld-Larsson K, Haligren A, Petersson LG, Twetman S. 2007. Effect of a dental cream containing amorphous calcium phosphate complexes on white spot lesion regression assessed by laser fluorescence. Oral health & preventive dentistry. 5(3).

Ando M, Van Der Veen MH, Schemehorn BR, Stookey GK. 2001. Comparative study to quantify demineralized enamel in deciduous and permanent teeth using laser–and light–induced fluorescence techniques. Caries research. 35(6):464-470.

Angmar-Månsson B, Ten Bosch J. 1987. Optical methods for the detection and quantification of caries. Advances in dental research. 1(1):14-20.

Aoki H. 1991. Science and medical applications of hydroxyapatite. Ishiyaku Euroamerica.

Arends J. 1980. Remineralization of artificial enamel lesions in vitro. Caries research. 14(6):351-358.

Årtun J, Thylstrup A. 1989. A 3-year clinical and sem study of surface changes of carious enamel lesions after inactivation. American journal of orthodontics and dentofacial orthopedics. 95(4):327-333.

Arx T. 1993. Developmental disturbances of permanent teeth following trauma to the primary dentition. Australian dental journal. 38(1):1-10.

Bachmann L, Zezell DM, Ribeiro AdC, Gomes L, Ito AS. 2006. Fluorescence spectroscopy of biological tissues—a review. Applied Spectroscopy Reviews. 41(6):575-590.

Bailey D, Adams G, Tsao C, Hyslop A, Escobar K, Manton D, Reynolds E, Morgan M. 2009. Regression of post-orthodontic lesions by a remineralizing cream. Journal of dental research. 88(12):1148-1153.

Batchelar DL, Davidson M, Dabrowski W, Cunningham IA. 2006. Bone-composition imaging using coherent-scatter computed tomography: Assessing bone health beyond bone mineral density. Medical physics. 33(4):904-915.

Beerens M, Van Der Veen M, Van Beek H, Ten Cate J. 2010. Effects of casein phosphopeptide amorphous calcium fluoride phosphate paste on white spot lesions and dental plaque after orthodontic treatment: A 3-month follow-up. European journal of oral sciences. 118(6):610-617.

Benedict H. 1928. Note on fluorescence of teeth in ultraviolet rays. Science. 67:442.

Benedict H. 1929. The fluorescence of teeth as another method of attack on the problem of dental caries. J Dent Res. 9:274-275.

Bergstrand F, Twetman S. 2011. A review on prevention and treatment of post-orthodontic white spot lesions–evidence-based methods and emerging technologies. The open dentistry journal. 5(1).

Bishara SE, Ostby AW. 2008. White spot lesions: Formation, prevention, and treatment. Seminars in Orthodontics. 14(3):174-182.
Bjelkhagen H. 1982. Early detection of enamel caries by the luminescence excited by visible laser light. Swed Dent J. 6(1):1-7.
Björkman UH, Sundström F, ten Bosch JJ. 1991. Fluorescence in dissolved fractions of human enamel. Acta Odontologica Scandinavica. 49(3):133-138.
Booij M, Ten Bosch J. 1982. A fluorescent compound in bovine dental enamel matrix compared with synthetic dityrosine. Archives of oral biology. 27(5):417-421.
Boyd R. 1992. Nonlinear optics. 1992. New York: Academic Press.
Brès E, Voegel JC, Frank R. 1990. High-resolution electron microscopy of human enamel crystals. Journal of microscopy. 160(2):183-201.
Bröchner A, Christensen C, Kristensen B, Tranæus S, Karlsson L, Sonnesen L, Twetman S. 2011. Treatment of post-orthodontic white spot lesions with casein phosphopeptide-stabilised amorphous calcium phosphate. Clinical oral investigations. 15(3):369-373.
Can M, Darling L, Fried D. 2008. High-resolution ps-oct of enamel remineralization. Proceedings of SPIE--the International Society for Optical Engineering: NIH Public Access.
Cate JT. 1990. In vitro studies on the effects of fluoride on de-and remineralization. Journal of dental research. 69(2_suppl):614-619.
Chan YL, Ngan AH, King NM. 2011. Nano-scale structure and mechanical properties of the human dentine-enamel junction. Journal of the mechanical behavior of biomedical materials. 4(5):785-795.
Chatterjee R, Kleinberg I. 1979. Effect of orthodontic band placement on the chemical composition of human incisor tooth plaque. Archives of oral biology. 24(2):97-100.
Chen H, Liu X, Dai J, Jiang Z, Guo T, Ding Y. 2013. Effect of remineralizing agents on white spot lesions after orthodontic treatment: A systematic review. American journal of orthodontics and dentofacial orthopedics. 143(3):376-382. e373.
Chen S-Y, Hsu C-YS, Sun C-K. 2008. Epi-third and second harmonic generation microscopic imaging of abnormal enamel. Optics express. 16(15):11670-11679.
Cloitre T, Panayotov IV, Tassery H, Gergely C, Levallois B, Cuisinier FJ. 2013. Multiphoton imaging of the dentine-enamel junction. Journal of biophotonics. 6(4):330-337.
Cochrane N, Reynolds E. 2009. Casein phosphopeptides in oral health. Food constituents and oral health. Elsevier. p. 185-224.
Cochrane N, Saranathan S, Cai F, Cross K, Reynolds E. 2008. Enamel subsurface lesion remineralisation with casein phosphopeptide stabilised solutions of calcium, phosphate and fluoride. Caries research. 42(2):88-97.
Cross K, Huq N, Reynolds E. 2007a. Casein phosphopeptides in oral health-chemistry and clinical applications. Current pharmaceutical design. 13(8):793-800.
Cross KJ, Huq NL, O'Brien-Simpson NM, Perich JW, Attard TJ, Reynolds EC. 2007b. The role of multiphosphorylated peptides in mineralized tissue regeneration. International Journal of Peptide Research and Therapeutics. 13(4):479-495.
Cross KJ, Huq NL, Palamara JE, Perich JW, Reynolds EC. 2005. Physicochemical characterization of casein phosphopeptide-amorphous calcium phosphate nanocomplexes. Journal of Biological Chemistry. 280(15):15362-15369.
Cury JA, Tenuta LMA. 2009. Enamel remineralization: Controlling the caries disease or treating early caries lesions? Brazilian Oral Research. 23:23-30.
Curzon MEJ FJ. 1983. Chemical composition of enamel. (ed) LE, editor.

Cuy JL, Mann AB, Livi KJ, Teaford MF, Weihs TP. 2002. Nanoindentation mapping of the mechanical properties of human molar tooth enamel. Archives of oral biology. 47(4):281-291.
Damen J, Exterkate R, Ten Cate J. 1997. Reproducibility of tmr for the determination of longitudinal mineral changes in dental hard tissues. Advances in dental research. 11(4):415-419.
De Jong EdJ, Sundström F, Westerling H, Tranaeus S, Ten Bosch J, Angmar-Månsson B. 1995. A new method for in vivo quantification of changes in initial enamel caries with laser fluorescence. Caries research. 29(1):2-7.
De Jong EdJ, Ten Bosch J. 1985. Error analysis of the microradiographic determination of mineral content in mineralised tissue slices. Physics in medicine and biology. 30(10):1067.
Denk W, Strickler JH, Webb WW. 1990. Two-photon laser scanning fluorescence microscopy. Science. 248(4951):73-76.
Derks A, Katsaros C, Frencken J, Van't Hof M, Kuijpers-Jagtman A. 2004. Caries-inhibiting effect of preventive measures during orthodontic treatment with fixed appliances. Caries research. 38(5):413-420.
Dickinson M, Wolf K, Mann A. 2007. Nanomechanical and chemical characterization of incipient in vitro carious lesions in human dental enamel. Archives of oral biology. 52(8):753-760.
Eastoe J. 1960. Organic matrix of tooth enamel. Nature. 187(4735):411.
Elfallah HM, Bertassoni LE, Charadram N, Rathsam C, Swain MV. 2015. Effect of tooth bleaching agents on protein content and mechanical properties of dental enamel. Acta biomaterialia. 20:120-128.
Everall NJ. 2009. Confocal raman microscopy: Performance, pitfalls, and best practice. Applied spectroscopy. 63(9):245A-262A.
Featherstone J. 2004a. The continuum of dental caries—evidence for a dynamic disease process. Journal of dental research. 83(1_suppl):39-42.
Featherstone J. 2004b. The continuum of dental caries—evidence for a dynamic disease process. Journal of dental research. 83(suppl 1):C39-C42.
Featherstone J, Duncan J, Cutress T. 1979. A mechanism for dental caries based on chemical processes and diffusion phenomena during in-vitro caries simulation on human tooth enamel. Archives of oral biology. 24(2):101-112.
Featherstone J, Lussi A. 2006. Understanding the chemistry of dental erosion. Dental erosion. Karger Publishers. p. 66-76.
Featherstone J, O'reilly M, Shariati M, Brugler S. 1986. Enhancement of remineralization in vitro and in vivo. Factors relating to demineralisation and remineralisation of the teeth. IRL Press. Oxford and Washington.
Featherstone J, Ten Cate J, Shariati M, Arends J. 1983. Comparison of artificial caries-like lesions by quantitative microradiography and microhardness profiles. Caries research. 17(5):385-391.
Featherstone JD. 1995. Clinical aspects of de/remineralization of teeth. International Association for Dental Research.
Fejerskov O. 1997. Concepts of dental caries and their consequences for understanding the disease. Community dentistry and oral epidemiology. 25(1):5-12.
Fejerskov O, Johnson N, Silverstone L. 1974. The ultrastructure of fluorosed human dental enamel. European journal of oral sciences. 82(5):357-372.
Fejerskov O, Nyvad B. 2003. Is dental caries an infectious disease? Diagnostic and treatment consequences for the practitioner. Nordic dentistry 2003 yearbook. Quintessence Publishing Co, Ltd. p. 141-152.
Ferrar J, Nakamoto K. 1994. Introductory raman spectroscopy. Acad. Press, inc. Harcourt Brace and Comp., Publishers, Boston–San Diego–NY–London–Sudney–Tokio–Toronto.

Gallagher RR, Balooch M, Balooch G, Wilson RS, Marshall SJ, Marshall GW. 2010. Coupled nanomechanical and raman microspectroscopic investigation of human third molar dej. Journal of dental biomechanics. 2010.

Gibson EA, Masihzadeh O, Lei TC, Ammar DA, Kahook MY. 2011. Multiphoton microscopy for ophthalmic imaging. Journal of ophthalmology. 2011.

Gilchrist F, Santini A, Harley K, Deery C. 2007. The use of micro-raman spectroscopy to differentiate between sound and eroded primary enamel. International journal of paediatric dentistry. 17(4):274-280.

Gorelick L, Geiger AM, Gwinnett AJ. 1982. Incidence of white spot formation after bonding and banding. American journal of orthodontics. 81(2):93-98.

Grasselli JG, Bulkin BJ. 1991. Analytical raman spectroscopy. Wiley.

Gwinnett AJ, Ceen RF. 1979. Plaque distribution on bonded brackets: A scanning microscope study. American journal of orthodontics. 75(6):667-677.

Hadler-Olsen S, Sandvik K, El-Agroudi MA, Øgaard B. 2011. The incidence of caries and white spot lesions in orthodontically treated adolescents with a comprehensive caries prophylactic regimen—a prospective study. The European Journal of Orthodontics. 34(5):633-639.

Haines D. 1968. Physical properties of human tooth enamel and enamel sheath material under load. Journal of biomechanics. 1(2):117IN17119-17118IN22125.

Hall A, Girkin J. 2004. A review of potential new diagnostic modalities for caries lesions. Journal of dental research. 83(1_suppl):89-94.

Hannig C, Hamkens A, Becker K, Attin R, Attin T. 2005. Erosive effects of different acids on bovine enamel: Release of calcium and phosphate in vitro. Archives of oral biology. 50(6):541-552.

He B, Huang S, Jing J, Hao Y. 2010. Measurement of hydroxyapatite density and knoop hardness in sound human enamel and a correlational analysis between them. Archives of oral biology. 55(2):134-141.

He L-H, Swain MV. 2009. Enamel—a functionally graded natural coating. Journal of dentistry. 37(8):596-603.

Helmchen F, Denk W. 2005. Deep tissue two-photon microscopy. Nature methods. 2(12):932.

Herzberg G. 1945. Infrared and raman spectra of polyatomic molecules. D. Van Nostrand Company.; New York.

Hicks J, Garcia-Godoy F, Flaitz C. 2005. Biological factors in dental caries enamel structure and the caries process in the dynamic process of demineralization and remineralization (part 2). Journal of clinical pediatric dentistry. 28(2):119-124.

Hollander F. 1935. The apparent radiopaque surface layer of the enamel. Dent Cosmos. 77:1187-1197.

Hsu DJ, Darling CL, Lachica MM, Fried D. 2008. Nondestructive assessment of the inhibition of enamel demineralization by co2 laser treatment using polarization sensitive optical coherence tomography. Journal of biomedical optics. 13(5):054027-054027-054029.

Huang S, Gao S, Yu H. 2009. Effect of nano-hydroxyapatite concentration on remineralization of initial enamel lesion in vitro. Biomedical Materials. 4(3):034104.

Huang TT, Jones AS, He LH, Darendeliler MA, Swain MV. 2007. Characterisation of enamel white spot lesions using x-ray micro-tomography. Journal of dentistry. 35(9):737-743.

Huminicki A, Dong C, Cleghorn B, Sowa M, Hewko M, Choo-Smith L-. 2010. Determining the effect of calculus, hypocalcification, and stain on using optical coherence tomography and polarized raman spectroscopy for detecting white spot lesions. International journal of dentistry. 2010.

Ichim I, Li Q, Li W, Swain M, Kieser J. 2007. Modelling of fracture behaviour in biomaterials. Biomaterials. 28(7):1317-1326.

Biostatgv. 2000. [accessed]. https://marne.u707.jussieu.fr/biostatgv.

Ismail A, Sohn W, Tellez M, Amaya A, Sen A, Hasson H, Pitts N. 2007. The international caries detection and assessment system (icdas): An integrated system for measuring dental caries. Community dentistry and oral epidemiology. 35(3):170-178.

Jiang W, Cao W. 2004. Second harmonic generation of shear waves in crystals. ieee transactions on ultrasonics, ferroelectrics, and frequency control. 51(2):153-162.

Jongebloed W, Arends J. 1981. Remineralization of artificial enamel lesions in vitro. Caries research. 15(1):60-69.

Kaehler T. 1994. Nanotechnology: Basic concepts and definitions. Clinical chemistry. 40(9):1797-1799.

KANI T, KANI M, ISOZAKI A, SHINTANI H, OHASHI T, TOKUMOTO T. 1989. Effect to apatite-containing dentifrices on dental caries in school children. Journal of Dental Health. 39(1):104-109.

Kawasaki K, Buchanan AV, Weiss KM. 2009. Biomineralization in humans: Making the hard choices in life. Annual review of genetics. 43:119-142.

Kidd EA, Nyvad B, Espelid I. 2008. Caries control for the individual patient. Dental caries. Blackwell Publishing Ltd. p. 487-504.

Koenig K, Schneckenburger H. 1994. Laser-induced autofluorescence for medical diagnosis. Journal of fluorescence. 4(1):17-40.

Lang NP, Hotz PR, Gusberti FA, Joss A. 1987. Longitudinal clinical and microbiological study on the relationship between infection with streptococcus mutans and the development of caries in humans. Molecular Oral Microbiology. 2(1):39-47.

Larsen M. 1986a. An investigation of the theoretical background for the stability of the calcium-phosphate salts and their mutual conversion in aqueous solutions. Archives of oral biology. 31(11):757-761.

Larsen M. 1986b. The nature of early caries lesions in enamel. Journal of dental research. 65(7):1030.

Larsen MJ. 1974. Chemically induced in vitro lesions in dental enamel. European journal of oral sciences. 82(7):496-509.

Larsen MJ, Fejerkov O. 1989. Chemical and structural challenges in remineralization of dental enamel lesions. European journal of oral sciences. 97(4):285-296.

Larsen MJ, Jensen S. 1986. Solubility study of the initial formation of calcium orthophosphates from aqueous solutions at ph 5–10. Archives of oral biology. 31(9):565-572.

Legeros RZ, Trautz OR, Legeros JP, Klein E, Shirra WP. 1967. Apatite crystallites: Effects of carbonate on morphology. Science. 155(3768):1409-1411.

Leventouri T, Chakoumakos B, Papanearchou N, Perdikatsis V. 2001. Comparison of crystal structure parameters of natural and synthetic apatites from neutron powder diffraction. Journal of materials research. 16(9):2600-2606.

Lewis IR, Edwards H. 2001. Handbook of raman spectroscopy: From the research laboratory to the process line. CRC Press.

Li L, Pan H, Tao J, Xu X, Mao C, Gu X, Tang R. 2008. Repair of enamel by using hydroxyapatite nanoparticles as the building blocks. Journal of Materials Chemistry. 18(34):4079-4084.

Lin P-Y, Lyu H-C, Hsu C-YS, Chang C-S, Kao F-J. 2011. Imaging carious dental tissues with multiphoton fluorescence lifetime imaging microscopy. Biomedical optics express. 2(1):149-158.

Lin S-J, Wu R-J, Tan H-Y, Lo W, Lin W-C, Young T-H, Hsu C-J, Chen J-S, Jee S-H, Dong C-Y. 2005. Evaluating cutaneous photoaging by use of multiphoton fluorescence and second-harmonic generation microscopy. Optics letters. 30(17):2275-2277.

Liu Y, Hsu C-YS. 2007. Laser-induced compositional changes on enamel: A ft-raman study. Journal of dentistry. 35(3):226-230.

Lo E, Zhi Q, Itthagarun A. 2010. Comparing two quantitative methods for studying remineralization of artificial caries. Journal of dentistry. 38(4):352-359.

Lopes CB, Pacheco M, Silveira Jr L, Duarte J, Cangussu MCT, Pinheiro A. 2007. The effect of the association of nir laser therapy bmps, and guided bone regeneration on tibial fractures treated with wire osteosynthesis: Raman spectroscopy study. Journal of Photochemistry and Photobiology B: Biology. 89(2-3):125-130.

Lucchese A, Gherlone E. 2012. Prevalence of white-spot lesions before and during orthodontic treatment with fixed appliances. European journal of orthodontics. 35(5):664-668.

Lussi A, Hibst R, Paulus R. 2004. Diagnodent: An optical method for caries detection. Journal of dental research. 83(1_suppl):80-83.

Lyubchanskii I, Dadoenkova N, Lyubchanskii M, Rasing T, Jeong J-W, Shin S-C. 2000. Second-harmonic generation from realistic film–substrate interfaces: The effects of strain. Applied Physics Letters. 76(14):1848-1850.

Manesh SK, Darling CL, Fried D. 2009. Nondestructive assessment of dentin demineralization using polarization-sensitive optical coherence tomography after exposure to fluoride and laser irradiation. Journal of Biomedical Materials Research Part B: Applied Biomaterials. 90(2):802-812.

Martinović BT, Ivanović M, Milosavljević Z, Mladenović R. 2015. Identifying basic chemical elements of hypomineralized enamel in first permanent molars. Vojnosanitetski pregled. 72(10).

McKee M, Addison W, Kaartinen M. 2005. Hierarchies of extracellular matrix and mineral organization in bone of the craniofacial complex and skeleton. Cells Tissues Organs. 181(3-4):176-188.

Mehta R, Nandlal B, Prashanth S. 2013. Comparative evaluation of remineralization potential of casein phosphopeptide-amorphous calcium phosphate and casein phosphopeptide-amorphous calcium phosphate fluoride on artificial enamel white spot lesion: An in vitro light fluorescence study. Indian journal of dental research. 24(6):681.

Mendes FM, Pinheiro SL, Bengtson AL. 2004. Effect of alteration in organic material of the occlusal caries on diagnodent readings. Brazilian Oral Research. 18(2):141-144.

Mohanty B, Dadlani D, Mahoney D, Mann AB. 2013. Characterizing and identifying incipient carious lesions in dental enamel using micro-raman spectroscopy. Caries research. 47(1):27-33.

Moron BM, Comar LP, Wiegand A, Buchalla W, Yu H, Buzalaf MA, Magalhaes AC. 2013. Different protocols to produce artificial dentine carious lesions in vitro and in situ: Hardness and mineral content correlation. Caries research. 47(2):162-170.

Najibfard K, Ramalingam K, Chedjieu I, Amaechi B. 2011. Remineralization of early caries by a nano-hydroxyapatite dentifrice. Journal of Clinical Dentistry. 22(5):139.

Odutuga A, Prout R. 1974. Lipid analysis of human enamel and dentine. Archives of oral biology. 19(8):729-731.

Øgaard B, Rølla G, Arends J. 1988. Orthodontic appliances and enamel demineralization: Part 1. Lesion development. American journal of orthodontics and dentofacial orthopedics. 94(1):68-73.

Oheim M, Michael DJ, Geisbauer M, Madsen D, Chow RH. 2006. Principles of two-photon excitation fluorescence microscopy and other nonlinear imaging approaches. Advanced drug delivery reviews. 58(7):788-808.

Oliver W. 1992. Wc oliver and gm pharr, j. Mater. Res. 7, 1564 (1992). J Mater Res. 7:1564.

Oliver WC, Pharr GM. 1992. An improved technique for determining hardness and elastic modulus using load and displacement sensing indentation experiments. Journal of materials research. 7(6):1564-1583.

Oliver WC, Pharr GM. 2004. Measurement of hardness and elastic modulus by instrumented indentation: Advances in understanding and refinements to methodology. Journal of materials research. 19(01):3-20.

Pharr G, Bolshakov A. 2002. Understanding nanoindentation unloading curves. Journal of materials research. 17(10):2660-2671.

Pinheiro AL, Lopes CB, Pacheco MT, Brugnera Jr A, Zanin FAA, Cangussú MCT, Silveira Jr L. 2010. Raman spectroscopy validation of diagnodent-assisted fluorescence readings on tibial fractures treated with laser phototherapy, bmps, guided bone regeneration, and miniplates. Photomedicine and laser surgery. 28(S2):S-89-S-97.

Pitts N. 2004. Are we ready to move from operative to non-operative/preventive treatment of dental caries in clinical practice? Caries research. 38(3):294-304.

Pleshko N, Boskey A, Mendelsohn R. 1991. Novel infrared spectroscopic method for the determination of crystallinity of hydroxyapatite minerals. Biophysical journal. 60(4):786-793.

Popowics T, Rensberger J, Herring S. 2004. Enamel microstructure and microstrain in the fracture of human and pig molar cusps. Archives of oral biology. 49(8):595-605.

Pretty I, Ellwood R. 2013. The caries continuum: Opportunities to detect, treat and monitor the re-mineralization of early caries lesions. Journal of dentistry. 41:S12-S21.

Pucéat E, Reynard B, Lécuyer C. 2004. Can crystallinity be used to determine the degree of chemical alteration of biogenic apatites? Chemical Geology. 205(1):83-97.

Radlanski RJ, Renz H, Willersinn U, Cordis CA, Duschner H. 2001. Outline and arrangement of enamel rods in human deciduous and permanent enamel. 3d-reconstructions obtained from clsm and sem images based on serial ground sections. European journal of oral sciences. 109(6):409-414.

Reed R, Xu C, Liu Y, Gorski J, Wang Y, Walker M. 2015a. Radiotherapy effect on nano-mechanical properties and chemical composition of enamel and dentine. Archives of oral biology. 60(5):690-697.

Reed R, Xu C, Liu Y, Gorski JP, Wang Y, Walker MP. 2015b. Radiotherapy effect on nano-mechanical properties and chemical composition of enamel and dentine. Archives of oral biology. 60(5):690-697.

Reynolds E. 1997. Remineralization of enamel subsurface lesions by casein phosphopeptide-stabilized calcium phosphate solutions. Journal of dental research. 76(9):1587-1595.

Reynolds E, Del Rio A. 1984. Effect of casein and whey-protein solutions on caries experience and feeding patterns of the rat. Archives of oral biology. 29(11):927-933.

Reynolds E, Johnson I. 1981. Effect of milk on caries incidence and bacterial composition of dental plaque in the rat. Archives of oral biology. 26(5):445-451.

Reynolds EC. 1998. Anticariogenic complexes of amorphous calcium phosphate stabilized by casein phosphopeptides: A review. Special Care in Dentistry. 18(1):8-16.

Robinson C. 1983. Alterations in the composition of permanent human enamel during carious attack. Demineralisation and Remineralisation of the Teeth.209-223.

Robinson C, Shore R, Brookes S, Strafford S, Wood S, Kirkham J. 2000. The chemistry of enamel caries. Critical Reviews in Oral Biology & Medicine. 11(4):481-495.

Robinson C, Weatherell J, Hallsworth A. 1971. Variation in composition of dental enamel within thin ground tooth sections. Caries research. 5(1):44-57.

Roveri N, Battistella E, Bianchi CL, Foltran I, Foresti E, Iafisco M, Lelli M, Naldoni A, Palazzo B, Rimondini L. 2009. Surface enamel remineralization: Biomimetic apatite nanocrystals and fluoride ions different effects. Journal of Nanomaterials. 2009:8.

Salehi H, Derely L, Vegh AG, Durand JC, Gergely C, Larroque C, Fauroux MA, Cuisinier FJG. 2013. Label-free detection of anticancer drug paclitaxel in living cells by confocal raman microscopy. Applied Physics Letters. 102(11):113701.

Sato K. 2007. Mechanism of hydroxyapatite mineralization in biological systems. Journal of the Ceramic Society of Japan. 115(1338):124-130.

Sato Y, Sato T, Niwa M, Aoki H. 2006. Precipitation of octacalcium phosphates on artificial enamel in artificial saliva. Journal of Materials Science: Materials in Medicine. 17(11):1173-1177.

Silverstone L. 1983. Remineralization and enamel caries: New concepts. Dental Update. 10(4):261-273.

Silverstone L, Hicks M, Featherstone M. 1988. Dynamic factors affecting lesion initiation and progression in human dental enamel. Part i. The dynamic nature of enamel caries. Quintessence international (Berlin, Germany: 1985). 19(10):683.

Silverstone L, Wefel J, Zimmerman B, Clarkson B, Featherstone M. 1981. Remineraiization of natural and artificial lesions in human dental enamel in vitro. Caries research. 15(2):138-157.

Simmer J, Fincham A. 1995. Molecular mechanisms of dental enamel formation. Critical Reviews in Oral Biology & Medicine. 6(2):84-108.

Slimani A, Nouioua F, Desoutter A, Levallois B, Cuisinier FJG, Tassery H, Terrer E, Salehi H. 2017. Confocal raman mapping of collagen cross-link and crystallinity of human dentin-enamel junction. J Biomed Opt. 22(8):1-8.

Slimani A, Tardivo D, Panayotov IV, Levallois B, Gergely C, Cuisinier F, Tassery H, Cloitre T, Terrer E. 2018. Multiphoton microscopy for caries detection with icdas classification. Caries research. 52(5):359-366.

So PT, Dong CY, Masters BR, Berland KM. 2000. Two-photon excitation fluorescence microscopy. Annual review of biomedical engineering. 2(1):399-429.

Stookey GK. 2005. Quantitative light fluorescence: A technology for early monitoring of the caries process. Dental Clinics. 49(4):753-770.

Stylianopoulos T, Poh M-Z, Insin N, Bawendi MG, Fukumura D, Munn LL, Jain RK. 2010. Diffusion of particles in the extracellular matrix: The effect of repulsive electrostatic interactions. Biophysical journal. 99(5):1342-1349.

Summitt JB, Robbins JW, Hilton TJ, Schwartz RS. 2006. Fundamentals of operative dentistry: A contemporary approach. Quintessence Pub.

Sundström F, Fredriksson K, Montan S, Hafström-Björkman U, Ström J. 1985. Laser-induced fluorescence from sound and carious tooth substance: Spectroscopic studies. Swed Dent J. 9(2):71-80.

Tassery H, Levallois B, Terrer E, Manton D, Otsuki M, Koubi S, Gugnani N, Panayotov I, Jacquot B, Cuisinier F. 2013. Use of new minimum intervention dentistry technologies in caries management. Australian dental journal. 58(s1):40-59.

Ten BJ. 1991. A review of quantitative method for studies of mineral content of intra-oral incipient caries lesion. J Dent Res. 70:2-14.

Ten Bosch J. 1996. Light scattering and related methods in caries diagnosis. Early Detection of Dental Caries I.81-90.

Ten Cate J. 2008. Remineralization of deep enamel dentine caries lesions. Australian dental journal. 53(3):281-285.

Ten Cate J, Mundorff-Shrestha S. 1995. Working group report 1: Laboratory models for caries (in vitro and animal models). Advances in dental research. 9(3):332-334.

Torres CRG, Borges AB, Torres LMS, Gomes IS, de Oliveira RS. 2011. Effect of caries infiltration technique and fluoride therapy on the colour masking of white spot lesions. Journal of dentistry. 39(3):202-207.

Valeur B, Berberan-Santos MN. 2012. Molecular fluorescence: Principles and applications. John Wiley & Sons.

Vandiver J, Dean D, Patel N, Bonfield W, Ortiz C. 2005. Nanoscale variation in surface charge of synthetic hydroxyapatite detected by chemically and spatially specific high-resolution force spectroscopy. Biomaterials. 26(3):271-283.

Wang X-J, Milner TE, de Boer JF, Zhang Y, Pashley DH, Nelson JS. 1999. Characterization of dentin and enamel by use of optical coherence tomography. Applied Optics. 38(10):2092.

Weatherell I, Robinson C, Hiller C. 1968. Distribution of carbonate in thin sections of dental enamel. Caries research. 2(1):1-9.

Weatherell J. 1975. Composition of dental enamel. British medical bulletin. 31(2):115-119.

Wentrup-Byrne E, Armstrong CA, Armstrong RS, Collins BM. 1997. Fourier transform raman microscopic mapping of the molecular components in a human tooth. Journal of Raman Spectroscopy. 28(2-3):151-158.

White D. 1992. The comparative sensitivity of intra-oral, in vitro, and animal models in the'profile'evaluation of topical fluorides. Journal of dental research. 71.

White D. 1995. The application of in vitro models to research on demineralization and remineralization of the teeth. Advances in dental research. 9(3):175-193.

White S. 2004. Benign tumor of jaw. Oral radiology Principles and interpretation.410-458.

Xu C, Reed R, Gorski JP, Wang Y, Walker MP. 2012. The distribution of carbonate in enamel and its correlation with structure and mechanical properties. Journal of materials science. 47(23):8035-8043.

Xu C, Yao X, Walker MP, Wang Y. 2009. Chemical/molecular structure of the dentin–enamel junction is dependent on the intratooth location. Calcified tissue international. 84(3):221.

Yamagishi K, Onuma K, Suzuki T, Okada F, Tagami J, Otsuki M, Senawangse P. 2005. Materials chemistry: A synthetic enamel for rapid tooth repair. Nature. 433(7028):819.

Yokoyama E, Kakino S, Matsuura Y. 2008. Raman imaging of carious lesions using a hollow optical fiber probe. Applied Optics. 47(23):4227-4230.

Zipfel WR, Williams RM, Christie R, Nikitin AY, Hyman BT, Webb WW. 2003a. Live tissue intrinsic emission microscopy using multiphoton-excited native fluorescence and second harmonic generation. Proceedings of the National Academy of Sciences. 100(12):7075-7080.

Zipfel WR, Williams RM, Webb WW. 2003b. Nonlinear magic: Multiphoton microscopy in the biosciences. Nature biotechnology. 21(11):1369.

Zoumi A, Yeh A, Tromberg BJ. 2002a. Imaging cells and extracellular matrix in vivo by using second-harmonic generation and two-photon excited fluorescence. P Natl Acad Sci USA. 99(17):11014-11019.

Zoumi A, Yeh A, Tromberg BJ. 2002b. Imaging cells and extracellular matrix in vivo by using second-harmonic generation and two-photon excited fluorescence. Proceedings of the National Academy of Sciences. 99(17):11014-11019.

Chapter 5

Forth Article

Remineralization systems: make a difference in reversible caries lesion treatment?

ABSTRACT

Different approaches have been developed to manage primitive caries lesions non-invasively through lesion remineralization in an attempt to prevent disease progression. The efficacy of GC Tooth Mousse cream (CPP-ACP) as a potent remineralizing agent has been extremely affirmed. Recently, nano-hydroxyapatite containing dentifrice "KAREX" has put on the market as a dental care product suitable for dental tissue renovation. In the present study, an *in vitro* caries model was used to compare the remineralizing effect of the two products. Each specimen was treated with the respective remineralizing agent for 5 min every 24h for 21 days, with the help of cotton applicator tip. Teeth scanned by confocal Raman microscopy to provide phosphate maps showing the net differences between affected and unaffected enamel areas. The prominent phosphate peak at 960 cm^{-1} was nominated to observe changes in its intensity. The width of the same peak measured by FWHM was calculated across each spectral map to evaluate the effect of remineralizing agents on crystalline structure of demineralized enamel. At the end of the treatment, a significant difference has attained in respect to phosphate gain in the body of lesions treated by nHA containing-dentifrice compared to the counterpart treated by CPP-ACP. However, ANOVA indicated no significant differences among the treatment groups with regard to enamel crystallinity. We can conclude that enamel surface layer permeability along with material consistency might represent key factors in subsurface lesion remineralization. Further studies of the biomimetic molecules involved in calcium, phosphate stabilization and nucleation may provide further improvements in the development of novel remineralization technologies.

Keywords: CPP-ACP, nHA containing-dentifrice, confocal Raman microscopy, phosphate maps, non-invasive treatment, full-width at half-maximum (FWHM).

5.1 INTRODUCTION

White spot lesion (WSL) represents an early stage of caries formation where an intact surface layer (ISL) overlays subsurface enamel demineralization which takes place due to imbalance between pathological and protective factors (Robinson et al. 2000). Non-invasive treatment of WSL through remineralization; represents the aim of modern dentistry. The clinical usage of calcium phosphate salts in enamel remineralization process was unsuccessful because these salts are insoluble and unable to provide bioavailable ions which are essential for enamel restoration. Novel technology assists in localizing bioavailable ions at tooth surface to promote enamel renovation becomes mandatory (Cross et al. 2007a).

Dairy products are among the nutrients the most recognized as exhibiting an anticariogenic activity (Reynolds 1998). The components largely responsible for this activity have been identified as bovine milk phosphoprotein, casein, calcium and phosphate (Reynolds and Del Rio 1984; Reynolds and Johnson 1981; Reynolds 1998). Casein phosphopeptides (CPP) containing the cluster sequence – Ser(P)-Ser(P)- Ser(P)-Glu-Glu – have a remarkable ability to stabilize amorphous calcium phosphate (ACP) in a metastable solution. The CPP binds high amounts of calcium and phosphate to forming nanoclusters of ACP through the multiple phosphoseryl residues, preventing their growth to the critical size required for nucleation and precipitation (Reynolds 1998). Thus, CPP tends to increasing calcium and phosphate levels in the subsurface lesions, thereby esthetically repair WSLs (Chen et al. 2013; Reynolds 1997). This tasteless, stable and highly soluble CPP-ACP has been registered as Recaldent^{TM} and commercialized in

dental professional products (Tooth Mousse^{TM}). GC Tooth Mousse cream containing 10% w/w CPP-ACP has been used clinically to treat mild to moderate fluorotic tooth enamel without surgical intervention (Cross et al. 2007a).

Nano-hydroxyapatite (nHA) is one of the most biocompatible and bioactive materials which have similarity to the apatite crystal of tooth enamel in morphology, crystal structure and crystallinity (Vandiver et al. 2005). Recently, many reports have shown that (nHA) has the potential to remineralize artificial carious lesions following addition to toothpastes, mouthwashes (Huang et al. 2009; Yamagishi et al. 2005). nHA displays high affinity to the tooth and can strongly adsorb on enamel surfaces (Roveri et al. 2009), promoting remineralization due to their size-specific effects corresponding to enamel ultrastructure (Li et al. 2008). Toothpaste comprising (nHA) has been commercially available in Japan since the 1980s, and was approved as an opposing caries agent in 1993 based on randomized anti-caries field trials in Japanese school children (KANI et al. 1989).

KAREK is a caries-inhibitory nHA containing-dentifrice, lately produced by Zahnpasta (dental care products, Bielefeld, Germany). It has antimicrobial effects thanks to the presence of active substances zinc and xylitol. This hydroxyapatite (HA) based toothpaste forms a protective layer on tooth surfaces and can initiate regeneration of attacked areas even in case of low salivary flow rates because the active ingredient is already present in mineral form and does not have to be formed from the saliva through remineralisation processes (Najibfard et al. 2011).

Confocal Raman microscopy is a powerful technique, measures the inelastic scattering of incident light which is used to analyze the internal structure of mineralized tissues. The spatial resolution of 300 nm; makes it a novel optical approach appropriate for incipient caries detection (Al-Obaidi et al. 2018).

The efficacy of Tooth Mousse™ cream as a potent remineralizing agent has been affirmed by many regulatory bodies around the world. Therefore, the purpose of the current study was to determine whether newly produced KAREX tooth paste is able to remineralize artificial subsurface enamel lesions and comparing its remineralizing effect with GC Tooth Mousse cream, being used as a criterion in this study.

5.2 MATERIALS & METHODS

12 sound premolars were extracted for orthodontic treatment and collected with patients' consent and approval of the local ethical research committee (process No. 2017-2907) before usage. Teeth were cleaned of debris, stored in de-ionized water with 0.1% antimicrobial thymol at 4°C until use.

Teeth were exposed to pH cycling chemical model to induce uniform, reproducible subsurface enamel lesions *in vitro* through the use of sequential series of exposure to de/remineralizing solutions. The regimen was repeated for a period of 6 days, the temperature maintained at 37 ◦C (Al-Obaidi et al. 2018). Thereafter, teeth were randomly divided into 2 groups and cut into two, each part being scanned by Raman microscopy two times: once after initial caries induction and once again after intervention to decrease sources of variation.

GC Tooth Mousse cream (Recaldent™, CPP-ACP) and KAREX tooth paste (dental care products, Griesheim, Germany) were applied to remineralize the formerly created lesions. Each specimen was treated with the respective remineralizing agent for 5 min every 24h for 21 days, with the help of cotton applicator tip. Treated samples washed with distilled water and placed in artificial saliva at 37°C. Artificial saliva was renewed every 24h just before immersion of freshly treated samples (Mehta et al. 2013). The artificial saliva was prepared according to a method

given by (Sato et al. 2006), using inorganic components similar to that of natural saliva. 3.90 mM $Na_3 PO_4$, 4.29 mM NaCl, 17.98 mM KCl, 1.1 mM $CaCl_2$, 0.08 mM $MgCl_2$, 0.05 mM H_2SO_4, 3.27 mM $NaHCO_3$, pH = 7.2. All chemical products were supplied by Sigma-Aldrich, France.

5.2.1 Raman microscopy:

Raman spectra were recorded using a Witec Confocal Raman Microscope System (Witec, Ulm, Germany). Excitation was assured by a frequency doubled Nd: YAG visible laser (Newport, Evry, France) at 532nm. Acquisition time of a single spectrum was adjusted to 0.05 s.

Chemical mapping of dental enamel was carried out over enamel cross section from outer surface toward DEJ. The prominent phosphate peak at 960 cm^{-1} attributed to symmetric stretching mode ν_1; was nominated as the inner standard to observe changes in PO_4^{3-} intensity. Furthermore, the width of the same PO_4^{3-} peak was calculated across each spectral map to evaluate the effect of remineralizing agents on crystalline structure of demineralized enamel. As peak width increases, crystallinity decreases (Xu et al. 2012). An indicative standardization bar showing the maximum and minimum sums of phosphate intensity across the enamel film; was adopted.

Representative Raman spectra were collected from the damaged and healthy enamel sites and enhanced after baseline correction using (SpectraGryph- optical spectroscopy software, Version 1.2.7, 2017). Thereafter, phosphate intensity at 960 cm^{-1} along with ($FWHM^{-1}$) values were obtained twice; once after artificial caries induction and over again after treatment with the remineralizing agents to detect the net differences in enamel inorganic component.

5.2.2 Viscosity measurement:

Viscosity of remineralizing agents was determined using FUNGILAB viscometer (FUNGILAB S.A. Ind., Spain). Spindle number (R7) was used and the rotation speed of the spindle was adjusted to 6.0 RPM.

5.2.3 Statistical analysis:

Statistical analysis was performed using ANOVA test for normally distributed data and Kruskal-Wallis ANOVA for data that were not normally distributed. All statistical procedures were performed at over all significant level of $\alpha = 0.05$ with SigmaPlot version 11.0 (Systat Software, Inc., USA).

Difference (D) between initial PO_4^{3-} intensity (I_i, after pH cycling) and final intensity (I_f, after treatment with the selected agents) was calculated for each specimen and the mean of this difference ($\bar{D}$) was calculated for each of the experimental groups. The ratio of the difference ($\bar{D}$) to the ($\bar{I_i}$ mean of I_i for each experimental group) was also calculated for each experimental group, which represents the rate of change in phosphate intensity of the specimens (Featherstone et al. 1983). The same calculation was repeated to measure the rate of change in FWHM value which is inversely proportional to enamel crystallinity as elucidated in Table 1.

$$(D) = I_f - I_i \ldots (1)$$

$$(\bar{D}) = \sum (D)/n \ldots\ldots\ldots\ldots (2)$$

$$(\bar{I_i}) = \sum (I_i)/n \ldots\ldots\ldots\ldots\ldots (3)$$

$$\% \text{ rate of change in the intensity (CI)} = (\bar{D}) / (\bar{I_i}) * 100 \ldots\ldots\ldots (4)$$

5.3 RESULTS:

Phosphate maps were constructed from phosphate peak intensity at 960 cm^{-1} before and after remineralization (Fig.1). Phosphate intensity reveals its amount within the inorganic crystals and directly related to the degree of enamel mineralization. Therefore, each pseudo color in these images signifies a certain amount of phosphate in accordance with the adjacent standardization bars.

The yellow tint designates high mineral content in the outermost enamel layer and the unaffected inside enamel layer which represents the end of the lesion. Whereas, the body of the lesion looks brown in color due to severe reduction in PO_4^{3-} amount in this area **(**Fig.1FA-GC). A slight reduction in lesion depth was observed after remineralization **(**double ended arrows in Fig.1ID &FD-KA), besides, a clear evidence of remineralization of the subsurface lesions and ISLs following treatment with nHA containing-dentifrice (arrows in Fig.1IC-KA, FC-KA).

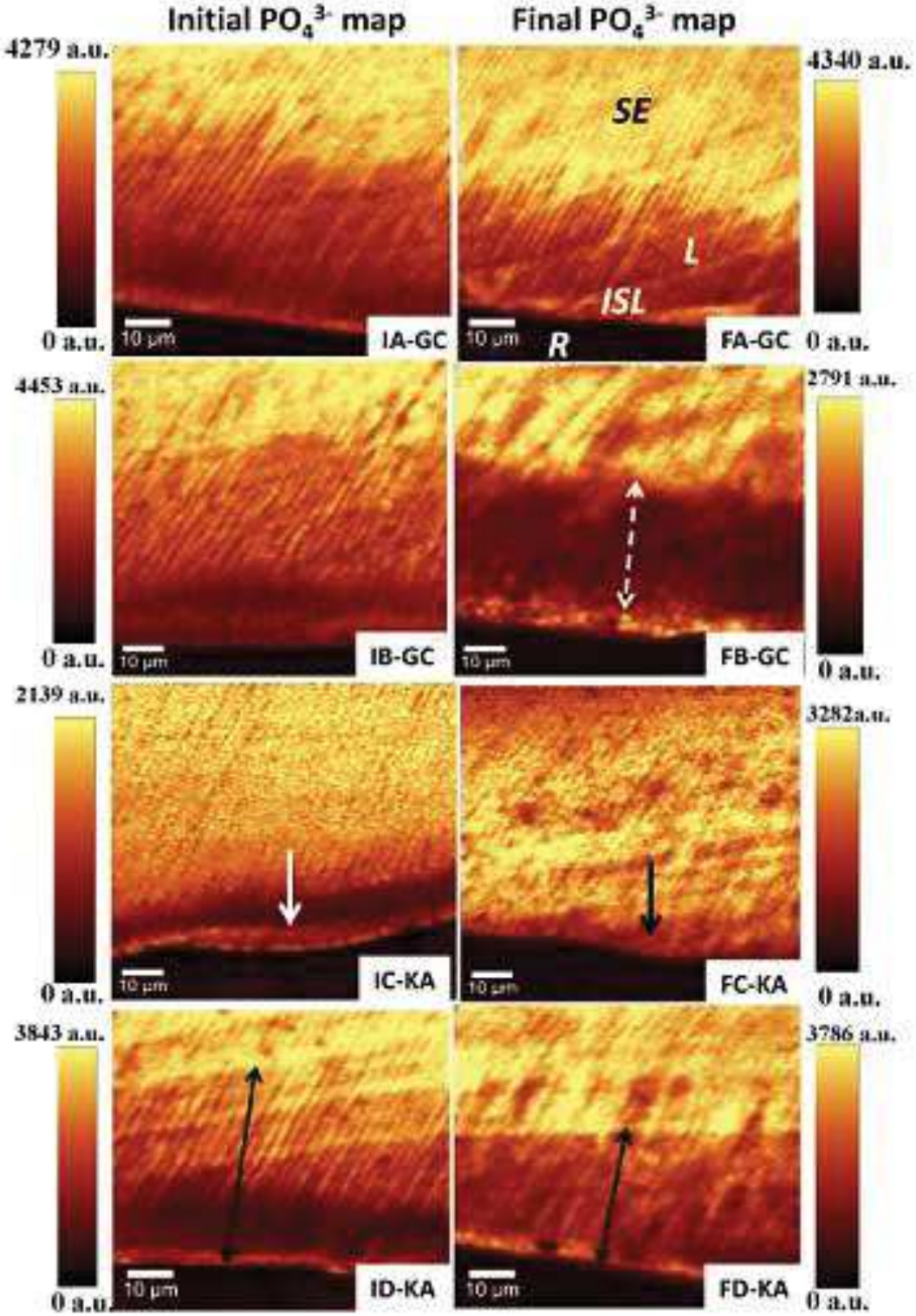

Figure 1. PO_4^{3-} maps of incipient lesions before & after treatment with remineraling agents. Indicative standardization bars on both sides demonstrate max. & min. values of PO_4^{3-} peak intensity at 960 cm^{-1}. **GC:** CPP-ACP tooth mousse. **KA:** KAREX (nHA containing-dentifrice). **I:** Initial. **F:** Final. Signs on Image (FA-GC) are valid for all images: **SE:** Sound Enamel, **L:** Lesion, **ISL:** Intact Surface Layer, **R:** Resin.

Data analysis verified that there were no significant differences ($p>0.05$) among the groups before and after treatment with CPP-ACP with respect to PO_4^{3-} intensity and enamel crystallinity in subsurface lesion & ISL zones (Fig.2A, B).

Analysis demonstrated that nHA containing-dentifrice significantly ($p<0.05$) promoted mineral gain in the enamel subsurface lesion and ISL areas (Fig.2C). However, no significant differences were noticed among the treatment groups with regard to enamel crystallinity (Fig.2D).

Correlated influence of CPP-ACP & nHA containing-dentifrice on the subsurface lesion and ISL areas are shown in (Fig.2E, F) to detect distinguished differences in their performance. The only significant difference was attained in respect to mineral gain in the body of lesions treated by dentifrice compared to the counterpart treated by CPP-ACP (Fig.2E). The statistical analysis showed no differences in the exerted effect of both products on mineral gain in ISL and on the degree of crystallinity in ISL and subsurface lesion zones (Fig.2E, F).

The rate of changes in phosphate intensity and FWHM value in ISL and subsurface lesion regions after treatment with remineralization agents are shown in (Table 1). The change in mineral gain proves that CPP-ACP exerted a minor reminerlizing effect on ISL of the lesion (+9.2%). While, mineral loss from the subsurface layer has detected after CPP-ACP application (-8.1%). nHA containing-dentifrice exhibits an important tendency to remineralizing subsurface lesions (+96.6%), and, to a lesser extent, ISL zone (+39.66). The table shows negative changes in FWHM value in ISL and subsurface lesion regions after treatment with remineralization agents; underlined an improvement in enamel crystallinity. CPP-ACP had a better effect on enamel texture than nHA containing-dentifrice.

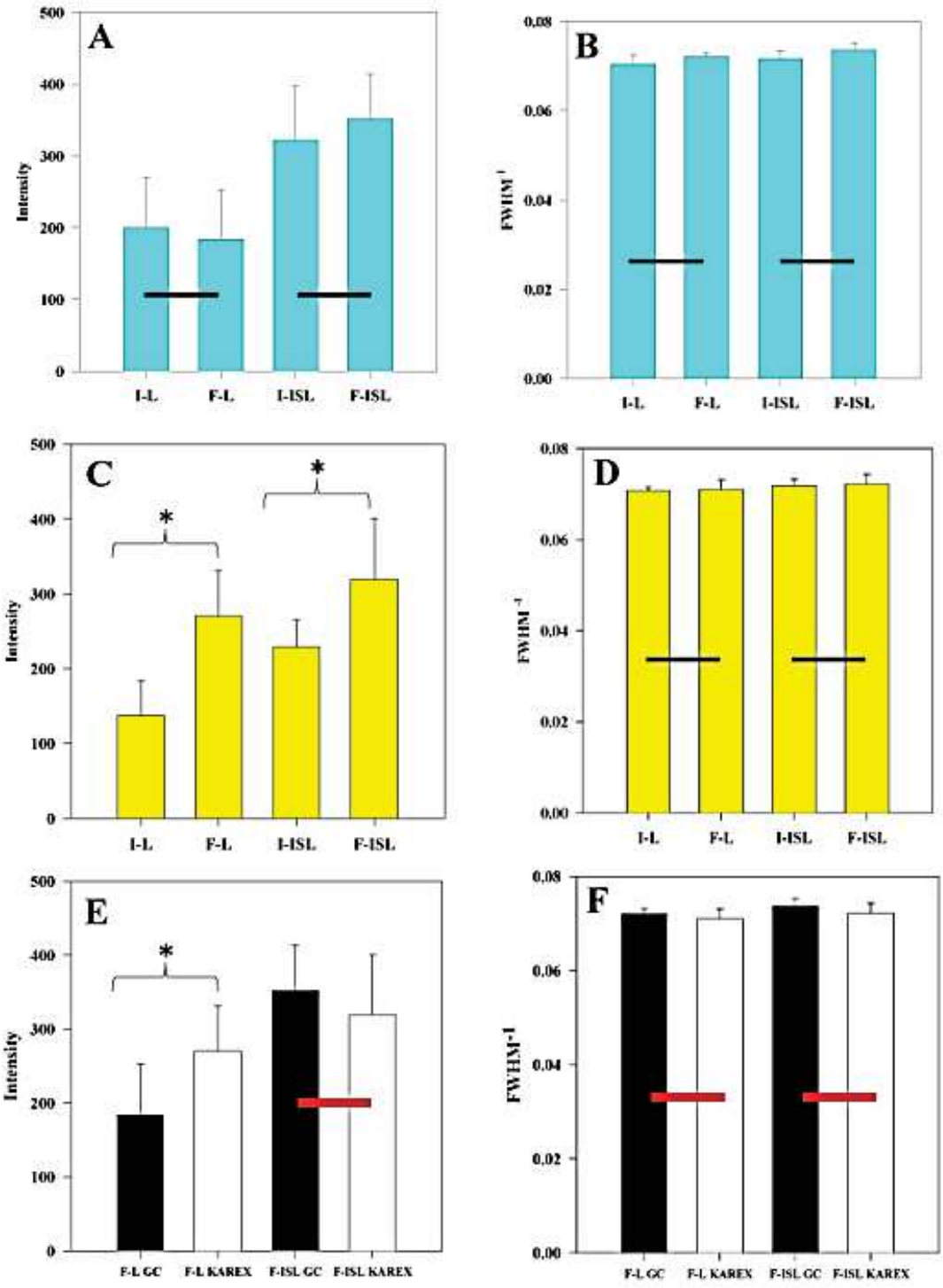

Figure 2. An overall mean and standard deviation (SD) were plotted to show: effect of: **(A)** CPP-ACP & **(C)** KAREX on PO_4^{3-} peak intensity at 960 cm^{-1}. Effect of: **(B)** CPP-ACP & **(D)** KAREX on enamel crystallinity represented by $FWHM^{-1}$ values. **(E&F)** Associating effect of CPP-ACP & KAREX on PO_4^{3-} peak intensity & $FWHM^{-1}$ respectively. Treatment effects of both agents were tested in **(L)** Lesion zone & **(ISL)** Intact Surface Lesion zone consecutively. **I:** Initial. **F:** Final. **GC:** CPP-ACP tooth mousse. **KAREX:** nHA containing-dentifrice. Asterisk (*) recurrently indicates a significant difference ($p< 0.05$) between the two groups. Horizontal bar indicates no significant difference ($p> 0.05$) among the groups linked by it.

5.4 DISCUSSION

Non-invasive management of non-cavitated caries lesions represents an essential goal of modern dentistry, involving remineralization systems to repair the enamel with bioavailable calcium & phosphate ions. The CPP acts as a delivery vehicle to co-localize bioavailable calcium and phosphate ions at the tooth surface. It can adapt its conformation to a wide range of surfaces, including the amorphous phases, thereby binding spontaneously forming clusters of calcium phosphate ions in a metastable solution, preventing their growth to the critical size required for nucleation (Reynolds 1998). The mechanism of action of CPP-ACP needs to be considered at a location inside the subsurface lesion, as well as at the surface of the lesion. The CPP-ACP has been determined to be amorphous electroneutral nanocomplexes with a hydrodynamic radius of 1.53 ± 0.04 nm (Cross et al. 2005). From the size and electroneutrality of the nanocomplexes, it would be predictable that they would enter the porosities of demineralized enamel and diffuse down concentrated ingredients into the lesion body. The released calcium, phosphate ions at the enamel surface will participate in a variety of equilibrium to form a range of calcium phosphate species, depending on the pH (Cochrane et al. 2008).

The process of diffusion into a subsurface lesion must be an overall electro neutral process. Therefore, diffusion potential into an enamel subsurface lesion can be characterized by the active ingredients of the neutral ion pair, $CaHPO_4^0$, diffuses down its ingredients into the lesion (Cochrane et al. 2008; Reynolds 1997). Once present in the enamel subsurface lesion, the CPP-ACP would release the weakly bound calcium and phosphate ions (Cochrane and Reynolds 2009; Cross et al. 2005), which would then deposit into crystal voids, promoting crystal growth at the hydroxyapatite (001) plane or along the c-axis; resulting in strengthening and widening of enamel rods (Brés et al. 1993). The CPPs have a high binding affinity for apatite (Cross et al.

2007b); therefore, on entering the lesion, the CPPs would bind to the more thermodynamically favored surface of an apatite crystal face. Hence, the release of bioavailable ions would be thermodynamically driven. This theory could explain the negative change in FWHM value illustrated by Table 1, where the reduced width of the phosphate band after treatment with CPP-ACP reflects a minor enhancement in enamel crystalline configuration.

However, supersaturation with respect to HA in which no spontaneous precipitation occurs, can't be expected to exist for a long period. After the contact between enamel apatite and the supersaturated solution; the mineral formation by growth of existing, partly demineralized crystals, largely reduces the supersaturation level in a way that a spontaneous nucleation is unlikely to occur (Larsen and Fejerkov 1989; Larsen and Jensen 1986). This could explicate the limited influence of remineralizing agents on enamel crystallinity reconstitution (Fig.2B, D).

Since the degree of hard tissue mineralization is directly related to phosphate sum-intensity (Akkus et al. 2016); Raman phosphate maps can show that CPP-ACP has a slight remineralization effect on ISL. Whereas, the dashed line in image (FB-GC, Fig.1); depicts an undesirable change in the mineral content of the subsurface layer (-8.1%). Previous studies (Arends 1980; Silverstone et al. 1981) indicated that mineral deposition is most easily formed superficially; making surface layer of the lesion appears harder and glossy. While the subsurface porous, demineralized part of the lesion remains unaltered, explaining why a proper remineralization of body of the lesion, rarely occurs (Fig.1, FB-GC).

Larsen (Larsen and Fejerkov 1989) (one of the pioneers in remineralization research), tested the results of enamel powder produced from intact teeth, suspended in remineralizing solutions. A reduction in pH value was observed during apatite formation because almost all phosphate in the aqueous phase prior to precipitation is in the form of H_3PO_4, $H_2PO_4^-$ and HPO_4^{2-} while the same

phosphate after the uptake in the apatite is mostly in the PO_4^{3-} form according to the following reaction (Larsen and Jensen 1986):

$$10\ Ca^{+2} + 3HPO_4^{2-} + 3H_2PO_4^{-} + 2\ H_2O \longrightarrow 2\ Ca_5(PO_4)_3OH + 11\ H^{+}$$

The released H^+ ions cause the pH to drop. The simultaneous pH decrease inhibits precipitation of calcium and phosphate in the aqueous phase, but it has a solubilizing effect on the enamel mineral (Larsen 1986a). This could explain the reduced amount of mineral that has been detected in subsurface lesions being treated with CPP-ACP. The impaired effect of CPP-ACP reported in this study is in accordance with previous observations stated in several clinical studies (Andersson et al. 2007; Bailey et al. 2009; Beerens et al. 2010; Bröchner et al. 2011), conducted to detect remineralizing effect of CPP-ACP cream *in vivo*. They failed to show any significant benefit of this product in reversing WSLs noninvasively. Even though, absence of effects might be due to ineffectiveness of this agent or insufficient sample sizes to detect significant differences. Thus, further researches to verify the efficacy of this combined therapy would be beneficial.

Nevertheless, the current findings seem to be inconsistent with those reported in former *in vitro* studies, tested effect of ion composition of CPP-ACP solutions on subsurface enamel lesion restoration. (Cochrane et al. 2008; Reynolds 1997) have demonstrated that CPP-ACP can promote remineralization of subsurface enamel lesions. The fact that they tested the effect of CPP-ACP solutions, while our current study has examined the remineralizing effect of CPP-ACP topical cream assigned to in-office/at home application could stand behind this discrepancy. Solutions are less viscous than creams, thus, better diffusion is predictable since viscosity is inversely proportional to the diffusivity (Stylianopoulos et al. 2010).

The surface chemical properties and morphological structure of nHA, combined with its chemical and physical similarity with natural enamel, have been claimed to play an important role in the remineralization of early caries lesions (Li et al. 2008). Many factors increased the potential of nHA to fill up defects and micropores on demineralized enamel such as increased surface area, increased proportion of atomicity, solubility properties of nHA (Kaehler 1994). When nHA penetrates the enamel pores, it will act as a template in the precipitation process. Thereby, it will constantly attract large amounts of Ca^{2+} and PO_4^{3-} from the remineralization solution to the enamel surface to fill the vacant positions of the enamel crystals. This in turn will reinforce crystal integrity and growth (Huang et al., 2009). Consequently, the deposition of nHA on outer enamel layer would probably block surface pores and restrict diffusion into subsurface lesion over the short-term remineralization. However, nHA is progressively transferred from the newly sediment apatite coating to inward. Finally, it is precipitated in the body of subsurface lesion in the long-term remineralization (Jongebloed and Arends 1981; Najibfard et al. 2011).

It is noteworthy that nHA containing-dentifrice has been tested in this study. Its influence was found to be superior to the CPP-ACP paste regarding to subsurface lesions remineralizatiion (Fig.2E). Phosphate maps in Fig.1A, B affirm that CPP-ACP has limited remineralizing influence on the body of lesion. Contrary to nHA containing-dentifrice (Fig.1C, D) which has triggered a patent remineralization of subsurface lesions (+96.6%).

Viscosity test confirmed that CPP-ACP cream is more viscous than nHA containing-dentifrice (2665 P versus 1846.65 P, respectively). As viscosity is inversely proportional to the diffusivity, diffusion process represents a limiting factor in the subsurface lesion remineralization (Arends 1980; Stylianopoulos et al. 2010). Consequently, nHA containing-dentifrice produced more profound remineralizaton of subsurface lesion thanks to its lower viscosity and thus better ionic

diffusion rates. Therefore, viscosity of the tested pastes could be considered as a key factor that might explain the discrepancy in their treating effect.

Fig.2 (A & C) describes the quantity of phosphate component; confirms that the outermost layers of teeth used to assess nHA containing-dentifrice capability; were basically less mineralized and thus more porous, than surface layers of teeth implicated in testing CPP-ACP efficacy. For mineral deposition to occur within the body of the lesion, calcium and phosphate ions must first penetrate enamel surface. Therefore, the presence of relatively mineralized and charged surface layer covering severely porous underlying enamel may result in restricted permeability of the ions and ion pairs necessary for mineral formation and subsequent underlying layer remineralization (Larsen and Fejerskov, 1989). In addition, the large variations in enamel chemical composition with respect to concentrated ingredients of specific mineral ions are therefore likely to result in large local variations in rates of both demineralization and remineralization (Robinson 1983; Robinson et al. 1971; Weatherell et al. 1968).

Remineralization systems represent a major advance in non-invasive treatment of incipient caries lesions. However, further studies of the biomimetic molecules involved in calcium, phosphate stabilization and nucleation may provide further improvements in the development of novel remineralization technologies.

5.5 CONCLUSION

CPP-ACP effect is confined to ISL making it a less permeable layer. These results are inconsistent with the proposed anticariogenic mechanism of the CPP, which is enhancement of remineralization through the localization of ACP at tooth surface. In addition, nHA containing - dentifrice has the potential to remineralize the whole lesion consistently. The study indicated a lack of reliable evidence supporting the effectiveness of remineralizing agents in WSLs

treatment. Likewise, de novo formation of crystals in body of the lesions remains an entirely unsolved problem. Largely, the present study points out that viscosity of the remineralizing material with enamel surface layer permeability represent serious obstacles to remineralization.

Remineralizing agent plus affected zone	Rate of change in PO_4^{3-} intensity	Rate of change in FWHM
CPP-ACP (ISL)	+9.20 %	-2.60 %
nHA based-dentifrice (ISL)	+39.66 %	-0.49 %
CPP-ACP (Body of lesion)	-8.12 %	-2.28 %
nHA based-dentifrice (Body of lesion)	+96.60 %	-0.31 %

Table 1 shows the rate of change in phosphate intensity & full-width at half-maximum (FWHM) values after treatment with different remineralizing agents estimated by special equation. **ISL:** Intact Surface Layer.

REFERENCES

Akkus A, Akkus A, Roperto R, Akkus O, Porto T, Teich S, Lang L. 2016. Evaluation of mineral content in healthy permanent human enamel by raman spectroscopy. Journal of clinical and experimental dentistry. 8(5):e546.

Al-Obaidi R, Salehi H, Desoutter A, Bonnet L, Etienne P, Terrer E, Jacquot B, Levallois B, Tassery H, Cuisinier F. 2018. Chemical & nano-mechanical study of artificial human enamel subsurface lesions. Scientific reports. 8(1):4047.

Alfano R, Yao S. 1981. Human teeth with and without dental caries studied by visible luminescent spectroscopy. Journal of dental research. 60(2):120-122.

Alsayed EZ, Hariri I, Nakashima S, Shimada Y, Bakhsh TA, Tagami J, Sadr A. 2016. Effects of coating materials on nanoindentation hardness of enamel and adjacent areas. Dental Materials. 32(6):807-816.

Amjad Z, Koutsoukos P, Nancollas G. 1981. The mineralization of enamel surfaces. A constant composition kinetics study. Journal of dental research. 60(10):1783-1792.

Anderson M. 2001. Current concepts of dental caries and its prevention. Operative Dentistry.11-18.

Andersson A, Sköld-Larsson K, Haligren A, Petersson LG, Twetman S. 2007. Effect of a dental cream containing amorphous calcium phosphate complexes on white spot lesion regression assessed by laser fluorescence. Oral health & preventive dentistry. 5(3).

Ando M, Van Der Veen MH, Schemehorn BR, Stookey GK. 2001. Comparative study to quantify demineralized enamel in deciduous and permanent teeth using laser–and light–induced fluorescence techniques. Caries research. 35(6):464-470.

Angmar-Månsson B, Ten Bosch J. 1987. Optical methods for the detection and quantification of caries. Advances in dental research. 1(1):14-20.

Aoki H. 1991. Science and medical applications of hydroxyapatite. Ishiyaku Euroamerica.

Arends J. 1980. Remineralization of artificial enamel lesions in vitro. Caries research. 14(6):351-358.

Årtun J, Thylstrup A. 1989. A 3-year clinical and sem study of surface changes of carious enamel lesions after inactivation. American journal of orthodontics and dentofacial orthopedics. 95(4):327-333.

Arx T. 1993. Developmental disturbances of permanent teeth following trauma to the primary dentition. Australian dental journal. 38(1):1-10.

Bachmann L, Zezell DM, Ribeiro AdC, Gomes L, Ito AS. 2006. Fluorescence spectroscopy of biological tissues—a review. Applied Spectroscopy Reviews. 41(6):575-590.

Bailey D, Adams G, Tsao C, Hyslop A, Escobar K, Manton D, Reynolds E, Morgan M. 2009. Regression of post-orthodontic lesions by a remineralizing cream. Journal of dental research. 88(12):1148-1153.

Batchelar DL, Davidson M, Dabrowski W, Cunningham IA. 2006. Bone-composition imaging using coherent-scatter computed tomography: Assessing bone health beyond bone mineral density. Medical physics. 33(4):904-915.

Beerens M, Van Der Veen M, Van Beek H, Ten Cate J. 2010. Effects of casein phosphopeptide amorphous calcium fluoride phosphate paste on white spot lesions and dental plaque after orthodontic treatment: A 3-month follow-up. European journal of oral sciences. 118(6):610-617.

Benedict H. 1928. Note on fluorescence of teeth in ultraviolet rays. Science. 67:442.

Benedict H. 1929. The fluorescence of teeth as another method of attack on the problem of dental caries. J Dent Res. 9:274-275.

Bergstrand F, Twetman S. 2011. A review on prevention and treatment of post-orthodontic white spot lesions–evidence-based methods and emerging technologies. The open dentistry journal. 5(1).

Bishara SE, Ostby AW. 2008. White spot lesions: Formation, prevention, and treatment. Seminars in Orthodontics. 14(3):174-182.
Bjelkhagen H. 1982. Early detection of enamel caries by the luminescence excited by visible laser light. Swed Dent J. 6(1):1-7.
Björkman UH, Sundström F, ten Bosch JJ. 1991. Fluorescence in dissolved fractions of human enamel. Acta Odontologica Scandinavica. 49(3):133-138.
Booij M, Ten Bosch J. 1982. A fluorescent compound in bovine dental enamel matrix compared with synthetic dityrosine. Archives of oral biology. 27(5):417-421.
Boyd R. 1992. Nonlinear optics. 1992. New York: Academic Press.
Brés E, Steuer P, VOEGEL JC, Frank R, Cuisinier F. 1993. Observation of the loss of the hydroxyapatite sixfold symmetry in a human fetal tooth enamel crystal. Journal of microscopy. 170(2):147-154.
Brès E, Voegel JC, Frank R. 1990. High-resolution electron microscopy of human enamel crystals. Journal of microscopy. 160(2):183-201.
Bröchner A, Christensen C, Kristensen B, Tranæus S, Karlsson L, Sonnesen L, Twetman S. 2011. Treatment of post-orthodontic white spot lesions with casein phosphopeptide-stabilised amorphous calcium phosphate. Clinical oral investigations. 15(3):369-373.
Cate JT. 1990. In vitro studies on the effects of fluoride on de-and remineralization. Journal of dental research. 69(2_suppl):614-619.
Chan YL, Ngan AH, King NM. 2011. Nano-scale structure and mechanical properties of the human dentine-enamel junction. Journal of the mechanical behavior of biomedical materials. 4(5):785-795.
Chatterjee R, Kleinberg I. 1979. Effect of orthodontic band placement on the chemical composition of human incisor tooth plaque. Archives of oral biology. 24(2):97-100.
Chen H, Liu X, Dai J, Jiang Z, Guo T, Ding Y. 2013. Effect of remineralizing agents on white spot lesions after orthodontic treatment: A systematic review. American journal of orthodontics and dentofacial orthopedics. 143(3):376-382. e373.
Chen S-Y, Hsu C-YS, Sun C-K. 2008. Epi-third and second harmonic generation microscopic imaging of abnormal enamel. Optics express. 16(15):11670-11679.
Cloitre T, Panayotov IV, Tassery H, Gergely C, Levallois B, Cuisinier FJ. 2013. Multiphoton imaging of the dentine-enamel junction. Journal of biophotonics. 6(4):330-337.
Cochrane N, Reynolds E. 2009. Casein phosphopeptides in oral health. Food constituents and oral health. Elsevier. p. 185-224.
Cochrane N, Saranathan S, Cai F, Cross K, Reynolds E. 2008. Enamel subsurface lesion remineralisation with casein phosphopeptide stabilised solutions of calcium, phosphate and fluoride. Caries research. 42(2):88-97.
Cross K, Huq N, Reynolds E. 2007a. Casein phosphopeptides in oral health-chemistry and clinical applications. Current pharmaceutical design. 13(8):793-800.
Cross KJ, Huq NL, O'Brien-Simpson NM, Perich JW, Attard TJ, Reynolds EC. 2007b. The role of multiphosphorylated peptides in mineralized tissue regeneration. International Journal of Peptide Research and Therapeutics. 13(4):479-495.
Cross KJ, Huq NL, Palamara JE, Perich JW, Reynolds EC. 2005. Physicochemical characterization of casein phosphopeptide-amorphous calcium phosphate nanocomplexes. Journal of Biological Chemistry. 280(15):15362-15369.
Cury JA, Tenuta LMA. 2009. Enamel remineralization: Controlling the caries disease or treating early caries lesions? Brazilian Oral Research. 23:23-30.
Curzon MEJ FJ. 1983. Chemical composition of enamel. (ed) LE, editor.
Cuy JL, Mann AB, Livi KJ, Teaford MF, Weihs TP. 2002. Nanoindentation mapping of the mechanical properties of human molar tooth enamel. Archives of oral biology. 47(4):281-291.

Damen J, Exterkate R, Ten Cate J. 1997. Reproducibility of tmr for the determination of longitudinal mineral changes in dental hard tissues. Advances in dental research. 11(4):415-419.

De Jong EdJ, Sundström F, Westerling H, Tranaeus S, Ten Bosch J, Angmar-Månsson B. 1995. A new method for in vivo quantification of changes in initial enamel caries with laser fluorescence. Caries research. 29(1):2-7.

De Jong EdJ, Ten Bosch J. 1985. Error analysis of the microradiographic determination of mineral content in mineralised tissue slices. Physics in medicine and biology. 30(10):1067.

Denk W, Strickler JH, Webb WW. 1990. Two-photon laser scanning fluorescence microscopy. Science. 248(4951):73-76.

Derks A, Katsaros C, Frencken J, Van't Hof M, Kuijpers-Jagtman A. 2004. Caries-inhibiting effect of preventive measures during orthodontic treatment with fixed appliances. Caries research. 38(5):413-420.

Dickinson M, Wolf K, Mann A. 2007. Nanomechanical and chemical characterization of incipient in vitro carious lesions in human dental enamel. Archives of oral biology. 52(8):753-760.

Eastoe J. 1960. Organic matrix of tooth enamel. Nature. 187(4735):411.

Elfallah HM, Bertassoni LE, Charadram N, Rathsam C, Swain MV. 2015. Effect of tooth bleaching agents on protein content and mechanical properties of dental enamel. Acta biomaterialia. 20:120-128.

Everall NJ. 2009. Confocal raman microscopy: Performance, pitfalls, and best practice. Applied spectroscopy. 63(9):245A-262A.

Featherstone J. 2004a. The continuum of dental caries—evidence for a dynamic disease process. Journal of dental research. 83(suppl 1):C39-C42.

Featherstone J. 2004b. The continuum of dental caries—evidence for a dynamic disease process. Journal of dental research. 83(1_suppl):39-42.

Featherstone J, Duncan J, Cutress T. 1979. A mechanism for dental caries based on chemical processes and diffusion phenomena during in-vitro caries simulation on human tooth enamel. Archives of oral biology. 24(2):101-112.

Featherstone J, Lussi A. 2006. Understanding the chemistry of dental erosion. Dental erosion. Karger Publishers. p. 66-76.

Featherstone J, O'reilly M, Shariati M, Brugler S. 1986. Enhancement of remineralization in vitro and in vivo. Factors relating to demineralisation and remineralisation of the teeth. IRL Press. Oxford and Washington.

Featherstone J, Ten Cate J, Shariati M, Arends J. 1983. Comparison of artificial caries-like lesions by quantitative microradiography and microhardness profiles. Caries research. 17(5):385-391.

Featherstone JD. 1995. Clinical aspects of de/remineralization of teeth. International Association for Dental Research.

Fejerskov O. 1997. Concepts of dental caries and their consequences for understanding the disease. Community dentistry and oral epidemiology. 25(1):5-12.

Fejerskov O, Johnson N, Silverstone L. 1974. The ultrastructure of fluorosed human dental enamel. European journal of oral sciences. 82(5):357-372.

Fejerskov O, Nyvad B. 2003. Is dental caries an infectious disease? Diagnostic and treatment consequences for the practitioner. Nordic dentistry 2003 yearbook. Quintessence Publishing Co, Ltd. p. 141-152.

Ferrar J, Nakamoto K. 1994. Introductory raman spectroscopy. Acad. Press, inc. Harcourt Brace and Comp., Publishers, Boston–San Diego–NY–London–Sudney–Tokio–Toronto.

Gallagher RR, Balooch M, Balooch G, Wilson RS, Marshall SJ, Marshall GW. 2010. Coupled nanomechanical and raman microspectroscopic investigation of human third molar dej. Journal of dental biomechanics. 2010.

Gibson EA, Masihzadeh O, Lei TC, Ammar DA, Kahook MY. 2011. Multiphoton microscopy for ophthalmic imaging. Journal of ophthalmology. 2011.

Gilchrist F, Santini A, Harley K, Deery C. 2007. The use of micro-raman spectroscopy to differentiate between sound and eroded primary enamel. International journal of paediatric dentistry. 17(4):274-280.

Gorelick L, Geiger AM, Gwinnett AJ. 1982. Incidence of white spot formation after bonding and banding. American journal of orthodontics. 81(2):93-98.

Grasselli JG, Bulkin BJ. 1991. Analytical raman spectroscopy. Wiley.

Gwinnett AJ, Ceen RF. 1979. Plaque distribution on bonded brackets: A scanning microscope study. American journal of orthodontics. 75(6):667-677.

Hadler-Olsen S, Sandvik K, El-Agroudi MA, Øgaard B. 2011. The incidence of caries and white spot lesions in orthodontically treated adolescents with a comprehensive caries prophylactic regimen—a prospective study. The European Journal of Orthodontics. 34(5):633-639.

Haines D. 1968. Physical properties of human tooth enamel and enamel sheath material under load. Journal of biomechanics. 1(2):117IN17119-17118IN22125.

Hall A, Girkin J. 2004. A review of potential new diagnostic modalities for caries lesions. Journal of dental research. 83(1_suppl):89-94.

Hannig C, Hamkens A, Becker K, Attin R, Attin T. 2005. Erosive effects of different acids on bovine enamel: Release of calcium and phosphate in vitro. Archives of oral biology. 50(6):541-552.

He B, Huang S, Jing J, Hao Y. 2010. Measurement of hydroxyapatite density and knoop hardness in sound human enamel and a correlational analysis between them. Archives of oral biology. 55(2):134-141.

He L-H, Swain MV. 2009. Enamel—a functionally graded natural coating. Journal of dentistry. 37(8):596-603.

Helmchen F, Denk W. 2005. Deep tissue two-photon microscopy. Nature methods. 2(12):932.

Herzberg G. 1945. Infrared and raman spectra of polyatomic molecules. D. Van Nostrand Company.; New York.

Hicks J, Garcia-Godoy F, Flaitz C. 2005. Biological factors in dental caries enamel structure and the caries process in the dynamic process of demineralization and remineralization (part 2). Journal of clinical pediatric dentistry. 28(2):119-124.

Hollander F. 1935. The apparent radiopaque surface layer of the enamel. Dent Cosmos. 77:1187-1197.

Hsu DJ, Darling CL, Lachica MM, Fried D. 2008. Nondestructive assessment of the inhibition of enamel demineralization by co2 laser treatment using polarization sensitive optical coherence tomography. Journal of biomedical optics. 13(5):054027-054027-054029.

Huang S, Gao S, Yu H. 2009. Effect of nano-hydroxyapatite concentration on remineralization of initial enamel lesion in vitro. Biomedical Materials. 4(3):034104.

Huang TT, Jones AS, He LH, Darendeliler MA, Swain MV. 2007. Characterisation of enamel white spot lesions using x-ray micro-tomography. Journal of dentistry. 35(9):737-743.

Huminicki A, Dong C, Cleghorn B, Sowa M, Hewko M, Choo-Smith L-. 2010. Determining the effect of calculus, hypocalcification, and stain on using optical coherence tomography and polarized raman spectroscopy for detecting white spot lesions. International journal of dentistry. 2010.

Ichim I, Li Q, Li W, Swain M, Kieser J. 2007. Modelling of fracture behaviour in biomaterials. Biomaterials. 28(7):1317-1326.

Biostatgv. 2000. [accessed]. https://marne.u707.jussieu.fr/biostatgv.

Ismail A, Sohn W, Tellez M, Amaya A, Sen A, Hasson H, Pitts N. 2007. The international caries detection and assessment system (icdas): An integrated system for measuring dental caries. Community dentistry and oral epidemiology. 35(3):170-178.

Jiang W, Cao W. 2004. Second harmonic generation of shear waves in crystals. ieee transactions on ultrasonics, ferroelectrics, and frequency control. 51(2):153-162.
Jongebloed W, Arends J. 1981. Remineralization of artificial enamel lesions in vitro. Caries research. 15(1):60-69.
Kaehler T. 1994. Nanotechnology: Basic concepts and definitions. Clinical chemistry. 40(9):1797-1799.
KANI T, KANI M, ISOZAKI A, SHINTANI H, OHASHI T, TOKUMOTO T. 1989. Effect to apatite-containing dentifrices on dental caries in school children. Journal of Dental Health. 39(1):104-109.
Kawasaki K, Buchanan AV, Weiss KM. 2009. Biomineralization in humans: Making the hard choices in life. Annual review of genetics. 43:119-142.
Kidd EA, Nyvad B, Espelid I. 2008. Caries control for the individual patient. Dental caries. Blackwell Publishing Ltd. p. 487-504.
Koenig K, Schneckenburger H. 1994. Laser-induced autofluorescence for medical diagnosis. Journal of fluorescence. 4(1):17-40.
Lang NP, Hotz PR, Gusberti FA, Joss A. 1987. Longitudinal clinical and microbiological study on the relationship between infection with streptococcus mutans and the development of caries in humans. Molecular Oral Microbiology. 2(1):39-47.
Larsen M. 1986a. An investigation of the theoretical background for the stability of the calcium-phosphate salts and their mutual conversion in aqueous solutions. Archives of oral biology. 31(11):757-761.
Larsen M. 1986b. The nature of early caries lesions in enamel. Journal of dental research. 65(7):1030.
Larsen MJ. 1974. Chemically induced in vitro lesions in dental enamel. European journal of oral sciences. 82(7):496-509.
Larsen MJ, Fejerkov O. 1989. Chemical and structural challenges in remineralization of dental enamel lesions. European journal of oral sciences. 97(4):285-296.
Larsen MJ, Jensen S. 1986. Solubility study of the initial formation of calcium orthophosphates from aqueous solutions at ph 5–10. Archives of oral biology. 31(9):565-572.
Legeros RZ, Trautz OR, Legeros JP, Klein E, Shirra WP. 1967. Apatite crystallites: Effects of carbonate on morphology. Science. 155(3768):1409-1411.
Leventouri T, Chakoumakos B, Papanearchou N, Perdikatsis V. 2001. Comparison of crystal structure parameters of natural and synthetic apatites from neutron powder diffraction. Journal of materials research. 16(9):2600-2606.
Lewis IR, Edwards H. 2001. Handbook of raman spectroscopy: From the research laboratory to the process line. CRC Press.
Li L, Pan H, Tao J, Xu X, Mao C, Gu X, Tang R. 2008. Repair of enamel by using hydroxyapatite nanoparticles as the building blocks. Journal of Materials Chemistry. 18(34):4079-4084.
Lin P-Y, Lyu H-C, Hsu C-YS, Chang C-S, Kao F-J. 2011. Imaging carious dental tissues with multiphoton fluorescence lifetime imaging microscopy. Biomedical optics express. 2(1):149-158.
Lin S-J, Wu R-J, Tan H-Y, Lo W, Lin W-C, Young T-H, Hsu C-J, Chen J-S, Jee S-H, Dong C-Y. 2005. Evaluating cutaneous photoaging by use of multiphoton fluorescence and second-harmonic generation microscopy. Optics letters. 30(17):2275-2277.
Liu Y, Hsu C-YS. 2007. Laser-induced compositional changes on enamel: A ft-raman study. Journal of dentistry. 35(3):226-230.
Lo E, Zhi Q, Itthagarun A. 2010. Comparing two quantitative methods for studying remineralization of artificial caries. Journal of dentistry. 38(4):352-359.
Lopes CB, Pacheco M, Silveira Jr L, Duarte J, Cangussu MCT, Pinheiro A. 2007. The effect of the association of nir laser therapy bmps, and guided bone regeneration on tibial fractures treated with wire osteosynthesis: Raman spectroscopy study. Journal of Photochemistry and Photobiology B: Biology. 89(2-3):125-130.

Lucchese A, Gherlone E. 2012. Prevalence of white-spot lesions before and during orthodontic treatment with fixed appliances. European journal of orthodontics. 35(5):664-668.
Lussi A, Hibst R, Paulus R. 2004. Diagnodent: An optical method for caries detection. Journal of dental research. 83(1_suppl):80-83.
Lyubchanskii I, Dadoenkova N, Lyubchanskii M, Rasing T, Jeong J-W, Shin S-C. 2000. Second-harmonic generation from realistic film–substrate interfaces: The effects of strain. Applied Physics Letters. 76(14):1848-1850.
Manesh SK, Darling CL, Fried D. 2009. Nondestructive assessment of dentin demineralization using polarization-sensitive optical coherence tomography after exposure to fluoride and laser irradiation. Journal of Biomedical Materials Research Part B: Applied Biomaterials. 90(2):802-812.
Martinović BT, Ivanović M, Milosavljević Z, Mladenović R. 2015. Identifying basic chemical elements of hypomineralized enamel in first permanent molars. Vojnosanitetski pregled. 72(10).
McKee M, Addison W, Kaartinen M. 2005. Hierarchies of extracellular matrix and mineral organization in bone of the craniofacial complex and skeleton. Cells Tissues Organs. 181(3-4):176-188.
Mehta R, Nandlal B, Prashanth S. 2013. Comparative evaluation of remineralization potential of casein phosphopeptide-amorphous calcium phosphate and casein phosphopeptide-amorphous calcium phosphate fluoride on artificial enamel white spot lesion: An in vitro light fluorescence study. Indian journal of dental research. 24(6):681.
Mendes FM, Pinheiro SL, Bengtson AL. 2004. Effect of alteration in organic material of the occlusal caries on diagnodent readings. Brazilian Oral Research. 18(2):141-144.
Mohanty B, Dadlani D, Mahoney D, Mann AB. 2013. Characterizing and identifying incipient carious lesions in dental enamel using micro-raman spectroscopy. Caries research. 47(1):27-33.
Moron BM, Comar LP, Wiegand A, Buchalla W, Yu H, Buzalaf MA, Magalhaes AC. 2013. Different protocols to produce artificial dentine carious lesions in vitro and in situ: Hardness and mineral content correlation. Caries research. 47(2):162-170.
Najibfard K, Ramalingam K, Chedjieu I, Amaechi B. 2011. Remineralization of early caries by a nano-hydroxyapatite dentifrice. Journal of Clinical Dentistry. 22(5):139.
Odutuga A, Prout R. 1974. Lipid analysis of human enamel and dentine. Archives of oral biology. 19(8):729-731.
Øgaard B, Rølla G, Arends J. 1988. Orthodontic appliances and enamel demineralization: Part 1. Lesion development. American journal of orthodontics and dentofacial orthopedics. 94(1):68-73.
Oheim M, Michael DJ, Geisbauer M, Madsen D, Chow RH. 2006. Principles of two-photon excitation fluorescence microscopy and other nonlinear imaging approaches. Advanced drug delivery reviews. 58(7):788-808.
Oliver W. 1992. Wc oliver and gm pharr, j. Mater. Res. 7, 1564 (1992). J Mater Res. 7:1564.
Oliver WC, Pharr GM. 1992. An improved technique for determining hardness and elastic modulus using load and displacement sensing indentation experiments. Journal of materials research. 7(6):1564-1583.
Oliver WC, Pharr GM. 2004. Measurement of hardness and elastic modulus by instrumented indentation: Advances in understanding and refinements to methodology. Journal of materials research. 19(01):3-20.
Pharr G, Bolshakov A. 2002. Understanding nanoindentation unloading curves. Journal of materials research. 17(10):2660-2671.
Pinheiro AL, Lopes CB, Pacheco MT, Brugnera Jr A, Zanin FAA, Cangussú MCT, Silveira Jr L. 2010. Raman spectroscopy validation of diagnodent-assisted fluorescence readings on tibial fractures treated with laser phototherapy, bmps, guided bone regeneration, and miniplates. Photomedicine and laser surgery. 28(S2):S-89-S-97.

Pitts N. 2004. Are we ready to move from operative to non-operative/preventive treatment of dental caries in clinical practice? Caries research. 38(3):294-304.
Pleshko N, Boskey A, Mendelsohn R. 1991. Novel infrared spectroscopic method for the determination of crystallinity of hydroxyapatite minerals. Biophysical journal. 60(4):786-793.
Popowics T, Rensberger J, Herring S. 2004. Enamel microstructure and microstrain in the fracture of human and pig molar cusps. Archives of oral biology. 49(8):595-605.
Pretty I, Ellwood R. 2013. The caries continuum: Opportunities to detect, treat and monitor the re-mineralization of early caries lesions. Journal of dentistry. 41:S12-S21.
Pucéat E, Reynard B, Lécuyer C. 2004. Can crystallinity be used to determine the degree of chemical alteration of biogenic apatites? Chemical Geology. 205(1):83-97.
Radlanski RJ, Renz H, Willersinn U, Cordis CA, Duschner H. 2001. Outline and arrangement of enamel rods in human deciduous and permanent enamel. 3d-reconstructions obtained from clsm and sem images based on serial ground sections. European journal of oral sciences. 109(6):409-414.
Reed R, Xu C, Liu Y, Gorski J, Wang Y, Walker M. 2015a. Radiotherapy effect on nano-mechanical properties and chemical composition of enamel and dentine. Archives of oral biology. 60(5):690-697.
Reed R, Xu C, Liu Y, Gorski JP, Wang Y, Walker MP. 2015b. Radiotherapy effect on nano-mechanical properties and chemical composition of enamel and dentine. Archives of oral biology. 60(5):690-697.
Reynolds E. 1997. Remineralization of enamel subsurface lesions by casein phosphopeptide-stabilized calcium phosphate solutions. Journal of dental research. 76(9):1587-1595.
Reynolds E, Del Rio A. 1984. Effect of casein and whey-protein solutions on caries experience and feeding patterns of the rat. Archives of oral biology. 29(11):927-933.
Reynolds E, Johnson I. 1981. Effect of milk on caries incidence and bacterial composition of dental plaque in the rat. Archives of oral biology. 26(5):445-451.
Reynolds EC. 1998. Anticariogenic complexes of amorphous calcium phosphate stabilized by casein phosphopeptides: A review. Special Care in Dentistry. 18(1):8-16.
Robinson C. 1983. Alterations in the composition of permanent human enamel during carious attack. Demineralisation and Remineralisation of the Teeth.209-223.
Robinson C, Shore R, Brookes S, Strafford S, Wood S, Kirkham J. 2000. The chemistry of enamel caries. Critical Reviews in Oral Biology & Medicine. 11(4):481-495.
Robinson C, Weatherell J, Hallsworth A. 1971. Variation in composition of dental enamel within thin ground tooth sections. Caries research. 5(1):44-57.
Roveri N, Battistella E, Bianchi CL, Foltran I, Foresti E, Iafisco M, Lelli M, Naldoni A, Palazzo B, Rimondini L. 2009. Surface enamel remineralization: Biomimetic apatite nanocrystals and fluoride ions different effects. Journal of Nanomaterials. 2009:8.
Salehi H, Derely L, Vegh AG, Durand JC, Gergely C, Larroque C, Fauroux MA, Cuisinier FJG. 2013. Label-free detection of anticancer drug paclitaxel in living cells by confocal raman microscopy. Applied Physics Letters. 102(11):113701.
Sato K. 2007. Mechanism of hydroxyapatite mineralization in biological systems. Journal of the Ceramic Society of Japan. 115(1338):124-130.
Sato Y, Sato T, Niwa M, Aoki H. 2006. Precipitation of octacalcium phosphates on artificial enamel in artificial saliva. Journal of Materials Science: Materials in Medicine. 17(11):1173-1177.
Silverstone L. 1983. Remineralization and enamel caries: New concepts. Dental Update. 10(4):261-273.
Silverstone L, Hicks M, Featherstone M. 1988. Dynamic factors affecting lesion initiation and progression in human dental enamel. Part i. The dynamic nature of enamel caries. Quintessence international (Berlin, Germany: 1985). 19(10):683.

Silverstone L, Wefel J, Zimmerman B, Clarkson B, Featherstone M. 1981. Remineraiization of natural and artificial lesions in human dental enamel in vitro. Caries research. 15(2):138-157.
Simmer J, Fincham A. 1995. Molecular mechanisms of dental enamel formation. Critical Reviews in Oral Biology & Medicine. 6(2):84-108.
Slimani A, Nouioua F, Desoutter A, Levallois B, Cuisinier FJG, Tassery H, Terrer E, Salehi H. 2017. Confocal raman mapping of collagen cross-link and crystallinity of human dentin-enamel junction. J Biomed Opt. 22(8):1-8.
Slimani A, Tardivo D, Panayotov IV, Levallois B, Gergely C, Cuisinier F, Tassery H, Cloitre T, Terrer E. 2018. Multiphoton microscopy for caries detection with icdas classification. Caries research. 52(5):359-366.
So PT, Dong CY, Masters BR, Berland KM. 2000. Two-photon excitation fluorescence microscopy. Annual review of biomedical engineering. 2(1):399-429.
Stookey GK. 2005. Quantitative light fluorescence: A technology for early monitoring of the caries process. Dental Clinics. 49(4):753-770.
Stylianopoulos T, Poh M-Z, Insin N, Bawendi MG, Fukumura D, Munn LL, Jain RK. 2010. Diffusion of particles in the extracellular matrix: The effect of repulsive electrostatic interactions. Biophysical journal. 99(5):1342-1349.
Summitt JB, Robbins JW, Hilton TJ, Schwartz RS. 2006. Fundamentals of operative dentistry: A contemporary approach. Quintessence Pub.
Sundström F, Fredriksson K, Montan S, Hafström-Björkman U, Ström J. 1985. Laser-induced fluorescence from sound and carious tooth substance: Spectroscopic studies. Swed Dent J. 9(2):71-80.
Tassery H, Levallois B, Terrer E, Manton D, Otsuki M, Koubi S, Gugnani N, Panayotov I, Jacquot B, Cuisinier F. 2013. Use of new minimum intervention dentistry technologies in caries management. Australian dental journal. 58(s1):40-59.
Ten BJ. 1991. A review of quantitative method for studies of mineral content of intra-oral incipient caries lesion. J Dent Res. 70:2-14.
Ten Bosch J. 1996. Light scattering and related methods in caries diagnosis. Early Detection of Dental Caries I.81-90.
Ten Cate J. 2008. Remineralization of deep enamel dentine caries lesions. Australian dental journal. 53(3):281-285.
Ten Cate J, Mundorff-Shrestha S. 1995. Working group report 1: Laboratory models for caries (in vitro and animal models). Advances in dental research. 9(3):332-334.
Torres CRG, Borges AB, Torres LMS, Gomes IS, de Oliveira RS. 2011. Effect of caries infiltration technique and fluoride therapy on the colour masking of white spot lesions. Journal of dentistry. 39(3):202-207.
Valeur B, Berberan-Santos MN. 2012. Molecular fluorescence: Principles and applications. John Wiley & Sons.
Vandiver J, Dean D, Patel N, Bonfield W, Ortiz C. 2005. Nanoscale variation in surface charge of synthetic hydroxyapatite detected by chemically and spatially specific high-resolution force spectroscopy. Biomaterials. 26(3):271-283.
Wang X-J, Milner TE, de Boer JF, Zhang Y, Pashley DH, Nelson JS. 1999. Characterization of dentin and enamel by use of optical coherence tomography. Applied Optics. 38(10):2092.
Weatherell I, Robinson C, Hiller C. 1968. Distribution of carbonate in thin sections of dental enamel. Caries research. 2(1):1-9.
Weatherell J. 1975. Composition of dental enamel. British medical bulletin. 31(2):115-119.
Wentrup-Byrne E, Armstrong CA, Armstrong RS, Collins BM. 1997. Fourier transform raman microscopic mapping of the molecular components in a human tooth. Journal of Raman Spectroscopy. 28(2-3):151-158.

White D. 1992. The comparative sensitivity of intra-oral, in vitro, and animal models in the'profile'evaluation of topical fluorides. Journal of dental research. 71.

White D. 1995. The application of in vitro models to research on demineralization and remineralization of the teeth. Advances in dental research. 9(3):175-193.

White S. 2004. Benign tumor of jaw. Oral radiology Principles and interpretation.410-458.

Xu C, Reed R, Gorski JP, Wang Y, Walker MP. 2012. The distribution of carbonate in enamel and its correlation with structure and mechanical properties. Journal of materials science. 47(23):8035-8043.

Xu C, Yao X, Walker MP, Wang Y. 2009. Chemical/molecular structure of the dentin–enamel junction is dependent on the intratooth location. Calcified tissue international. 84(3):221.

Yamagishi K, Onuma K, Suzuki T, Okada F, Tagami J, Otsuki M, Senawangse P. 2005. Materials chemistry: A synthetic enamel for rapid tooth repair. Nature. 433(7028):819.

Yokoyama E, Kakino S, Matsuura Y. 2008. Raman imaging of carious lesions using a hollow optical fiber probe. Applied Optics. 47(23):4227-4230.

Zipfel WR, Williams RM, Christie R, Nikitin AY, Hyman BT, Webb WW. 2003a. Live tissue intrinsic emission microscopy using multiphoton-excited native fluorescence and second harmonic generation. Proceedings of the National Academy of Sciences. 100(12):7075-7080.

Zipfel WR, Williams RM, Webb WW. 2003b. Nonlinear magic: Multiphoton microscopy in the biosciences. Nature biotechnology. 21(11):1369.

Zoumi A, Yeh A, Tromberg BJ. 2002a. Imaging cells and extracellular matrix in vivo by using second-harmonic generation and two-photon excited fluorescence. Proceedings of the National Academy of Sciences. 99(17):11014-11019.

Zoumi A, Yeh A, Tromberg BJ. 2002b. Imaging cells and extracellular matrix in vivo by using second-harmonic generation and two-photon excited fluorescence. P Natl Acad Sci USA. 99(17):11014-11019.

Chapter 6

Conclusion and perspective

Conclusion and perspective

The scope of this thesis was promotion of minimally invasive treatment system by identifying novel techniques in imaging the dental enamel, providing a detailed characterization of its organic and inorganic components to assist in early caries detection and tissue preservation.

In addition, the comparison of a modified in vitro caries induction system with an existing model showed that the modified system presents an adequate alternative to the later, in producing enamel subsurface lesions swiftly; that meet the whole criteria of natural incipient caries lesions.

Moreover, the chemical properties of nano-hydroxyapatite particles have been shown to play a significant role in remineralization of early caries lesions compared to the limited potential of casein phosphopeptides in localizing amorphous calcium phosphate at tooth surface. To add to that, the imaging systems used in this research have demonstrated the fundamental role of organic matrix in enamel integrity that must be taking into account to optimize the newly developed remineralizing dental products based on calcium phosphate salts. In sight of the results of this study, immense efforts are ongoing to develop new remineralization product based upon a peptide or a protein extracted from seashells. The new product should be of flowable consistency to overcome the problem of viscous, thickened materials that restricts their penetration inside enamel to diffuse their active ingredients and to compensate for the loss in enamel composition.

APPENDICES

Article 1

SCIENTIFIC REPORTS

OPEN

Chemical & Nano-mechanical Study of Artificial Human Enamel Subsurface Lesions

Received: 8 November 2017
Accepted: 22 February 2018
Published online: 06 March 2018

R. Al-Obaidi[1], H. Salehi[1], A. Desoutter[1], L. Bonnet[3], P. Etienne[3], E. Terrer[1,2], B. Jacquot[2], B. Levallois[1], H. Tassery[1,2] & F. J. G. Cuisinier[1]

White lesions represent an early phase of caries formation. 20 human sound premolars were subjected to pH cycling procedure to induce subsurface lesions (SLs) *in vitro*. In addition, 2 teeth with naturally developed white spot lesions (WSLs) were used as references. All specimens characterized by confocal Raman microscopy being used for the first time in examining white & subsurface lesions and providing a high resolution chemical and morphological map based on phosphate peak intensity alterations at 960 cm^{-1}. Nanoindentation technique was used to measure Hardness (H) and Young's modulus (E) of enamel. Phosphate map of examined samples exhibited presence of intact surface layer (ISL) followed by severe depletion in (PO_4^{3-}) peak in the area corresponding to the body of the lesion. In all examined groups, the mechanical properties of enamel were decreased in lesion area and found to be inversely related to penetration depth of indenter owing to enamel hierarchical structure. By combining the above two techniques, we linked mechanical properties of enamel to its chemical composition and ensured that the two methods are highly sensitive to detect small changes in enamel composition. Further work is required to bring these two excellent tools to clinical application to perceive carious lesions at an early stage of development.

Subsurface enamel demineralization is known as white spot lesions (WSLs); they represent the early stage of caries formation where affected surfaces seem to be intact upon gentle probing. However, with absence of effective treatment, cavitation may occur thereby increasing the necessity of invasive restorative treatments[1,2].

The WSL presents itself as a milky white opacity on smooth surfaces of teeth[3]. By examining histological sections of WSL, four zones could be distinguished: relatively intact surface layer (ISL), body of the lesion, dark zone and translucent zone which represents advancing front of the lesion[4].

The translucency of enamel is an optical phenomenon that depends on size of intercrystalline spaces. In early stages, active caries requires air drying to be visible, as the dissolution process of crystals at outer enamel surface begins. Further enlargement of intercrystalline spaces results in white patch visible without dryness. The effect of dehydration on enamel translucency is resulting from replacement of water content around enamel prisms with air. In a heterogeneous system, like enamel prisms surrounded by a fluid medium, scattering occurs due to difference in refractive indices (RI) of the two involved components. As RI of enamel is approximately 1.65, while that of water is 1.33 and of air is 1.00. Hence, larger difference in RI values, produces greater scattering at the enamel/air interface[5].

Every day, demineralization and remineralization occur in the mouth several times as an active process, with progression or reversal of dental caries being the end result. The process of dental caries can be modeled in the laboratory to produce the early manifestation of caries, namely, the subsurface lesions (SLs). The dynamic nature of the process has been modeled in numerous laboratories by various pH cycling models[6,7] in an attempt to simulate intraoral conditions in which enamel is subjected to repeated sequences of de/remineralization periods. The advantage of those models is that much can be learned about the processes involved, in a shorter period of time.

Transverse microradiography (TMR) is an essential method to determine the amount of mineral gain or loss in subsurface carious lesions *in vitro*. In addition, it has become a standard method, by which other recently developed caries detection techniques are compared and validated[8,9]. Though, preparing sections as thin as 100 µm that need to be very plane to ensure accuracy of the measurements; representing a major problem for this

[1]LBN, Univ. Montpellier, Montpellier, France. [2]Aix Marseille University, Marseille, France. [3]Laboratoire Charles Coulomb (L2C), UMR 5221 CNRS-Université de Montpellier, Montpellier, FR-34095, France. Correspondence and requests for materials should be addressed to R.A.-O. (email: rand.salih.mh@gmail.com)

method. This fact makes this technique destructive and time consuming. Particularly, in case of enamel, probably because of its brittleness, this method was frequently found to yield irregular sections[10].

Per contra, Raman microscopy which is a non-invasive technique; requires minimal specimen preparation, less expensive in term of cost and allows for simultaneous characterization of organic and inorganic tooth phases[11]. The high spatial resolution (300 nm) makes it an excellent tool for analyzing human enamel components, enabling the detection of WSL at an early stage of development[12]. Lesion depth measurements obtained from Raman scans; are based on phosphate peak intensity alterations which are closely related to its content in a given section[13]. This fact is even making the definition of the outer surface of a lesion easier when it is difficult to delineate it under TMR[14].

Nanoindentation (NI) technique enables investigations of local mechanical properties under various loading regimes based on load displacement data of indentations on submicron scale. Using this technique to measure mechanical characteristics at multiple locations within the same enamel sample is appropriate because it can accurately measure the mechanical properties of very small volumes with fine spatial resolution and show high sensitivity to any change affecting their values[15,16].

Our approach of combining confocal Raman microscopy, being used for the first time in examining white and subsurface lesions, with nanoindentation technique will add chemico-mechanical specificity in providing important information about an artificial model of subsurface lesions in human teeth to facilitate the future investigations on the efficacy WSLs treatments.

Materials and Methods

pH cycling procedure. (2) Premolars with naturally developed WSL (used as references for comparison purposes), in addition to (20) sound premolars (without any enamel developmental defects), were employed in this study. These teeth were extracted for orthodontic reasons and were used after obtaining approval of the local ethical research committee (process No. 2017–2907) and informed consent from all subjects. All procedures were carried out in accordance with relevant guidelines and regulations.

The number of teeth required in this study was calculated by using BiostaTGV site[17]. By comparing two means that were observed during our preliminary studies; we found that the minimum number of teeth in each group is 5 teeth per group.

Teeth washed with de-ionized water to remove any debris, stored in de-ionized water with 0.1% antimicrobial thymol and kept in refrigerator at 4 °C until use. Teeth were polished with non-fluoridated paste and further cleaned ultrasonically[18].

To create enamel subsurface lesions; 20 sound teeth were randomly divided into 4 groups which undergone 5, 6, 7 and 8 pH cycles respectively. Each cycle lasted 24 h. Different numbers of cycles were used in order to produce SLs that resemble, as much as possible, the naturally developed white lesions which classified as score 1 and 2 according to ICDAS[19]. Teeth were subjected to pH cycling procedure; using a demineralizing solution (0.075 M/L acetic acid, 1.0 mM/L calcium chloride and 2.0 mM/L potassium phosphate, pH = 4.3) and a remineralizing solution (150 mM/L potassium chloride, 1.5 mM/L calcium nitrate, 0.9 mM/L potassium phosphate, pH = 7). All chemicals were supplied by Sigma-Aldrich, France.

The procedure includes the immersion of each tooth in 20 ml of demineralizing solution for 6 hours at 37 °C. Then it removed and rinsed with distilled water for 2 min. before immersion in 20 ml of remineralizing solution for 18 hours at 37 °C. Adhesive tape disk of 6 mm diameter was cut and burnished on the buccal surface of each tooth. An acid resistant nail varnish was used to cover the whole surface of each tooth; the tape was removed leaving a window of 6 mm in diameter on buccal surface.

After the achievement of different number of cycles; teeth were divided longitudinally into two halves by using high speed diamond saw (Isomet 2000, Buehler, USA) to produce cross sections of teeth which then embedded in self-curing acrylic resin and keeping the cross sectioned surfaces exposed. The sections were polished by SiC papers #800, #1000 and #1200, followed by diamond pastes, using a polishing machine (Escil, France).

Raman microscopy. Raman spectra are recorded using a Witec Confocal Raman Microscope System alpha 300 R (Witec Inc., Ulm, Germany). Excitation in the confocal Raman microscopy is assured by a frequency doubled Nd: YAG laser (Newport, Evry, France) at a wavelength of 532 nm. The incident laser beam is focused onto the sample through a ×20 NIKON objective (Nikon, Tokyo, Japan). Then Raman backscattered radiation mixed with Rayleigh scattered are passed through an edge filter to block the Rayleigh's. Acquisition time of a single spectrum was set to 0.05 s. Each spectrum corresponding to a spatial unit defined as a voxel ($300\,nm \times 300\,nm \times 1\,\mu m$). All data acquisition and processing were performed using Image Plus software from Witec.

Chemical mapping of dental enamel was carried out over cross sections of all specimens with naturally and artificially developed subsurface lesions. The phosphate (PO_4^{3-}) ion has four internal vibrational modes. We chose to observe changes in intensity of the strongest peak at 960 cm^{-1} which is attributed to ν_1 (PO_4^{3-}) symmetric stretching mode.

Using an indicative look-up table (LUT), red hues indicate highest phosphate intensities, $CO_3^{2-}/PO4^{3-}$ ratio and crystallinity rates while purple hues represent lowest value of previous variables in chosen region. K-mean cluster analysis (KMCA) divides data into K mutually exclusive clusters which are compact and well-separated. Each cluster represents a zone depending upon magnitude of its phosphate peak intensity. Four zones with pseudo color were distinguished[11].

Crystallinity degree in enamel is determined by measuring changes in peaks ratio of symmetric mode of phosphate at 960 cm^{-1} over 950 cm^{-1} [20].

Raman peak at 1070 cm^{-1} is assigned to B-type carbonated hydroxyapatite (CHA).The ratio of intensities of carbonate to phosphate at (1070/960 cm^{-1}) were calculated throughout the whole section of each sample in order to detect variations in carbonate content in different zones of each sample[21].

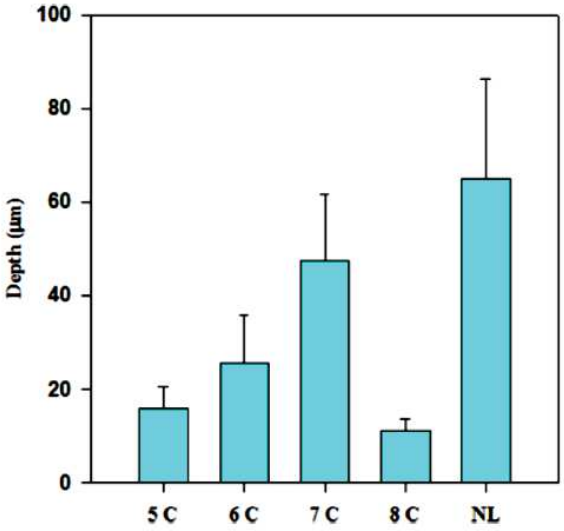

Figure 1. The relation between means of lesion depth determined by measuring variations in PO_4^{3-} peak intensity at 960 cm^{-1} & number of cycles (C). SD values are represented by error bars. (NL) natural lesion.

Nanoindentation technique. A nanoindenter equipped with a Berkovich tip (CSM, Switzerland), was used to measure hardness (H) and Young's modulus (E) of enamel. Tests were made in lesion, intermediate and sound enamel areas respectively. Indentations with a maximum load of 10 mN were marked on the samples where nanoindentation test was performed. The distance between each 2 neighboring indentations was at least 10 µm. A load of 20 µN was set for all tests, and loading and unloading time was 270 s. At least; ten indentations were done on each zone of the examined enamel surface.

H and E variables of samples were obtained from load-displacement loading/unloading curves, using Oliver and Pharr method[22], which is the most successful model for nanoindentation data analysis.

The hardness (H) is calculated at the maximum force according to the following relation:

$$H = \frac{F}{A_p} \tag{1}$$

where F is the maximum force and A_p is the projected surface contact area between the indenter and the sample.

The Young's modulus (E) of the sample can be obtained using the slope (S) at the beginning of the unloading curve according to the following relations:

$$E^* = \frac{\sqrt{\pi}}{2\beta}\frac{S}{\sqrt{A_p}} \tag{2}$$

and

$$\frac{1}{E^*} = \frac{1-\nu^2}{E} + \frac{1-\nu_i^2}{E_i} \tag{3}$$

where β is a geometrical constant depending upon indenter shape (1.034 in our case), E_i (1070 GPa) and ν_i (0.07) are Young's modulus and Poisson's coefficient of diamond indenter respectively. ν is the Poisson's coefficient of the sample which equals to 0.3 for enamel[23].

Overall mean and standard deviation (SD) for lesion depth (measured from Raman's data), penetration depth (Pd), H and E of different groups (from nanoindentation test) were calculated. Statistical analysis was performed using One Way ANOVA Analysis of Variance for all experimental groups, followed by multiple comparison procedures between each two pairs with Holm-Sidak method. All statistical procedures were performed at over all significant level of $\alpha = 0.05$ with SigmaPlot version 11.0 (Systat Software, Inc., USA).

Results

Depth of artificial subsurface lesions was measured and compared to that of natural lesion. Depth measurements were based on phosphate peak intensity alterations and found to increase linearly with gradual rise in number of cycles except for 8 cycles lesion, where a considerable loss of enamel layer has taken place. A statistically significant difference ($p < 0.05$) was found between all examined groups (Fig. 1).

Raman acquisitions were carried out from outer enamel surface towards dentin-enamel junction (DEJ). Images constructed from phosphate peak intensity at 960 cm^{-1} are shown in (Fig. 2A,D,G,J). All examined

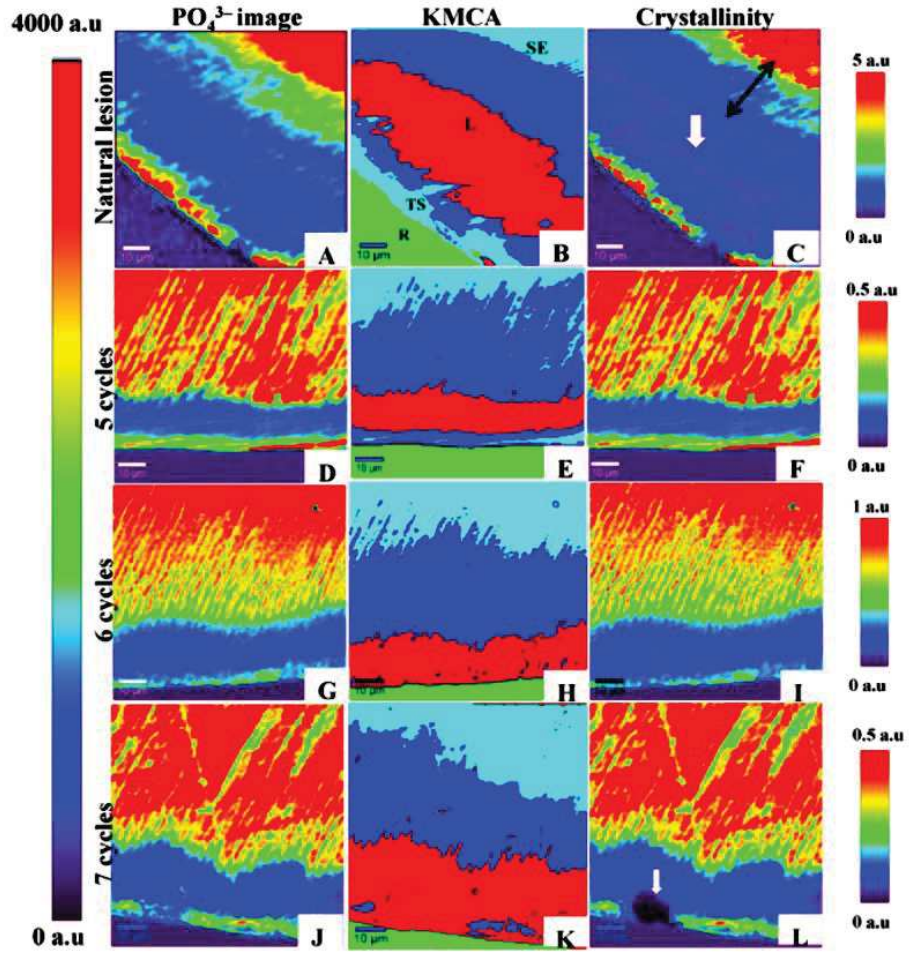

Figure 2. Natural lesion versus *in-vitro* lesions exposed to 5, 6 and 7 cycles. (**A**,**D**,**G** and **J**) images constructed from phosphate peak intensity at 960 cm^{-1}. Look Up Table (LUT) on the left. (**B**,**E**,**H** and **K**) K-mean cluster analysis (KMCA) images, green zones are corresponding to embedding resin. (**C**,**F**,**I**, and **L**) images of crystallinity (phosphate peaks ratio at (960) over (950) cm^{-1}). Individual LUT on the right. Purple zones are corresponding to embedding resin. Crystallinity images are almost following phosphate pattern in the 1st group of images, except for C and L images; where we can observe the presence of purple hues (white solid arrows) in lesion area which indicate total loss of crystallinity in lesion area. (Following symbols in image (**B**) are valid for all images: SE; sound enamel, L; lesion, TS; tooth surface, R; resin).

samples exhibited phosphate signal at outer enamel surface which indicates the presence of ISL. A severe depletion in (PO_4^{3-}) peak in the area corresponding to body of the lesion. At greater distances into the enamel; phosphate peak intensity converges to that of sound enamel signaling the end of the lesion.

The reconstructed images of enamel crystallinity of all groups, almost exhibit a pattern similar to that of PO_4^{3-} images (Fig. 2C,F,I,L). Each pseudo color in these images; represents a special crystallinity value. Leveled color scale bars are designed to estimate the value of each color. Crystallinity decreases abruptly in lesion zone (blue). Thereafter; it starts to increase gradually in the intermediate zone (green, yellow hues) before it reaches to its maximum value in sound enamel (red area) beyond subsurface lesion.

Results of K-mean cluster analysis of data set of four clusters are shown in (Fig. 2B,E,H,K). Images constructed via KMCA demonstrating clusters with four distinguished colors: acrylic resin (green), sound enamel with two different intensities of phosphate (in turquoise zone, PO_4^{3-} intensity is stronger than that in blue zone) and demineralized lesion body (red).

Reconstructed images derived from $CO_3^{2-}/PO4^{3-}$ ratio (Fig. 3A–D) were used to analyze changes in enamel inorganic components in each zone of the lesion. They revealed an increase in $CO_3^{2-}/PO4^{3-}$ ratio in lesion zone in comparison to sound enamel zone.

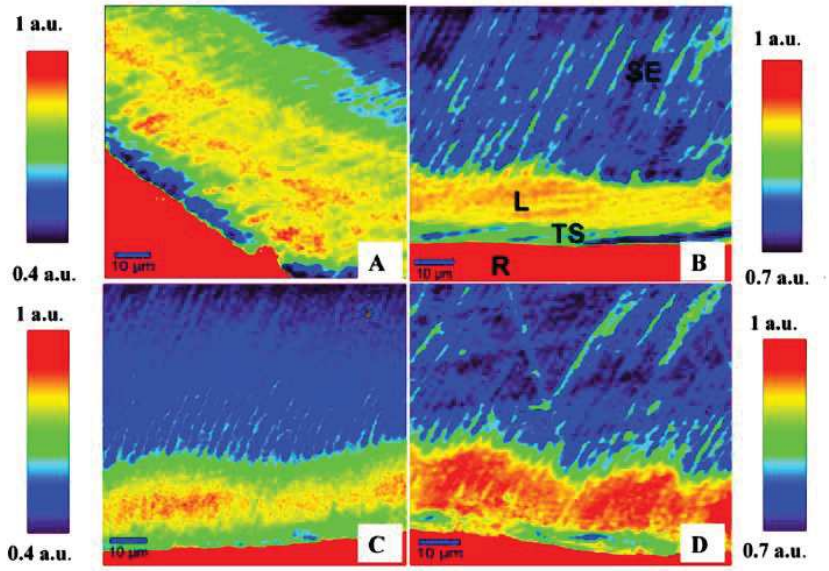

Figure 3. (A) Natural lesion versus *in-vitro* lesions (B,C,D) exposed to 5, 6 and 7 cycles respectively. Images constructed from CO_3^{2-}/PO_4^{3-} ratio at (1070 cm^{-1}) over (960 cm^{-1}). Individual LUT on left & right where red hues indicate highest CO_3^{2-}/PO_4^{3-} ratio and purple hues represent lowest values of the same ratio. (Following symbols in image B are valid for all images: SE; sound enamel, L; lesion, TS; tooth surface, R; resin).

Nanoindentation load-displacement curve is drawn from applied load versus depth profile (Fig. 4B). Curves were derived from different indentations made in three zones of enamel: unaffected enamel close to dentin, lesion area which is confined to enamel surface and intermediate zone which lies between the two areas to show differences in penetration depth of indenter tip.

H and E of enamel were determined in all zones of each group to measure intra-tooth variations. A reduction in two variables value was detected in lesion area in all examined groups (Fig. 4C,D). E rates display a positive relationship with those of H, except for the natural lesion (NL) where E value is smaller than expected. Difference was found to be significant ($p < 0.05$) by comparing E value of (NL) with those of other artificial lesions. While, the difference was found to be non-significant ($p > 0.05$) by comparing changes in rates of Pd and H of lesions (Table 1).

Discussion

Chemical composition and mechanical properties of WSLs and subsurface artificial lesions were described using Raman microscopy and nanoindentation techniques. Both techniques tested the same areas of each sample.

To our knowledge, confocal Raman microscopy has been used for the first time in this study to detect WSLs and experimentally induced subsurface lesions. It can provide a high resolution chemical and morphological map of examined specimen, detecting even very small changes in its chemical composition. Data analysis of each acquired scan which is comprised of tenth thousands of single spectrums, is used to reconstruct different Raman detailed images. Transverse microradiography is a quantitative method depending on x-ray absorbance of an object and images reflect mineral concentration in mineralized tissue slices[24]. Systematic and random errors represent the two sources of errors that could affect x-ray absorbance measurement. The crucial factor with regard to systematic errors is the beam inhomogeneity, while, film choice is the vital factor in respect to random errors[24]. Moreover, artifacts result from inadequate section preparation as we mentioned before, may incorrectly be interpreted as additional demineralization in the lesion part of the specimen. Furthermore, TMR is usually applied, to determine overall changes in mineral content and not detailed structures of biological tissues[25]. TMR resolution is dependent on X-ray detector resolution, i.e., silver grain diameter of radiographic film and on the microscope scanner used to read the film. High resolution microradiograph is with a pixel resolution of 2.15 µm[26], comparing to a voxel size of ($300 \times nm \times 300\,nm \times 1\,\mu m$ for confocal Raman microscopy. Hence, Raman microscopy could be considered as a superior alternative for Raman spectroscopy and transverse microradiography[12].

Deepest subsurface lesion that we could produce *in vitro* is shallower than naturally developed one, in spite of lower concentrations of calcium, phosphate, and even lower pH values that have been used to induce a faster demineralization *in vitro*. Besides that, thickness of subsurface lesions reported by other studies[27,28] was greater than thickness of this study. However, there is less detailed information about these fabricated lesions, in particular, the evidences concerning the presence of ISL.

Enamel is composed of large number of hydroxyapatite crystals (HACs); represented by the chemical formula $Ca_{10}(PO4)_6(OH)_2$ with incorporation of many cations and anions in their lattice resulting in the formation of

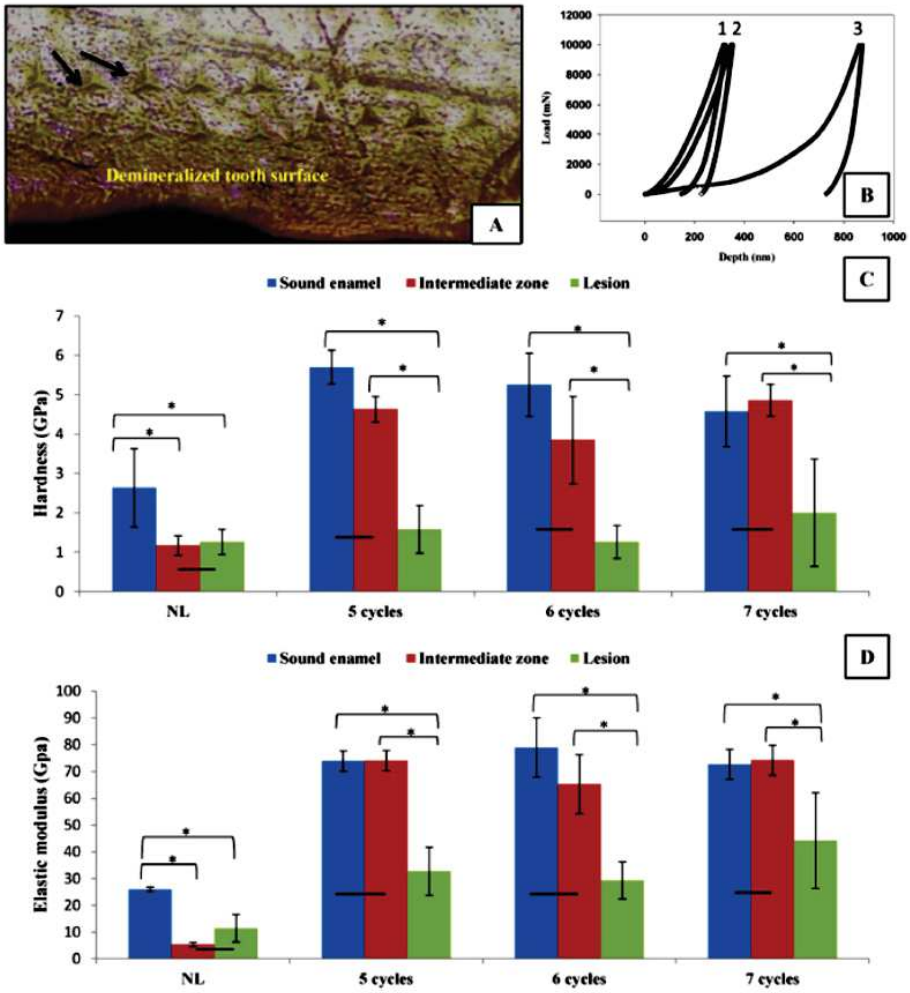

Figure 4. (**A**) Optical microscopic image of polished enamel surface with prints of Berkovich tip indenter in lesion zone. (**B**) A graph demonstrating the nanoindentation load-displacement curves in: 1 sound enamel, 2 intermediate zone & 3 lesion area. The difference in penetration depth (Pd) between the three zones is very obvious; indicating an inverse relationship between the reduction in hardness value and the increase in the depth of penetration. (**C** and **D**) bar graphs showing H and E mean values in all zones in: Natural lesion versus artificial lesions after 5, 6 and 7 cycles consecutively. Asterisk (*) shows a statistically significant difference ($p < 0.05$) between zones connected by bracket within each group. Horizontal bar indicates no significant difference ($p > 0.05$) among subgroups marked by it.

different kinds of apatite. The main substituent in biological apatite is carbonate ion (CO_3^{2-}) which substitutes the phosphate group (PO_4^{3-}) to form B-type CHA containing 4–6 wt % carbonate[29,30]. Incorporation of carbonate into enamel increases its dissolution rate by interfering with crystal structure[31]. In particular, crystallinity, i.e., crystal size and perfection of apatite are of great importance, because small, more imperfect crystals due to presence of substituents, make them more susceptible to acid dissolution and caries progression[32]. Therefore, lowering in enamel crystallinity in lesion zone of our samples could be related to the increase in CO_3^{2-}/PO_4^{3-} ratio in the same zone[33–35].

KMCA method assembles set of spectra of the same or close intensities in a well-recognized cluster[11]. High resolution images constructed by KMCA visibly reveal changes in enamel structure associated with number of cycles. As ISL becomes thinner, less mineralized and more porous; thickness of demineralized area increases progressively with time, until the eighth cycle, where enamel surface dissolved. These results emphasize the fact that degree of enamel dissolution strengthens with repeated and prolonged variations in pH values.

Mechanical properties of enamel are inconstant and dependent on its chemical composition and structural organization. Enamel is anisotropic material where prisms are arranged in pattern perpendicular to their long axis, so that any variations in its prisms direction and composition may lead to differences in its mechanical properties[36].

Tested area	Pd (µm) Mean ± SD	H (GPa) Mean ± SD	E (GPa) Mean ± SD
SE	0.3 ± 0.01	4.5 ± 0.67	74.7 ± 3.3
NWSL	0.54 ± 0.09	1.26 ± 0.32	11.4 ± 5.2
5 cycles lesion	0.5 ± 0.08	1.58 ± 0.61	32.8 ± 9
6 cycles lesion	0.6 ± 0.24	1.1 ± 0.52	27.5 ± 8.2
7 cycles lesion	0.5 ± 0.2	2 ± 1.4	42.5 ± 18.4

Table 1. Penetration depth (Pd), Hardness (H), elastic modulus (E) in lesion area of natural white spot lesion (N = 2) & artificial lesions of 5, 6 & 7 cycles (N = 5 in each group). Difference was found to be significant ($p < 0.05$ between E value of NL (natural lesion) & those of other artificial lesions, while non-significant difference ($p > 0.05$) was found between Pd and H values of all kinds of lesions.

Our results showed no significant difference between mechanical properties of intermediate zone and lesion area of NL (Fig. 4C,D) contrary to other artificial lesions. Simultaneously, we exclusively observed that crystallinity degree has obviously declined in intermediate zone of NL (Fig. 2C, double ended black arrow) which indicates an alteration in crystal size and shape and consequently reduced apatite perfection which constitutes the structural unit of enamel prisms. These modifications in enamel structure could help in explaining the reduced mechanical properties of intermediate zone of WSL.

Outer enamel layers are harder than inner layers which are close to DEJ, where enamel becomes less compact due to increase inter-prismatic voids and less mineralized due to decrease mineral density and increase organic matrix contents. This could explain the low H and E values for sound enamel in NWSL group (Fig. 4C,D), where indentations in this zone were made next to DEJ because of extensive depth of NWSL (>60 µm)[37,38].

Table 1 demonstrates how the mechanical properties of enamel (hardness and elastic modulus) are inversely related to penetration depth of indenter owing to enamel hierarchical structure. Obtained average values of H ~ 4.5 GPa and E ~ 74.7 GPa for sound enamel at 10 mN load are consistent with values reported in previous study where E ~ 80 GPa and H ~ 4 GPa[39].

Mechanical properties were considerably reduced in demineralized enamel compared to sound enamel as a result of inorganic substance loss (Table 1). Records obtained from the above two methods show similar changes across the lesion and represent a mechanism for linking mechanical properties of enamel to its composition which is in coincident with prior studies[35,40].

We can conclude that our protocol is reliable to reproduce subsurface lesions *in vitro* in a relatively short period as long as it is limited to seven cycles to ensure the presence of highly mineralized ISL which represents the characteristic feature of these lesions which complicates their clinical non-invasive treatment. These artificial models with methods of characterization, particularly confocal Raman microscopy, are typical to test the efficacy of remineralizing dental products. Our work certifies that the two methods are highly sensitive to detect small changes in enamel composition. Further work is required to facilitate their use in the dental clinic to detect carious lesions at an early stage of formation.

References

1. Derks, A., Katsaros, C., Frencken, J., Van't Hof, M. & Kuijpers-Jagtman, A. Caries-inhibiting effect of preventive measures during orthodontic treatment with fixed appliances. *Caries research* **38**, 413–420 (2004).
2. Bergstrand, F. & Twetman, S. A review on prevention and treatment of post-orthodontic white spot lesions–evidence-based methods and emerging technologies. *The open dentistry journal* **5** (2011).
3. Summitt, J. B., Robbins, J. W., Hilton, T. J. & Schwartz, R. S. *Fundamentals of operative dentistry: a contemporary approach*. (Quintessence Pub., 2006).
4. Gorelick, L., Geiger, A. M. & Gwinnett, A. J. Incidence of white spot formation after bonding and banding. *American journal of orthodontics* **81**, 93–98 (1982).
5. Wang, X.-J. *et al.* Characterization of dentin and enamel by use of optical coherence tomography. *Applied Optics* **38**, 2092, https://doi.org/10.1364/ao.38.002092 (1999).
6. Ten Cate, J. & Mundorff-Shrestha, S. Working group report 1: laboratory models for caries (*in vitro* and animal models). *Advances in dental research* **9**, 332–334 (1995).
7. Featherstone, J. The continuum of dental caries—evidence for a dynamic disease process. *Journal of dental research* **83**, C39–C42 (2004).
8. Hsu, D. J., Darling, C. L., Lachica, M. M. & Fried, D. Nondestructive assessment of the inhibition of enamel demineralization by CO2 laser treatment using polarization sensitive optical coherence tomography. *Journal of biomedical optics* **13**, 054027-054027-054029 (2008).
9. Manesh, S. K., Darling, C. L. & Fried, D. Nondestructive assessment of dentin demineralization using polarization-sensitive optical coherence tomography after exposure to fluoride and laser irradiation. *Journal of Biomedical Materials Research Part B: Applied Biomaterials* **90**, 802–812 (2009).
10. Lo, E., Zhi, Q. & Itthagarun, A. Comparing two quantitative methods for studying remineralization of artificial caries. *Journal of dentistry* **38**, 352–359 (2010).
11. Salehi, H. *et al.* Label-free detection of anticancer drug paclitaxel in living cells by confocal Raman microscopy. *Applied Physics Letters* **102**, 113701, https://doi.org/10.1063/1.4794871 (2013).
12. Desoutter, A. *et al.* in *Proc. of SPIE Vol.* 892907–892901 (2014).
13. Akkus, A. *et al.* Evaluation of mineral content in healthy permanent human enamel by Raman spectroscopy. *Journal of clinical and experimental dentistry* **8**, e546 (2016).
14. Ten, B. J. A review of quantitative method for studies of mineral content of intra-oral incipient caries lesion. *J. Dent. Res.* **70**, 2–14 (1991).
15. Dickinson, M., Wolf, K. & Mann, A. Nanomechanical and chemical characterization of incipient *in vitro* carious lesions in human dental enamel. *Archives of oral biology* **52**, 753–760 (2007).
16. Alsayed, E. Z. *et al.* Effects of coating materials on nanoindentation hardness of enamel and adjacent areas. *Dental Materials* **32**, 807–816 (2016).

17. iPLESP. BiostaTGV, https://marne.u707. jussieu.fr/biostatgv (2000).
18. Elfallah, H. M., Bertassoni, L. E., Charadram, N., Rathsam, C. & Swain, M. V. Effect of tooth bleaching agents on protein content and mechanical properties of dental enamel. *Acta biomaterialia* **20**, 120–128, https://doi.org/10.1016/j.actbio.2015.03.035 (2015).
19. Ismail, A. *et al.* The International Caries Detection and Assessment System (ICDAS): an integrated system for measuring dental caries. *Community dentistry and oral epidemiology* **35**, 170–178 (2007).
20. Slimani, A. *et al.* Confocal Raman mapping of collagen cross-link and crystallinity of human dentin-enamel junction. *J Biomed Opt* **22**, 1–8, https://doi.org/10.1117/1.JBO.22.8.086003 (2017).
21. Xu, C., Yao, X., Walker, M. P. & Wang, Y. Chemical/molecular structure of the dentin–enamel junction is dependent on the intratooth location. *Calcified tissue international* **84**, 221 (2009).
22. Oliver, W. C. & Pharr, G. M. Measurement of hardness and elastic modulus by instrumented indentation: Advances in understanding and refinements to methodology. *Journal of materials research* **19**, 3–20 (2004).
23. Haines, D. Physical properties of human tooth enamel and enamel sheath material under load. *Journal of biomechanics* **1**, 117IN17119–17118IN22125 (1968).
24. de Jong, Ed. J. & Ten Bosch, J. Error analysis of the microradiographic determination of mineral content in mineralised tissue slices. *Physics in medicine and biology* **30**, 1067 (1985).
25. Damen, J., Exterkate, R. & Ten Cate, J. Reproducibility of TMR for the determination of longitudinal mineral changes in dental hard tissues. *Advances in dental research* **11**, 415–419 (1997).
26. Can, A. M., Darling, C. L. & Fried, D. In *Proceedings of SPIE–the International Society for Optical Engineering*. 68430T–68431 (NIH Public Access).
27. Moron, B. M. *et al.* Different protocols to produce artificial dentine carious lesions *in vitro* and *in situ*: hardness and mineral content correlation. *Caries research* **47**, 162–170, https://doi.org/10.1159/000345362 (2013).
28. Mohanty, B., Dadlani, D., Mahoney, D. & Mann, A. B. Characterizing and identifying incipient carious lesions in dental enamel using micro-Raman spectroscopy. *Caries research* **47**, 27–33, https://doi.org/10.1159/000342432 (2013).
29. Aoki, H. *Science and medical applications of hydroxyapatite*. (Ishiyaku Euroamerica, 1991).
30. Leventouri, T., Chakoumakos, B., Papanearchou, N. & Perdikatsis, V. Comparison of crystal structure parameters of natural and synthetic apatites from neutron powder diffraction. *Journal of materials research* **16**, 2600–2606 (2001).
31. Legeros, R. Z., Trautz, O. R., Legeros, J. P., Klein, E. & Shirra, W. P. Apatite crystallites: effects of carbonate on morphology. *Science* **155**, 1409–1411 (1967).
32. Pleshko, N., Boskey, A. & Mendelsohn, R. Novel infrared spectroscopic method for the determination of crystallinity of hydroxyapatite minerals. *Biophysical journal* **60**, 786–793 (1991).
33. Simmer, J. & Fincham, A. Molecular mechanisms of dental enamel formation. *Critical Reviews in Oral Biology & Medicine* **6**, 84–108 (1995).
34. Pucéat, E., Reynard, B. & Lécuyer, C. Can crystallinity be used to determine the degree of chemical alteration of biogenic apatites? *Chemical Geology* **205**, 83–97 (2004).
35. Xu, C., Reed, R., Gorski, J. P., Wang, Y. & Walker, M. P. The Distribution of Carbonate in Enamel and its Correlation with Structure and Mechanical Properties. *Journal of materials science* **47**, 8035–8043, https://doi.org/10.1007/s10853-012-6693-7 (2012).
36. Radlanski, R. J., Renz, H., Willersinn, U., Cordis, C. A. & Duschner, H. Outline and arrangement of enamel rods in human deciduous and permanent enamel. 3D-reconstructions obtained from CLSM and SEM images based on serial ground sections. *European journal of oral sciences* **109**, 409–414 (2001).
37. Cuy, J. L., Mann, A. B., Livi, K. J., Teaford, M. F. & Weihs, T. P. Nanoindentation mapping of the mechanical properties of human molar tooth enamel. *Archives of oral biology* **47**, 281–291 (2002).
38. He, B., Huang, S., Jing, J. & Hao, Y. Measurement of hydroxyapatite density and Knoop hardness in sound human enamel and a correlational analysis between them. *Archives of oral biology* **55**, 134–141 (2010).
39. Chan, Y. L., Ngan, A. H. & King, N. M. Nano-scale structure and mechanical properties of the human dentine-enamel junction. *Journal of the mechanical behavior of biomedical materials* **4**, 785–795, https://doi.org/10.1016/j.jmbbm.2010.09.003 (2011).
40. Gallagher, R. R. *et al.* Coupled Nanomechanical and Raman Microspectroscopic Investigation of Human Third Molar DEJ. *Journal of dental biomechanics* **2010**, https://doi.org/10.4061/2010/256903 (2010).

Acknowledgements

This work is partially supported by grants from Iraqi government represented by Ministry of Higher Education and Scientific Research.

Author Contributions

Al-Obaidi R. contributed to conception, design, acquisition, analysis and interpretation of data, prepared Figures 1–4 and drafted the manuscript. Salehi H. contributed to acquisition, analysis and interpretation of data, prepared Figures 2 and 3. Desoutter A. and Bonnet L. contributed to data acquisition. Etienne P., Terrer E., Jacquot B., Levallois B., Tassery H. contributed to conception. Cuisinier F.J.G. contributed to conception, design, analysis and interpretation of data. All authors reviewed the manuscript and gave final approval.

Additional Information

Competing Interests: The authors declare no competing interests.

Publisher's note: Springer Nature remains neutral with regard to jurisdictional claims in published maps and institutional affiliations.

Article 2

Nihon University School of Dentistry
Journal of Oral Science

Enamel Subsurface Lesions: Formation and Assessment in vitro.

Journal:	*Journal of Oral Science*
Manuscript ID	Draft
Manuscript Type:	Original Article
Date Submitted by the Author:	n/a
Complete List of Authors:	Al-Obaidi, Rand; LBN Salehi, Hamideh ; LBN Desoutter, Alban ; LBN Tassery, Herve ; LBN Cuisinier, Frederic ; LBN
Keywords:	White spot lesion, pH cycling model, Raman microscopy

Enamel Subsurface Lesions: Formation and Assessment *in vitro*.

R. Al-Obaidi[1]*, H. Salehi[1], A. Desoutter[1], H. Tassery [1, 2] and F. J. G. Cuisinier[1].

Rand Al-Obaidi, Hamideh Salehi, Alban Desoutter, Frederic Cuisinier

[1]Labratory of Bioengineering & Nano-science, Montpellier University, Montpellier, France.

Herve Tassery

[2]Labratory of Bioengineering & Nano-science, Aix Marseille University, Marseille, France

Corresponding author: Rand Al-Obaidi*

545, Av du Pr JL Viala

34193 Cedex 5 Montpellier-France

Phone: +33 6 41380158

rand.salih.mh@gmail.com

ABSTRACT

This study aims to compare two pH-cycling models used to induce subsurface lesion (SL) with a less demineralized surface layer, besides, developing new technologies for assessing them through demonstrating the performance of confocal Raman microscopy in WSL detection. 12 sound premolars were subjected to two models (A & B) to induce (SL). Teeth had in vivo formed white lesions were used as a positive control. All specimens were inspected by SOPROLIFE camera and Raman microscopy to detect small changes in appearance and structure of enamel. Changes in the tooth natural color throughout the treatment were recorded via the camera. Phosphate maps with their spectra constructed from phosphate peak at 960 cm^{-1} are shown here. Depth of lesions was measured based on phosphate peak intensity variations. Protocol B is reliable to reproduce SLs in a relatively short period. Both protocols have intrinsic limitations as they could not completely simulate the complex intraoral conditions leading to WSL formation with respect to lesion depth and preservation of intact surface layer (ISL). Raman microscopy could be considered the gold standard for hard tissue mineralization analyses.

Keywords: White spot lesion (WSL), pH cycling model, Raman microscopy.

INTRODUCTION

Dental caries is a multifactorial disease resulting from a dynamic disparity present in the oral cavity in alternating periods of dissolution and mineral loss (1). White spot lesions (WSLs) represent an early stage of caries formation where subsurface enamel demineralization takes place. WSL formation can be reconstituted in the laboratory through the use of chemical systems in a relatively short period (2). pH cycling model is a chemical system involves exposition of dental enamel to combinations of de/ remineralization phases planned to mimic the dynamics of mineral loss and gain involved in caries formation supporting the possible mechanisms of caries prevention and/or remineralization and clinical trials planning (3).

Soprolife light-induced fluorescence assessor system (Acteon, La Ciotat, France) is newly released apparatus for detection and assessment of incipient dental caries, founded on imaging and auto-fluorescence of dental tissues (4).

Raman microscopy is a non-invasive spectroscopic method with minimal specimen preparation that provides details on the biochemistry and molecular structure of mineralized tissues. Its high spatial resolution (300 nm), makes it a novel optical approach for analyzing calcified tissue components and detecting early changes in its composition (5).

The incremental prevalence of mild hypomineralization due to developmental defects on tooth surfaces poses a challenge for caries detection and prevention. pH-cycling models enable the development of subsurface lesions in a relatively short periods which representing up to 6 to 12 months of clinical lesion progression. The present study was designed to compare two chemical models with respect to their potential to induce artificial caries confined to enamel surface and demonstrate their ability to mimic the intra-oral conditions that lead to WSL formation. In addition,

it anticipates developing new technology for assessing subsurface lesions through demonstrating the performance of Raman microscopy in incipient caries detection.

MATERIALS & METHODS

Sound premolars collected with informed consent from all subjects and approval of the local ethical research committee (process No. 2017-2907) before being used in this research.

4 premolars had in vivo formed WSLs were used as reference (positive control). 12 sound teeth were randomly divided into 3 groups which were exposed to two pH cycling models; A & B respectively. Teeth were undergone 7, 8 and 14 cycles respectively. Each cycle lasted 24h. Different numbers of cycles were used to produce artificial early caries lesions with various severities of lesion depths to measure the representative characteristics of early caries lesions, such as fluorescence loss, color changes and amount of mineral loss by the intraoral camera and the confocal microscopy.

The first model (A) is described by Featherstone (6) has held for 14 days. The demineralizing solution is composed of 2.0 mM $Ca(NO_3)_2 \cdot 4H_2O$), 2.0 mM KH_2PO_4, 75.0 mM CH_3COOH, at pH = 4.4). Remineralizing solution composition is 1.5 mM $Ca(NO_3)_2 \cdot 4H_2O$), 0.9 mM KH_2PO_4, 130 mM KCl, 20 mM $NaC_2H_6AsO_2 \cdot 3H_2O$, at pH = 7.

Second model (B) (7) uses a demineralizing solution (0.075 M L^{-1} CH_3COOH, 1.0 mM $CaCl_2$, 2.0 mM KH_2PO_4, at pH= 4.3). The remineralizing solution contains (150 mM KCl, 1.5 mM $Ca(NO_3)$, 0.9 mM KH_2PO_4, at pH = 7). All chemical products were supplied by Sigma-Aldrich, France.

Each tooth was immersed in 20 ml of demineralizing solution for 6 hours. Then it was removed and rinsed with running water before being immersed in 20 ml of remineralizing solution for 18 hours. The temperature maintained at 37 ◦C. Teeth were sectioned longitudinally into two halves to have cross sections of teeth which then were embedded in self-curing acrylic resin, having the cross sectioned surface of samples facing the surface that is to be polished later.

Soprolife Camera:

The camera can be used to capture high resolution images of caries lesions, which will critically facilitate clinical assessments (8). All teeth were filmed with it pre- and post-intervention in order to detect changes in enamel surface appearance. The camera provides anatomical images in (daylight mode) and fluorescent images in (diagnostic mode). The light is provided by 4 blue-light LEDs of wavelength 450 nm.

Raman microscopy:

Raman spectra were recorded using a Witec Confocal Raman Microscope System alpha 300R (Witec, Ulm, Germany). Excitation is assured by a frequency doubled Nd: YAG laser (Newport, Evry, France) at 532nm. Enamel chemical mapping was started at the outer surface and ending before dentin enamel junction (DEJ). The phosphate (PO_4^{3-}) ion has four vibrational modes. The peak at 960 cm^{-1} is assigned to ν_1 vibration peak of the phosphate group in enamel which was selected as the inner standard to observe changes in intensity of the strongest peak at 960 cm^{-1}. Using an indicative look-up table (LUT), yellow and dark brown hues indicate maximum and minimum phosphate intensity in a chosen area.

Overall mean and standard deviation (SD) of lesion depth were calculated. Statistical analysis was performed using One Way ANOVA Analysis of Variance. All statistical procedures were performed at over all significant level of $\alpha = 0.05$ with SigmaPlot 11.0 (Systat Software; Inc., USA).

RESULTS

Image pairs were recorded using the intraoral camera as an additional method for visual inspection (Fig.1A, B, C, D). A & B represent images in daylight mode before intervention. C& D represent images exhibiting changes in enamel surface appearance after 8 cycles-protocol A and 7 cycles-protocol B consecutively. Depth of artificial lesions was measured and compared to that of natural lesions based on phosphate peak intensity variations in dental section. A statistically significant difference ($p<0.05$) in depth was found between positive control group and 8 cycles-B. The difference was significant between 7 & 8 cycle lesions (protocol B) as well. A non-significant difference ($p>0.05$) was detected between other groups (Fig.1 E).

Phosphate maps with their corresponding spectra presented in (Fig. 2A, B, C, D, E) are constructed from phosphate peak intensity at 960 cm^{-1}. All examined samples exhibited an important phosphate signal at outer enamel surface which indicates the presence of ISL. Then, there was a severe depletion in PO_4^{3-} peak in the area corresponding to body of the lesion. At greater distances into the enamel; the intensity meets that of sound enamel indicating end of the lesion.

DISCUSSION

This paper aims to compare two pH-cycling models, focusing on their strengths, limitations and the period required to induce subsurface lesion. The Chemical composition of subsurface lesions was described using Raman microscopy which can detect very small changes by identifying variations in phosphate intensity that reflects the amount of mineral content in the target zone (9). Data analysis of each acquired scan which is comprised of tenth thousands of spectra; was used to reconstruct different detailed images.

Natural WSLs formed in complex intraoral conditions due to imbalance between pathological factors that cause demineralization and protective factors that drive to remineralization. De/remineralization occur in the mouth several times every day as a dynamic process that takes much longer than in the laboratory models (10). Therefore, WSLs are more sophisticated than *in vitro* subsurface lesions (SLs) in respect to chemical composition of enamel and lesion depth due to the presence of saliva and plaque *in vivo*. WSLs are quite variable; ISL is almost present due to strong possibility of remineralization from the oral environment. While the amount of mineral loss from the subsurface lesion is completely inconstant (10).

Subsurface lesion produced by protocol A after 8 cycles was invisible after inspection with the camera (Fig.1C) even after prolonged dryness due to humble demineralization and thus small changes in the chemical composition of enamel represented by PO_4^{3-} peak intensity (Fig.2A). After 14 cycles; changes became more evident with the formation of pronounced subsurface lesion accompanied by undermining of ISL (Fig.2B). However, protocol B was able to induce first changes in enamel appearance after merely 3 cycles. Severely white enamel became evident after only 7 cycles (Fig.1D) along with chemical map showing a deep lesion with intense decrease in phosphate

amount in lesion body and presence of ISL (Fig.2 C). A distinct dissolution of the outer surface was encountered after 8 cycles (Fig.2 D).

When light enters sound enamel which is a low light scattering material, it travels an average distance of 0.1 mm before being scattered (11). When minerals are lost from enamel due to demineralization, they will be partly replaced by water which leads to increase differences in refractive index (RI) between sound and demineralized enamel leading to greater scattering at the enamel/ air interface (12). When the lesion is dried, the water is replaced by air and the average refractive index declines even more, leading to an even whiter lesion. Besides that, whiteness of the initial lesions is an optical phenomenon, resulted from increased porosity within the enamel crystalline structure (11; 13).

Thus, changes in enamel appearance could be detected only when distinct subsurface lesion is developed owing to interior opacity and subsurface scattering effect (14). Chemical protocols have limitations regarding lesion depth and ISL conservation due to the difficulty to completely simulate the complex intraoral conditions that leading to WSL development (15). Protocol A induced slight change in enamel appearance after 8 cycles. Whereas, protocol B produced deep subsurface lesion after only 7 cycles. The latter model is less time consuming and reliable to reproduce SLs *in vitro* in a relatively short period as long as it is limited to seven cycles to ensure the presence of ISL which represents the characteristic feature of these lesions that complicates their non-invasive treatment. These subsurface lesions are essential in profile studies for rapid and low-cost testing of developing and recently marketed remineralizing dental products (3).

Raman microscopy could be considered as the gold standard for hard tissue mineralization analyses. Further work is required to present this tool to clinical application to perceive carious lesions at an early stage of development.

ACKNOWLEDGEMENTS

The authors wish to acknowledge the financial support of Ministry of Higher Education in Iraqi

COMPETING FINANCIAL INTERESTS

The authors declare that they have no conflict of interest.

REFERENCES

1. Featherstone J, Duncan J, Cutress T (1979) A mechanism for dental caries based on chemical processes and diffusion phenomena during in-vitro caries simulation on human tooth enamel. Archives of oral biology 24, 101-12.
2. Larsen MJ (1974) Chemically induced in vitro lesions in dental enamel. European journal of oral sciences 82, 496-509.
3. White D (1995) The application of in vitro models to research on demineralization and remineralization of the teeth. Advances in dental research 9, 175-93.
4. Tassery H, Levallois B, Terrer E, Manton D, Otsuki M et al. (2013) Use of new minimum intervention dentistry technologies in caries management. Australian dental journal 58, 40-59.
5. Slimani A, Nouioua F, Desoutter A, Levallois B, Cuisinier FJG et al. (2017) Confocal Raman mapping of collagen cross-link and crystallinity of human dentin-enamel junction. J Biomed Opt 22, 1-8.
6. Featherstone J, O'reilly M, Shariati M, Brugler S (1986) Enhancement of remineralization in vitro and in vivo. Factors relating to demineralisation and remineralisation of the teeth. IRL Press. Oxford and Washington.
7. Al-Obaidi R, Salehi H, Desoutter A, Bonnet L, Etienne P et al. (2018) Chemical & Nano-mechanical Study of Artificial Human Enamel Subsurface Lesions. Scientific reports 8, 4047.
8. Pitts N (2004) Are we ready to move from operative to non-operative/preventive treatment of dental caries in clinical practice? Caries research 38, 294-304.
9. Mohanty B, Dadlani D, Mahoney D, Mann AB (2013) Characterizing and identifying incipient carious lesions in dental enamel using micro-Raman spectroscopy. Caries research 47, 27-33.
10. Featherstone J (2004) The continuum of dental caries—evidence for a dynamic disease process. Journal of dental research 83, 39-42.
11. Angmar-Månsson B, Ten Bosch J (1987) Optical methods for the detection and quantification of caries. Advances in dental research 1, 14-20.
12. Wang X-J, Milner TE, de Boer JF, Zhang Y, Pashley DH, Nelson JS (1999) Characterization of dentin and enamel by use of optical coherence tomography. Applied Optics 38, 2092.
13. Torres CRG, Borges AB, Torres LMS, Gomes IS, de Oliveira RS (2011) Effect of caries infiltration technique and fluoride therapy on the colour masking of white spot lesions. Journal of dentistry 39, 202-7.
14. Årtun J, Thylstrup A (1989) A 3-year clinical and SEM study of surface changes of carious enamel lesions after inactivation. American journal of orthodontics and dentofacial orthopedics 95, 327-33.
15. White D. (1992) The comparative sensitivity of intra-oral, in vitro, and animal models in the'profile'evaluation of topical fluorides. Journal of dental research 71.

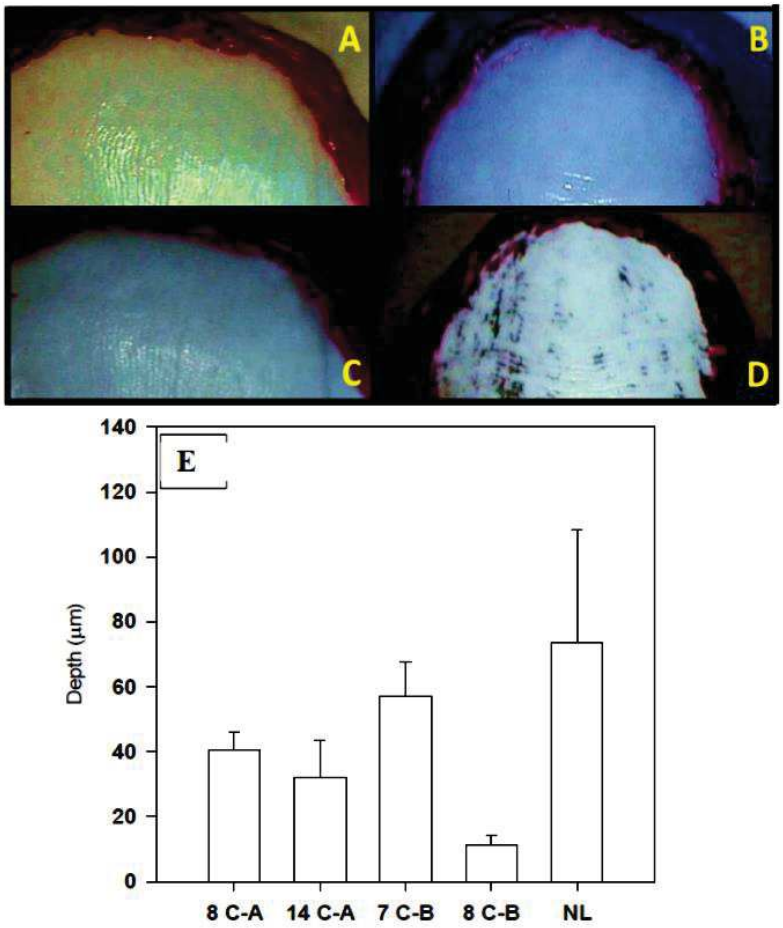

Fig. 1 Anatomical images in daylight mode made by intraoral camera. (A & B) Teeth before cycling. (C) Image after 8 cycles- Protocol A. (D) Image after 7 cycles- Protocol B. (E) Depth of lesions based on PO_4^{3-} intensity, produced by: Protocol A after 8 cycles (8C-A), on the same group, test has continued till 14 cycles (14 C-A). Protocol B after 7cycles (7C-B) and after 8 cycles (8 C-B). (NWL) natural white lesion. SD values are represented by error bars.

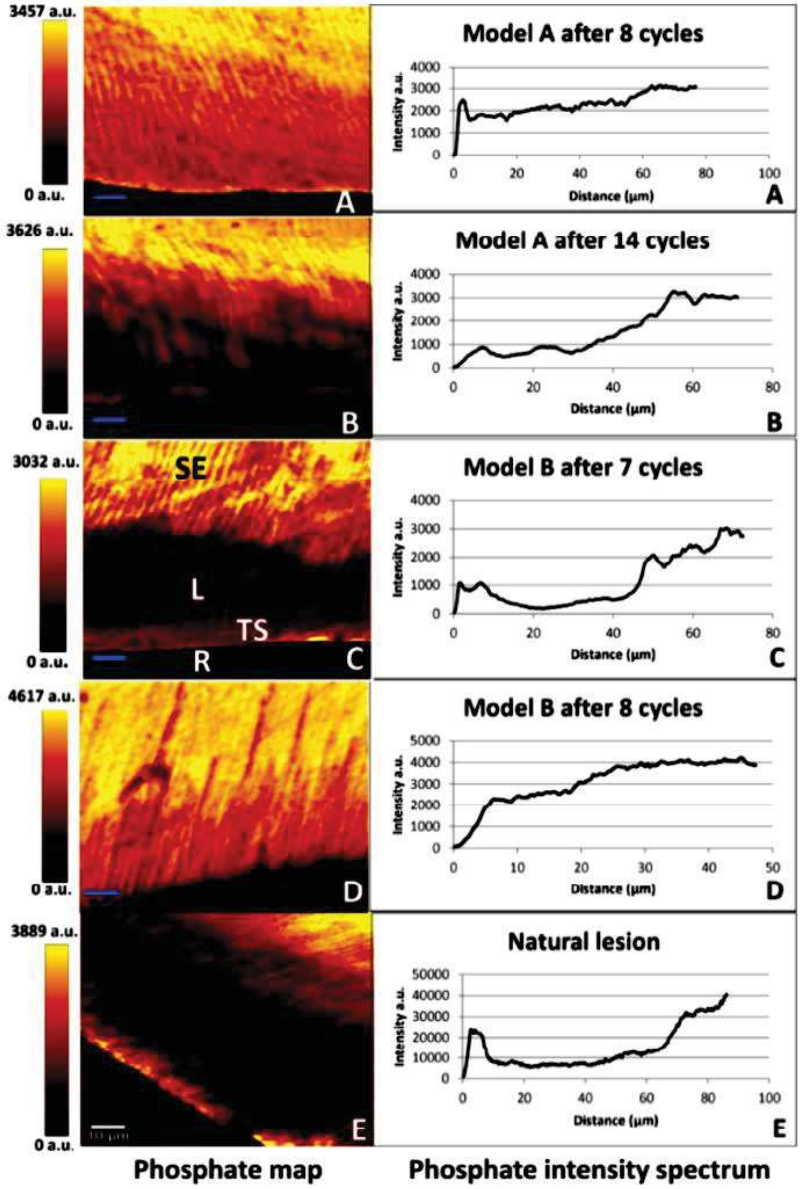

Fig. 2 Phosphate maps with their correspondent spectrums constructed from phosphate peak at 960 cm^{-1}. (A & B) demonstrating lesions produced by protocol A after 8 and 14 cycles. (C & D) Protocol

B after 7 and 8 cycles. (E) Natural lesion. Individual LUTs on the left. (Following symbols fixed on image (C) are valid for all images: SE; sound enamel, L; lesion, TS; tooth surface, R; resin.

Article 3

Journal of
Dental Research

Remineralization systems: make a difference in reversible caries treatment?

Journal:	*Journal of Dental Research*
Manuscript ID	Draft
Manuscript Type:	Research Reports
Date Submitted by the Author:	n/a
Complete List of Authors:	Al-Obaidi, Rand; LBN, Salehi, Hamideh; Université de Montpellier, Laboratoire Bio ingénierie et Nanosciences (LBN) Desoutter, Alban; Université de Montpellier, Laboratoire Bio ingénierie et Nanosciences (LBN) Levallois, Bernard; LBN JACQUOT, Bruno Tassery, Hervé; LBN 4203 Montpellier, operative dentistry; AMU university, Cuisinier, Frédéric
Keywords:	Caries treatment, Demineralization, Enamel biomineralization/formation, Hydroxyapatite, Minimally invasive dentistry
Abstract:	Different approaches have been developed to manage primitive caries lesions non-invasively through lesion remineralization in an attempt to prevent disease progression. The efficacy of GC Tooth Mousse cream (CPP-ACP) as a potent remineralizing agent has been extremely affirmed. Recently, nano-hydroxyapatite containing dentifrice "KAREX" has put on the market as a dental care product suitable for dental tissue renovation. In the present study, an in vitro caries model was used to compare the remineralizing effect of the two products. Each specimen was treated with the respective remineralizing agent for 5 min every 24h for 21 days, with the help of cotton applicator tip. Teeth scanned by confocal Raman microscopy to provide phosphate maps showing the net differences between affected and unaffected enamel areas. The prominent phosphate peak at 960 cm −1 was nominated to observe changes in its intensity. The width of the same peak measured by FWHM was calculated across each spectral map to evaluate the effect of remineralizing agents on crystalline structure of demineralized enamel. At the end of the treatment, a significant difference has attained in respect to phosphate gain in the body of lesions treated by nHA containing-dentifrice compared to the counterpart treated by CPP-ACP. However, ANOVA indicated no significant differences among the treatment groups with regard to enamel crystallinity. We can conclude that enamel surface layer permeability along with material formulation might represent key factors in subsurface lesion remineralization. Further studies of the biomimetic molecules involved in calcium, phosphate stabilization and nucleation may provide further

	improvements in the development of novel remineralization technologies.

Remineralization systems: make a difference in reversible caries treatment?

R. Al-Obaidi[1], H. Salehi[1], A. Desoutter[1], B. Levallois[1], B. Jacquot[2], H. Tassery[1, 2] and F. J. G. Cuisinier[1].

R. Al-Obaidi, H. Salehi, A. Desoutter, B. Levallois, F. J. G. Cuisinier, H. Tassery.

[1]LBN, University of Montpellier, Montpellier, France.

E-mail: rand.salih.mh@gmail.com

B. Jacquot. H. Tassery.

[2]Aix Marseille University, Marseille, France.

E-mail: herve.tassery@gmail.com

ABSTRACT

Different approaches have been developed to manage primitive caries lesions non-invasively through lesion remineralization in an attempt to prevent disease progression. The efficacy of GC Tooth Mousse cream (CPP-ACP) as a potent remineralizing agent has been extremely affirmed. Recently, nano-hydroxyapatite containing dentifrice "KAREX" has put on the market as a dental care product suitable for dental tissue renovation. In the present study, an *in vitro* caries model was used to compare the remineralizing effect of the two products. Each specimen was treated with the respective remineralizing agent for 5 min every 24h for 21 days, with the help of cotton applicator tip. Teeth scanned by confocal Raman microscopy to provide phosphate maps showing the net differences between affected and unaffected enamel areas. The prominent phosphate peak at 960 cm^{-1} was nominated to observe changes in its intensity. The width of the same peak measured by FWHM was calculated across each spectral map to evaluate the effect of remineralizing agents on crystalline structure of demineralized enamel. At the end of the treatment, a significant difference has attained in respect to phosphate gain in the body of lesions treated by nHA containing-dentifrice compared to the counterpart treated by CPP-ACP. However, ANOVA indicated no significant differences among the treatment groups with regard to enamel crystallinity. We can conclude that enamel surface layer permeability along with

material formulation might represent key factors in subsurface lesion remineralization. Further studies of the biomimetic molecules involved in calcium, phosphate stabilization and nucleation may provide further improvements in the development of novel remineralization technologies.

Keywords: CPP-ACP, nHA containing-dentifrice, confocal Raman microscopy, phosphate maps, non-invasive treatment, full-width at half-maximum (FWHM).

INTRODUCTION

White spot lesion (WSL) represents an early stage of caries formation where an intact surface layer (ISL) overlays subsurface enamel demineralization which takes place due to imbalance between pathological and protective factors (Robinson et al. 2000). Non-invasive treatment of WSL through remineralization; represents the aim of modern dentistry. The clinical usage of calcium phosphate salts in enamel remineralization process was unsuccessful because these salts are insoluble and unable to provide bioavailable ions which are essential for enamel restoration. Novel technology assists in localizing bioavailable ions at tooth surface to promote enamel renovation becomes mandatory (Cross et al. 2007a).

Dairy products are among the nutrients the most recognized as exhibiting an anticariogenic activity (Reynolds 1998). The components largely responsible for this activity have been identified as bovine milk phosphoprotein, casein, calcium and phosphate (Reynolds and Del Rio 1984; Reynolds and Johnson 1981; Reynolds 1998). Casein phosphopeptides (CPP) containing the cluster sequence – Ser(P)-Ser(P)- Ser(P)-Glu-Glu – have a remarkable ability to stabilize amorphous calcium phosphate (ACP) in a metastable solution. The CPP binds high amounts of calcium and phosphate to forming nanoclusters of ACP through the multiple phosphoseryl residues, preventing their growth to the critical size required for nucleation and precipitation (Reynolds 1998). Thus, CPP tends to increasing calcium and phosphate levels in the subsurface lesions, thereby esthetically repair WSLs (Chen et al. 2013; Reynolds 1997). This tasteless, stable and highly soluble CPP-ACP has been registered as Recaldent™ and commercialized in dental professional products (Tooth Mousse™). GC Tooth Mousse cream containing 10% w/w

CPP-ACP has been used clinically to treat mild to moderate fluorotic tooth enamel without surgical intervention (Cross et al. 2007a).

Nano-hydroxyapatite (nHA) is one of the most biocompatible and bioactive materials which have similarity to the apatite crystal of tooth enamel in morphology, crystal structure and crystallinity (Vandiver et al. 2005). Recently, many reports have shown that (nHA) has the potential to remineralize artificial carious lesions following addition to toothpastes, mouthwashes (Huang et al. 2009; Yamagishi et al. 2005). nHA displays high affinity to the tooth and can strongly adsorb on enamel surfaces (Roveri et al. 2009), promoting remineralization due to their size-specific effects corresponding to enamel ultrastructure (Li et al. 2008). Toothpaste comprising (nHA) has been commercially available in Japan since the 1980s, and was approved as an opposing caries agent in 1993 based on randomized anti-caries field trials in Japanese school children (KANI et al. 1989).

KAREK is a caries-inhibitory nHA containing-dentifrice, lately produced by Zahnpasta (dental care products, Bielefeld, Germany). It has antimicrobial effects thanks to the presence of active substances zinc and xylitol. This hydroxyapatite (HA) based toothpaste forms a protective layer on tooth surfaces and can initiate regeneration of attacked areas even in case of low salivary flow rates because the active ingredient is already present in mineral form and does not have to be formed from the saliva through remineralisation processes (Najibfard et al. 2011).

Confocal Raman microscopy is a powerful technique, measures the inelastic scattering of incident light which is used to analyze the internal structure of mineralized tissues. The spatial resolution of 300 nm; makes it a novel optical approach appropriate for incipient caries detection (Al-Obaidi et al. 2018).

The efficacy of Tooth Mousse™ cream as a potent remineralizing agent has been affirmed by many regulatory bodies around the world. Therefore, the purpose of the current study was to determine whether newly produced KAREX tooth paste is able to remineralize artificial subsurface enamel lesions and comparing its remineralizing effect with GC Tooth Mousse cream, being used as a criterion in this study.

MATERIALS & METHODS

12 sound premolars were extracted for orthodontic treatment and collected with patients' consent and approval of the local ethical research committee (process No. 2017-2907) before usage.

Teeth were cleaned of debris, stored in de-ionized water with 0.1% antimicrobial thymol at 4°C until use.

Teeth were exposed to pH cycling chemical model to induce uniform, reproducible subsurface enamel lesions *in vitro* through the use of sequential series of exposure to de/remineralizing solutions. The regimen was repeated for a period of 6 days, the temperature maintained at 37 ◦C (Al-Obaidi et al. 2018). Thereafter, teeth were randomly divided into 2 groups and cut into two, each part being scanned by Raman microscopy two times: once after initial caries induction and once again after intervention to decrease sources of variation.

GC Tooth Mousse cream (Recaldent™, CPP-ACP) and KAREX tooth paste (dental care products, Griesheim, Germany) were applied to remineralize the formerly created lesions. Each specimen was treated with the respective remineralizing agent for 5 min every 24h for 21 days, with the help of cotton applicator tip. Treated samples washed with distilled water and placed in artificial saliva at 37°C. Artificial saliva was renewed every 24h just before immersion of freshly treated samples (Mehta et al. 2013). The artificial saliva was prepared according to a method given by (Sato et al. 2006), using inorganic components similar to that of natural saliva. 3.90 mM Na_3PO_4, 4.29 mM NaCl, 17.98 mM KCl, 1.1 mM $CaCl_2$, 0.08 mM $MgCl_2$, 0.05 mM H_2SO_4, 3.27 mM $NaHCO_3$, pH = 7.2. All chemical products were supplied by Sigma-Aldrich, France.

Raman microscopy:

Raman spectra were recorded using a Witec Confocal Raman Microscope System (Witec, Ulm, Germany). Excitation was assured by a frequency doubled Nd: YAG visible laser (Newport, Evry, France) at 532nm. Acquisition time of a single spectrum was adjusted to 0.05 s.

Chemical mapping of dental enamel was carried out over enamel cross section from outer surface toward DEJ. The prominent phosphate peak at 960 cm^{-1} attributed to symmetric stretching mode ν_1; was nominated as the inner standard to observe changes in PO_4^{3-} intensity. Furthermore, the width of the same PO_4^{3-} peak was calculated across each spectral map to evaluate the effect of remineralizing agents on crystalline structure of demineralized enamel. As

peak width increases, crystallinity decreases (Xu et al. 2012). An indicative standardization bar showing the maximum and minimum sums of phosphate intensity across the enamel film; was adopted.

Representative Raman spectra were collected from the damaged and healthy enamel sites and enhanced after baseline correction using (SpectraGryph- optical spectroscopy software, Version 1.2.7, 2017). Thereafter, phosphate intensity at 960 cm^{-1} along with ($FWHM^{-1}$) values were obtained twice; once after artificial caries induction and over again after treatment with the remineralizing agents to detect the net differences in enamel inorganic component.

Viscosity measurement:

Viscosity of remineralizing agents was determined using FUNGILAB viscometer (FUNGILAB S.A. Ind., Spain). Spindle number (R7) was used and the rotation speed of the spindle was adjusted to 6.0 RPM.

STATISTICAL ANALYSIS:

Statistical analysis was performed using ANOVA test for normally distributed data and Kruskal-Wallis ANOVA for data that were not normally distributed. All statistical procedures were performed at over all significant level of $\alpha = 0.05$ with SigmaPlot version 11.0 (Systat Software, Inc., USA).

Difference (D) between initial PO_4^{3-} intensity (I_i, after pH cycling) and final intensity (I_f, after treatment with the selected agents) was calculated for each specimen and the mean of this difference ($\bar{D}$) was calculated for each of the experimental groups. The ratio of the difference ($\bar{D}$) to the ($\bar{I_i}$) was also calculated for each experimental group, which represents the rate of change in phosphate intensity of the specimens (Featherstone et al. 1983). The same calculation was repeated to measure the rate of change in FWHM value which is inversely proportional to enamel crystallinity as elucidated in Table 1.

$$(D) = I_f - I_i \ldots (1)$$

$$(\bar{D}) = \sum (D)/n \ldots\ldots\ldots (2)$$

$(I_i^-) = \sum (I_i)/n$..... (3)

% rate of change in the intensity (CI) = $(D^-)/(I_i^-)$* 100..... (4)

RESULTS:

Phosphate maps were constructed from phosphate peak intensity at 960 cm^{-1} before and after remineralization (Fig.1). Phosphate intensity reveals its amount within the inorganic crystals and directly related to the degree of enamel mineralization. Therefore, each pseudo color in these images signifies a certain amount of phosphate in accordance with the adjacent standardization bars.

The yellow tint designates high mineral content in the outermost enamel layer and the unaffected inside enamel layer which represents the end of the lesion. Whereas, the body of the lesion looks brown in color due to severe reduction in PO_4^{3-} amount in this area (Fig.1FA-GC). A slight reduction in lesion depth was observed after remineralization (double ended arrows in Fig.1ID &FD-KA), besides, a clear evidence of remineralization of the subsurface lesions and ISLs following treatment with nHA containing-dentifrice (arrows in Fig.1IC-KA, FC-KA).

Data analysis verified that there were no significant differences ($p>0.05$) among the groups before and after treatment with CPP-ACP with respect to PO_4^{3-} intensity and enamel crystallinity in subsurface lesion & ISL zones (Fig.2A, B).

Analysis demonstrated that nHA containing-dentifrice significantly ($p<0.05$) promoted mineral gain in the enamel subsurface lesion and ISL areas (Fig.2C). However, no significant differences were noticed among the treatment groups with regard to enamel crystallinity (Fig.2D).

Correlated influence of CPP-ACP & nHA containing-dentifrice on the subsurface lesion and ISL areas are shown in (Fig.2E, F) to detect distinguished differences in their performance. The only significant difference was attained in respect to mineral gain in the body of lesions treated by dentifrice compared to the counterpart treated by CPP-ACP (Fig.2E). The statistical analysis showed no differences in the exerted effect of both products on mineral gain in ISL and on the degree of crystallinity in ISL and subsurface lesion zones (Fig.2E, F).

The rate of changes in phosphate intensity and FWHM value in ISL and subsurface lesion regions after treatment with remineralization agents are shown in (Table 1). The change in mineral gain proves that CPP-ACP exerted a minor reminerlizing effect on ISL of the lesion

(+9.2%). While, mineral loss from the subsurface layer has detected after CPP-ACP application (-8.1%). nHA containing-dentifrice exhibits an important tendency to remineralizing subsurface lesions (+96.6%), and, to a lesser extent, ISL zone (+39.66). The table shows negative changes in FWHM value in ISL and subsurface lesion regions after treatment with remineralization agents; underlined an improvement in enamel crystallinity. CPP-ACP had a better effect on enamel texture than nHA containing-dentifrice.

DISCUSSION

Non-invasive management of non-cavitated caries lesions represents an essential goal of modern dentistry, involving remineralization systems to repair the enamel with bioavailable calcium & phosphate ions. The CPP acts as a delivery vehicle to co-localize bioavailable calcium and phosphate ions at the tooth surface. It can adapt its conformation to a wide range of surfaces, including the amorphous phases, thereby binding spontaneously forming clusters of calcium phosphate ions in a metastable solution, preventing their growth to the critical size required for nucleation (Reynolds 1998). The mechanism of action of CPP-ACP needs to be considered at a location inside the subsurface lesion, as well as at the surface of the lesion. The CPP-ACP has been determined to be amorphous electroneutral nanocomplexes with a hydrodynamic radius of 1.53 ± 0.04 nm (Cross et al. 2005). From the size and electroneutrality of the nanocomplexes, it would be predictable that they would enter the porosities of demineralized enamel and diffuse down concentration gradients into the lesion body. The released calcium, phosphate ions at the enamel surface will participate in a variety of equilibrium to form a range of calcium phosphate species, depending on the pH (Cochrane et al. 2008).

The process of diffusion into a subsurface lesion must be an overall electro neutral process. Therefore, diffusion potential into an enamel subsurface lesion can be characterized by the active gradients of the neutral ion pair, $CaHPO_4^0$, diffuses down its gradients into the lesion (Cochrane et al. 2008; Reynolds 1997). Once present in the enamel subsurface lesion, the CPP-ACP would release the weakly bound calcium and phosphate ions (Cochrane and Reynolds 2009; Cross et al. 2005), which would then deposit into crystal voids, promoting crystal growth at the hydroxyapatite (001) plane or along the c-axis; resulting in strengthening and widening of enamel rods (Huq et al., 2000). The CPPs have a high binding affinity for apatite (Cross et al.

2007b); hence, on entering the lesion, the CPPs would bind to the more thermodynamically favored surface of an apatite crystal face. Hence, the release of bioavailable ions would be thermodynamically driven. This theory could explain the negative change in FWHM value illustrated by Table 1, where the reduced width of the phosphate band after treatment with CPP-ACP reflects a minor enhancement in enamel crystalline configuration.

However, supersaturation with respect to HA in which no spontaneous precipitation occurs, can't be expected to exist for a long period. After the contact between enamel apatite and the supersaturated solution; the mineral formation by growth of existing, partly demineralized crystals, largely reduces the supersaturation level in a way that a spontaneous nucleation is unlikely to occur (Larsen and Fejerskov 1989; Larsen and Jensen 1986). This could explicate the limited influence of remineralizing agents on enamel crystallinity reconstitution (Fig.2B, D).

Since the degree of hard tissue mineralization is directly related to phosphate sum-intensity (Akkus et al. 2016); Raman phosphate maps can show that CPP-ACP has a slight remineralization effect on ISL. Whereas, the dashed line in image (FB-GC, Fig.1); depicts an undesirable change in the mineral content of the subsurface layer (-8.1%). Previous studies (Arends 1980; Silverstone et al. 1981) indicated that mineral deposition is most easily formed superficially; making surface layer of the lesion appears harder and glossy. While the subsurface porous, demineralized part of the lesion remains unaltered, explaining why a proper remineralization of body of the lesion, rarely occurs (Fig.1, FB-GC).

Larsen (Larsen and Fejerskov 1989) (one of the pioneers in remineralization research), tested the results of enamel powder produced from intact teeth, suspended in remineralizing solutions. A reduction in pH value was observed during apatite formation because almost all phosphate in the aqueous phase prior to precipitation is in the form of H_3PO_4, $H_2PO_4^-$ and HPO_4^{2-} while the same phosphate after the uptake in the apatite is mostly in the PO_4^{3-} form according to the following reaction (Larsen and Jensen 1986):

$$10\ Ca^{+2} + 3HPO_4^{2-} + 3H_2PO_4^- + 2\ H_2O \longrightarrow 2\ Ca_5(PO_4)_3OH + 11\ H^+$$

The released H^+ ions cause the pH to drop. The simultaneous pH decrease inhibits precipitation of calcium and phosphate in the aqueous phase, but it has a solubilizing effect on the enamel mineral (Larsen 1986). This could explain the reduced amount of mineral that has been detected in subsurface lesions being treated with CPP-ACP. The impaired effect of CPP-ACP reported in this study is in accordance with previous observations stated in several clinical studies

(Andersson et al. 2007; Bailey et al. 2009; Beerens et al. 2010; Bröchner et al. 2011), conducted to detect remineralizing effect of CPP-ACP cream *in vivo*. They failed to show any significant benefit of this product in reversing WSLs noninvasively. Even though, absence of effects might be due to ineffectiveness of this agent or insufficient sample sizes to detect significant differences. Thus, further researches to verify the efficacy of this combined therapy would be beneficial.

Nevertheless, the current findings seem to be inconsistent with those reported in former *in vitro* studies, tested effect of ion composition of CPP-ACP solutions on subsurface enamel lesion restoration. (Cochrane et al. 2008; Reynolds 1997) have demonstrated that CPP-ACP can promote remineralization of subsurface enamel lesions. The fact that they tested the effect of CPP-ACP solutions, while our current study has examined the remineralizing effect of CPP-ACP topical cream assigned to in-office/at home application could stand behind this discrepancy. Solutions are less viscous than creams, thus, better diffusion is predictable since viscosity is inversely proportional to the diffusivity (Stylianopoulos et al. 2010).

The surface chemical properties and morphological structure of nHA, combined with its chemical and physical similarity with natural enamel, have been claimed to play an important role in the remineralization of early caries lesions (Li et al. 2008). Many factors increased the potential of nHA to fill up defects and micropores on demineralized enamel such as increased surface area, increased proportion of atomicity, solubility properties of nHA (Kaehler 1994). When nHA penetrates the enamel pores, it will act as a template in the precipitation process. Thereby, it will constantly attract large amounts of Ca^{2+} and PO_4^{3-} from the remineralization solution to the enamel surface to fill the vacant positions of the enamel crystals. This in turn will reinforce crystal integrity and growth (Huang et al., 2009). Consequently, the deposition of nHA on outer enamel layer would probably block surface pores and restrict diffusion into subsurface lesion over the short-term remineralization. However, nHA is progressively transferred from the newly sediment apatite coating to inward. Finally, it is precipitated in the body of subsurface lesion in the long-term remineralization (Jongebloed and Arends 1981; Najibfard et al. 2011).
It is noteworthy that nHA containing-dentifrice has been tested in this study. Its influence was found to be superior to the CPP-ACP paste regarding to subsurface lesions remineralizatiion (Fig.2E). Phosphate maps in Fig.1A, B affirm that CPP-ACP has limited remineralizing

influence on the body of lesion. Contrary to nHA containing-dentifrice (Fig.1C, D) which has triggered a patent remineralization of subsurface lesions (+96.6%).

Viscosity test confirmed that CPP-ACP cream is more viscous than nHA containing-dentifrice (2665 P versus 1846.65 P, respectively). As viscosity is inversely proportional to the diffusivity, diffusion process represents a limiting factor in the subsurface lesion remineralization (Arends 1980; Stylianopoulos et al. 2010). Consequently, nHA containing-dentifrice produced more profound remineralizaton of subsurface lesion thanks to its lower viscosity and thus better ionic diffusion rates. Therefore, viscosity of the tested pastes could be considered as a key factor that might explain the discrepancy in their treating effect.

Fig.2 (A & C) describes the quantity of phosphate component; confirms that the outermost layers of teeth used to assess nHA containing-dentifrice capability; were basically less mineralized and thus more porous, than surface layers of teeth implicated in testing CPP-ACP efficacy. For mineral deposition to occur within the body of the lesion, calcium and phosphate ions must first penetrate enamel surface. Therefore, the presence of relatively mineralized and charged surface layer covering severely porous underlying enamel may result in restricted permeability of the ions and ion pairs necessary for mineral formation and subsequent underlying layer remineralization (Larsen and Fejerskov, 1989). In addition, the large variations in enamel chemical composition with respect to concentration gradients of specific mineral ions are therefore likely to result in large local variations in rates of both demineralization and remineralization (Robinson 1983; Robinson et al. 1971; Weatherell et al. 1968).

Remineralization systems represent a major advance in non-invasive treatment of incipient caries lesions. However, further studies of the biomimetic molecules involved in calcium, phosphate stabilization and nucleation may provide further improvements in the development of novel remineralization technologies.

CONCLUSION

CPP-ACP effect is confined to ISL making it a less permeable layer. These results are inconsistent with the proposed anticariogenic mechanism of the CPP, which is enhancement of remineralization through the localization of ACP at tooth surface. In addition, nHA containing - dentifrice has the potential to remineralize the whole lesion consistently. The study indicated a lack of reliable evidence supporting the effectiveness of remineralizing agents in WSLs treatment. Likewise, de novo formation of crystals in body of the lesions remains an entirely

unsolved problem. Largely, the present study points out that viscosity of the remineralizing material with enamel surface layer permeability represent serious obstacles to remineralization.

ACKNOWLEDGEMENTS

The authors would like to acknowledge the contribution of Iraqi government represented by Ministry of Higher Education and Scientific Research. Special thanks to Dr. Friedrich Menges (developer of Spekwin32 & Spectragryph) for his unconditional help and support.

COMPETING FINANCIAL INTERESTS

Authors declare no competing financial and non-financial interests in relation to the work described.

REFERENCES

Akkus A, Akkus A, Roperto R, Akkus O, Porto T, Teich S, Lang L. 2016. Evaluation of mineral content in healthy permanent human enamel by raman spectroscopy. Journal of clinical and experimental dentistry. 8(5):e546.

Al-Obaidi R, Salehi H, Desoutter A, Bonnet L, Etienne P, Terrer E, Jacquot B, Levallois B, Tassery H, Cuisinier F. 2018. Chemical & nano-mechanical study of artificial human enamel subsurface lesions. Scientific reports. 8(1):4047.

Andersson A, Sköld-Larsson K, Haligren A, Petersson LG, Twetman S. 2007. Effect of a dental cream containing amorphous calcium phosphate complexes on white spot lesion regression assessed by laser fluorescence. Oral health & preventive dentistry. 5(3).

Arends J. 1980. Remineralization of artificial enamel lesions in vitro. Caries research. 14(6):351-358.

Bailey D, Adams G, Tsao C, Hyslop A, Escobar K, Manton D, Reynolds E, Morgan M. 2009. Regression of post-orthodontic lesions by a remineralizing cream. Journal of dental research. 88(12):1148-1153.

Beerens M, Van Der Veen M, Van Beek H, Ten Cate J. 2010. Effects of casein phosphopeptide amorphous calcium fluoride phosphate paste on white spot lesions and dental plaque after orthodontic treatment: A 3-month follow-up. European journal of oral sciences. 118(6):610-617.

Bröchner A, Christensen C, Kristensen B, Tranæus S, Karlsson L, Sonnesen L, Twetman S. 2011. Treatment of post-orthodontic white spot lesions with casein phosphopeptide-stabilised amorphous calcium phosphate. Clinical oral investigations. 15(3):369-373.

Chen H, Liu X, Dai J, Jiang Z, Guo T, Ding Y. 2013. Effect of remineralizing agents on white spot lesions after orthodontic treatment: A systematic review. American journal of orthodontics and dentofacial orthopedics. 143(3):376-382. e373.

Cochrane N, Reynolds E. 2009. Casein phosphopeptides in oral health. Food constituents and oral health. Elsevier. p. 185-224.

Cochrane N, Saranathan S, Cai F, Cross K, Reynolds E. 2008. Enamel subsurface lesion remineralisation with casein phosphopeptide stabilised solutions of calcium, phosphate and fluoride. Caries research. 42(2):88-97.

Cross K, Huq N, Reynolds E. 2007a. Casein phosphopeptides in oral health-chemistry and clinical applications. Current pharmaceutical design. 13(8):793-800.

Cross KJ, Huq NL, O'Brien-Simpson NM, Perich JW, Attard TJ, Reynolds EC. 2007b. The role of multiphosphorylated peptides in mineralized tissue regeneration. International Journal of Peptide Research and Therapeutics. 13(4):479-495.

Cross KJ, Huq NL, Palamara JE, Perich JW, Reynolds EC. 2005. Physicochemical characterization of casein phosphopeptide-amorphous calcium phosphate nanocomplexes. Journal of Biological Chemistry. 280(15):15362-15369.

Featherstone J, Ten Cate J, Shariati M, Arends J. 1983. Comparison of artificial caries-like lesions by quantitative microradiography and microhardness profiles. Caries research. 17(5):385-391.

Huang S, Gao S, Yu H. 2009. Effect of nano-hydroxyapatite concentration on remineralization of initial enamel lesion in vitro. Biomedical Materials. 4(3):034104.

Jongebloed W, Arends J. 1981. Remineralization of artificial enamel lesions in vitro. Caries research. 15(1):60-69.

Kaehler T. 1994. Nanotechnology: Basic concepts and definitions. Clinical chemistry. 40(9):1797-1799.

KANI T, KANI M, ISOZAKI A, SHINTANI H, OHASHI T, TOKUMOTO T. 1989. Effect to apatite-containing dentifrices on dental caries in school children. Journal of Dental Health. 39(1):104-109.

Larsen M. 1986. An investigation of the theoretical background for the stability of the calcium-phosphate salts and their mutual conversion in aqueous solutions. Archives of oral biology. 31(11):757-761.

Larsen MJ, Fejerskov O. 1989. Chemical and structural challenges in remineralization of dental enamel lesions. European journal of oral sciences. 97(4):285-296.

Larsen MJ, Jensen S. 1986. Solubility study of the initial formation of calcium orthophosphates from aqueous solutions at ph 5–10. Archives of oral biology. 31(9):565-572.

Li L, Pan H, Tao J, Xu X, Mao C, Gu X, Tang R. 2008. Repair of enamel by using hydroxyapatite nanoparticles as the building blocks. Journal of Materials Chemistry. 18(34):4079-4084.

Mehta R, Nandlal B, Prashanth S. 2013. Comparative evaluation of remineralization potential of casein phosphopeptide-amorphous calcium phosphate and casein phosphopeptide-amorphous calcium phosphate fluoride on artificial enamel white spot lesion: An in vitro light fluorescence study. Indian journal of dental research. 24(6):681.

Najibfard K, Ramalingam K, Chedjieu I, Amaechi B. 2011. Remineralization of early caries by a nano-hydroxyapatite dentifrice. Journal of Clinical Dentistry. 22(5):139.

Reynolds E. 1997. Remineralization of enamel subsurface lesions by casein phosphopeptide-stabilized calcium phosphate solutions. Journal of dental research. 76(9):1587-1595.

Reynolds E, Del Rio A. 1984. Effect of casein and whey-protein solutions on caries experience and feeding patterns of the rat. Archives of oral biology. 29(11):927-933.

Reynolds E, Johnson I. 1981. Effect of milk on caries incidence and bacterial composition of dental plaque in the rat. Archives of oral biology. 26(5):445-451.

Reynolds EC. 1998. Anticariogenic complexes of amorphous calcium phosphate stabilized by casein phosphopeptides: A review. Special Care in Dentistry. 18(1):8-16.

Robinson C. 1983. Alterations in the composition of permanent human enamel during carious attack. Demineralisation and Remineralisation of the Teeth.209-223.

Robinson C, Shore R, Brookes S, Strafford S, Wood S, Kirkham J. 2000. The chemistry of enamel caries. Critical Reviews in Oral Biology & Medicine. 11(4):481-495.

Robinson C, Weatherell J, Hallsworth A. 1971. Variation in composition of dental enamel within thin ground tooth sections. Caries research. 5(1):44-57.

Roveri N, Battistella E, Bianchi CL, Foltran I, Foresti E, Iafisco M, Lelli M, Naldoni A, Palazzo B, Rimondini L. 2009. Surface enamel remineralization: Biomimetic apatite nanocrystals and fluoride ions different effects. Journal of Nanomaterials. 2009:8.

Sato Y, Sato T, Niwa M, Aoki H. 2006. Precipitation of octacalcium phosphates on artificial enamel in artificial saliva. Journal of Materials Science: Materials in Medicine. 17(11):1173-1177.

Silverstone L, Wefel J, Zimmerman B, Clarkson B, Featherstone M. 1981. Remineraiization of natural and artificial lesions in human dental enamel in vitro. Caries research. 15(2):138-157.

Stylianopoulos T, Poh M-Z, Insin N, Bawendi MG, Fukumura D, Munn LL, Jain RK. 2010. Diffusion of particles in the extracellular matrix: The effect of repulsive electrostatic interactions. Biophysical journal. 99(5):1342-1349.

Vandiver J, Dean D, Patel N, Bonfield W, Ortiz C. 2005. Nanoscale variation in surface charge of synthetic hydroxyapatite detected by chemically and spatially specific high-resolution force spectroscopy. Biomaterials. 26(3):271-283.

Weatherell I, Robinson C, Hiller C. 1968. Distribution of carbonate in thin sections of dental enamel. Caries research. 2(1):1-9.

Xu C, Reed R, Gorski JP, Wang Y, Walker MP. 2012. The distribution of carbonate in enamel and its correlation with structure and mechanical properties. Journal of materials science. 47(23):8035-8043.

Yamagishi K, Onuma K, Suzuki T, Okada F, Tagami J, Otsuki M, Senawangse P. 2005. Materials chemistry: A synthetic enamel for rapid tooth repair. Nature. 433(7028):819.

Table 1 shows the rate of change in phosphate intensity & full-width at half-maximum (FWHM) values after treatment with different remineralizing agents estimated by special equation. **ISL:** Intact Surface Layer.

Figure 1. PO_4^{3-} maps of incipient lesions before & after treatment with remineraling agents. Indicative standardization bars on both sides demonstrate max. & min. values of PO_4^{3-} peak intensity at 960 cm^{-1}. **GC:** CPP-ACP tooth mousse. **KA:** KAREX (nHA containing-dentifrice). **I:** Initial. **F:** Final. Signs on Image (FA-GC) are valid for all images: **SE:** Sound Enamel, **L:** Lesion, **ISL:** Intact Surface Layer, **R:** Resin.

Figure 2. An overall mean and standard deviation (SD) were plotted to show: effect of: **(A)** CPP-ACP & **(C)** KAREX on PO_4^{3-} peak intensity at 960 cm^{-1}. Effect of: **(B)** CPP-ACP & **(D)** KAREX on enamel crystallinity represented by $FWHM^{-1}$ values. **(E&F)** Associating effect of CPP-ACP & KAREX on PO_4^{3-} peak intensity & $FWHM^{-1}$ respectively. Treatment effects of both agents were tested in (**L**) Lesion zone & (**ISL**) Intact Surface Lesion zone consecutively. **I:** Initial. **F:** Final. **GC:** CPP-ACP tooth mousse. **KAREX:** nHA containing-dentifrice. Asterisk (*) recurrently indicates a significant difference ($p < 0.05$) between the two groups. Horizontal bar indicates no significant difference ($p > 0.05$) among the groups linked by it.

Title page:

Total word count (Abstract to Acknowledgments)	3527
Total word count (excluding abstract, acknowledgment)	3199
Abstract word count	257
Total number of figures and tables	3
Number of references	39
Keywords	Raman microscopy Non-invasive treatment Mineral components CPP-ACP nHA containing-dentifrice

Remineralizing agent plus affected zone	Rate of change in PO_4^{3-} intensity	Rate of change in FWHM
CPP-ACP (ISL)	+9.20 %	-2.60 %
nHA based-dentifrice (ISL)	+39.66 %	-0.49 %
CPP-ACP (Body of lesion)	-8.12 %	-2.28 %
nHA based-dentifrice (Body of lesion)	+96.60 %	-0.31 %

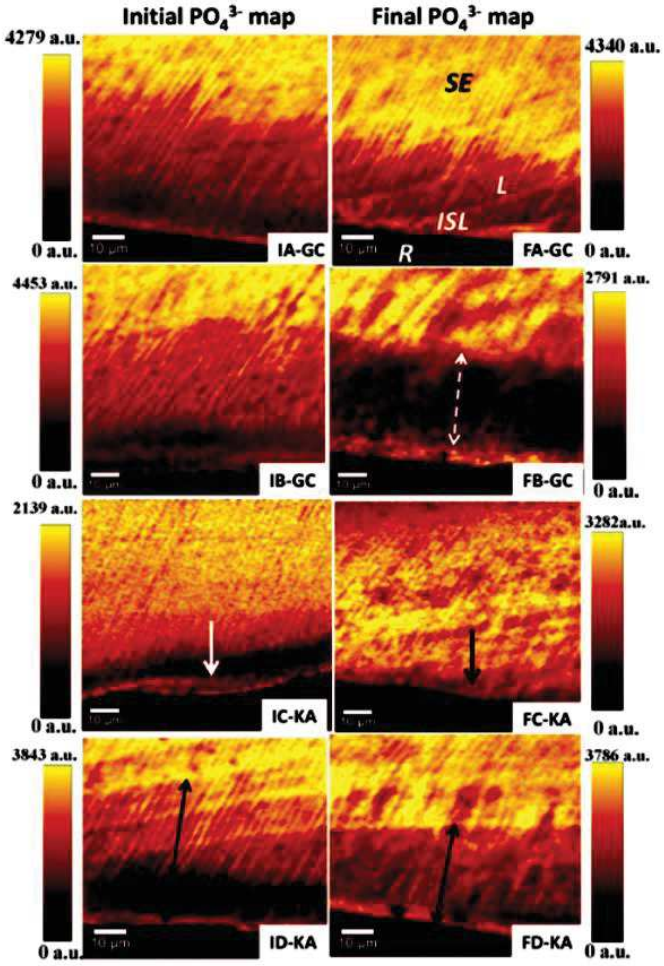

1

42x62mm (300 x 300 DPI)

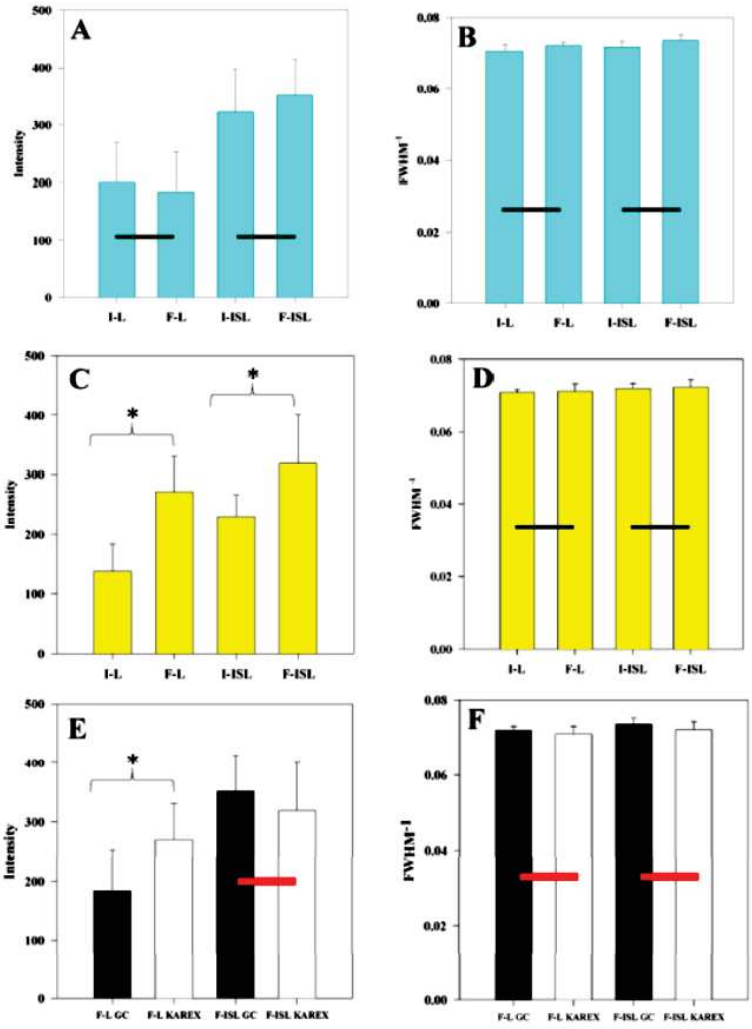

2

63x83mm (300 x 300 DPI)

Article 4

Liaison between Changes in Chemical Composition of Enamel Subsurface Lesions and The Emitted Nonlinear Optical Signals.

R. Al-Obaidi*[1], H. Salehi[1], H. Tassery[1, 2], B. Jacquot[2], F. J. G. Cuisinier[1], C. Gergely[3] &T. Cloitre[3]

R. Al-Obaidi, H. Salehi, F. J. G. Cuisinier, H. Tassery.

[1]LBN, University of Montpellier, Montpellier, France.

E-mail: rand.salih.mh@gmail.com

B. Jacquot. H. Tassery.

[2]Aix Marseille University, Marseille, France.

E-mail: herve.tassery@gmail.com

C. Gergely, T. Cloitre.

[3]Laboratoire Charles Coulomb (L2C), University of Montpellier, CNRS, Montpellier, France.

E-mail: csilla.gergely@umontpellier.fr

ABSTRACT

Enamel can be regarded as a functionally graded natural biocomposite, which will require special attention using high-resolution characterization methods to fully appreciate the significance of such a structure. Measurements on 14 human teeth were made using two incident lights of different wavelengths; released by confocal Raman microscopy and multi-photon microscopy (MPM). Phosphate peak intensity at 960 cm^{-1} together with organic to mineral ratio at (2931/430 cm^{-1}) and nonlinear optical signals (SHG second harmonic generation and 2PEF two-photon excitation fluorescence) spectra; were recorded from the damaged and healthy enamel sites. Raman spectral maps showed that the higher the organic/mineral ratio in the demineralized enamel, the lower is the intensity of mineral component in the same zone. Moreover, MPM

outcomes demonstrated an evident red shift of the fluorescence spectrum from carious enamel compared to that from sound enamel, in addition to the emergence of SHG peak from lesion zone of two specimens. These findings present another indication of carious lesion formation. By comparing 2PEF images with the structural motifs observed by confocal Raman imaging system; the morphological similarity of the acquired images is quite evident. The main conclusion is that 2PEF intensity increases with caries progression, thereby; any change in 2PEF intensity reflects changes in chemical composition of enamel. These findings may provide an important basis for potentially valuable applications in the clinical diagnosis of tooth pathological conditions. In addition, the outcomes expose the fundamental role of organic matrix in enamel integrity and reparation.

Keywords: non-invasive optical techniques, organic matrix, mineral components, auto-fluorescence (AF).

INTRODUCTION

Hydroxyapatite crystals (HACs) constitute about 96% of minerals in enamel [1]. While the proteins and lipids comprise around 3% of organic material in enamel that surrounds the mineral crystals. However, the organic matrix plays a paramount role in enamel integrity [2-4].

Dental caries formation and progression happen due to an imbalance between de/remineralization periods in enamel. When demineralization proceeds; white spot lesion (WSL) develops, signaling changes in enamel chemical composition [5]. Improving the diagnostic ability of initial caries lesions; will improve the potential of treatment without surgical intervention. Therefore, the development of new diagnostic technologies with high sensitivity and high specificity became compulsory. Based on the light scattering and autofluorescence (AF)

properties, spectroscopic and microscopic methods can have the potential to detect dental caries rather early [6]. Thus, the development of an effective, minimally invasive imaging modality is vital for investigating a variety of physiological phenomena and pathological conditions in dentistry.

Raman effect is resulted from the energy difference between the incoming excitation light and the scattered photons which is proportional to the vibrational energy of the molecules within the sample under study [7]. Confocal Raman microscopy is a powerful technique that measures the inelastic scattering of incident light which is used to analyze the internal structure of mineralized tissues. The spatial resolution of Raman microscopy (300 nm) makes it a sensitive diagnostic tool appropriate for early caries detection [8].

Fluorescence is a phenomenon by which an object is excited by a light of particular wavelength and then emits light at higher wavelength [6]. The molecules that can absorb photons and emit the energy as a photon with a red shifted wavelength known as fluoro or chromophores [9] which are responsible for fluorescence in enamel [10]. In dental research, Benedict [11] was one of the pioneers who described enamel fluorescence and thereafter proposed it as a method to detect dental caries [12]. The source of two-photon excitation fluorescence (2PEF) in dental tissues may vary with diverse excitation mechanisms involved and concerning both organic and inorganic components [13,14]. Enamel rod or prism is the basic unit of enamel structure filled with inorganic HA crystals, bounded by a sheath rich in organic components, giving rise to the 2PEF. Whereas the inorganic crystalline regions inside the prisms reveal low or no fluorescence due to low organic content [15]. Whereas dentin is a relatively elastic structure composed of collagen fibers [14] which generates strong SHG and 2PEF signals [16,17]. Multi-photon microscopy (MPM) has become a preferred imaging modality in biological research [18,19], providing a powerful means of visualizing dental

tissues, in both healthy and carious conditions [20,21]. MPM is a nonlinear imaging approach where fluorophores are excited by simultaneous absorption of two (or more) low-energy photons. 2PEF refers to the light emitted when a fluorophore absorbs two photons of equal wavelength arrive within a period of an attosecond (1×10^{-18} of second) and collaborate to excite the molecule [22]. Concurrently, these photons can also induce second harmonic generation (SHG) which is a coherent, nonlinear process that generates particularly strong signals when the molecules are well-ordered in non-centrosymmetric biological structures [16]. The major advantage of MPM lies in its capability to create images simultaneously based on the fluorescence signals produced by the process of multiphoton excitation (2PEF) and second harmonic generation (SHG) [17]. Collecting 2PEF signals is considered to be a promising technique for tissue auto-fluorescence imaging that allows deeper sample penetration and reduced photodamage thanks to laser excitation feature that produces signal only at the focal point [23,24].

The present research aims to correlate fluorescence-based results provided by multi-photon microscopy (MPM) with confocal Raman microscopy records regarding the phosphate level at 960 cm^{-1} and the organic matrix at ~2931 cm^{-1} in healthy and demineralized enamel of extracted human teeth.

MATERIALS & METHODS

14 sound premolars were extracted from patients aged between 13 to 14 years for orthodontic reasons. All teeth were collected with informed consent from all subjects and after approval of the local ethical research committee (process No. 2017-2907) before being used in this research. All procedures were carried out in accordance with relevant guidelines and regulations. The number of teeth required in this study was calculated by using BiostaTGV site [25].

Teeth were washed with de-ionized water to remove any debris, stored in de-ionized water with 0.1% antimicrobial thymol and kept at 4°C until use. All teeth were exposed to pH cycling chemical model [26] to create uniform, reproducible subsurface enamel lesions *in vitro*. Teeth were then sectioned longitudinally into two halves by using high speed diamond saw (Isomet 2000, Buehler, USA) to produce cross sections of teeth which then embedded in self-curing acrylic resin (GC, Japan), having the cross sectioned surface of the samples facing the surface that is to be polished later. For further details see [26].

Raman microscopy:

Witec Confocal Raman Microscope System alpha 300R (Witec, Ulm, Germany) was used to register Raman spectra. Excitation in the confocal Raman microscopy was assured by a frequency doubled Nd: YAG laser (Newport, Evry, France) that illuminated the inspected sample with a visible light of wavelength 532 nm. Raman spectra were attained using a ×20 objective with numerical aperture of 0.46 (Nikon, Tokyo, Japan) focused on the specimens. Then Raman backscattered radiation mixed with Rayleigh scattered light were passed through an edge filter to block the Rayleigh's. Exposure time of a single spectrum was set to 0.05 s. Each spectrum corresponding to a spatial unit is defined as a voxel ($300\,nm \times 300\,nm \times 1\,\mu m$). All data acquisition and processing were performed using Image Plus software from Witec inc [27].

Raman linear mapping of dental enamel was attained from enamel cross section, starting at the outer enamel surface and ending in the inner enamel ahead of the dentin enamel junction (DEJ). Raman peak at 960 cm^{-1} is assigned to ν_1 vibration mode of the phosphate group in enamel which was selected as the inner standard to observe changes in sum-intensity of the strongest PO_4^{3-} peak. The 2931cm^{-1} Raman band attributed to the C–H stretching/deformation of organic

matrix in enamel, was related to the phosphate peak at (ν_2) 430 cm^{-1}. The later peak was chosen as the internal standard for the normalization adjustment and calculation of organic to mineral components ratio in the sound and carious enamel in order to evaluate the variances in the chemical composition of enamel [28]. Red and violet hues of an indicative look-up table (LUT); designate the maximum and minimum phosphate intensities and organic/mineral ratio in a chosen area respectively [27].

Multiphoton Microscopy (MPM)

For further investigations, each cross section was scanned by MPM to support the results provided by Raman microscopy. 2PEF images were registered with a custom-built multiphoton microscope based on a SliceScope upright microscope (MPSS-1000P) equipped with a Multiphoton Scan Head (MP-2000), both from Scientifica LTD. For sample excitation, we used a Spectra-Physics Tsunami Ti-Sapphire laser operated in pulsed mode, wavelength range, 760 to 900nm, typically 870 nm, repetition rate 80 MHz; pulse duration ~100 fs. The laser beam was focused on the sample by a Nikon CFI75 LWD-16x-W objective (NA 0.8, water immersion). Images were created by laser raster scanning the sample. The fuorescence signal was epi-collected through the objective; separated from the backscattered laser light and SHG signal by the combination of a 735nm long pass dichroic mirror (87-065 Edmund Optics), a 750 nm short pass filter (FESH0750, Thor Labs), and a 475-nm long-pass filter (84-705, Edmund Optics); and then detected with a photomultiplier tube (R928P; Hamamatsu). The SHG signal was collected through a 1.4-NA oil-immersion condenser (U-AAC, Olympus), filtered by using a 482nm long pass dichroic mirror (86-331, Edmund Optics) and a 447 nm high-performance band-pass filter (48-074, Edmund Optics) and then detected by a H7422P photomultiplier (Hamamatsu). The method enables acquisition of in-depth Z-stacks of 2-dimensional images of the sample based on

their nonlinear optical response (SHG and 2PEF emission) when excited in the infrared domain. Recorded images were treated by Image J software (http://rsb.info.nih.gov/ij/; National Institutes of Health, Bethesda, MD, USA) through the use of green lookup table.

Nonlinear Optical Spectroscopy

2PEF and SHG spectra were obtained using a fiber coupled imaging spectrometer and a back-illuminated CCD (Acton SP215i and PIXIS 400B Excelon, Princeton Instruments). 2PEF signal was epi-collected and coupled via the optical fiber using achromatic lenses. The backscattered laser light was filtered out with the same 735nm long pass dichroic /750-nm short-pass filter combination.

Statistical analyses:

Phosphate intensity at 960 cm^{-1} together with ratio of intensities of two Raman peaks (2931 to 430 cm^{-1}) and nonlinear optical (SHG and 2PEF) spectra were gathered from the damaged and healthy enamel sites. Data were plotted and the mean and the standard deviation were calculated. Statistical analyses were performed using Kruskal-Wallis One Way ANOVA Analysis of Variance on Ranks for data that were not normally distributed. All statistical tests were made at over all significant level of $\alpha = 0.05$ with SigmaPlot version 11.0 (Systat Software, Inc., USA). Representative Raman spectra along with nonlinear optical spectra were enhanced (after baseline correction) by using (SpectraGryph- optical spectroscopy software, Version 1.2.7, 2017).

RESULTS

Phosphate map was mounted from phosphate peak intensity at 960 cm^{-1} is presented in (Fig. 1A). According to the adjacent (LUT); highest PO_4^{3-} peak intensity is demonstrated by sound unaffected enamel (region 1) which looks red in color. Whereas, an important decrease in PO_4^{3-} intensity is revealed by the subsurface lesion (region 2). The demineralized area is delineated by double ended black arrow in (Fig. 1A). Fig.1B shows a false image constructed from organic/mineral ratio at (2931/430 cm^{-1}) with a noticeable difference perceived between region 1 & 2. In accordance with the corresponding LUT; the red shade in region 2 confirms a marked increase in the amount of enamel organic matrix compared to the degraded blue shade observed in region 1. Representative Raman spectra from both regions are presented in (Fig. 1C). The two spectra vary significantly in respect to PO_4^{3-} peak intensity at two internal vibrational modes v_1 & v_2 consecutively. Moreover, the original peak at 2931cm^{-1} related to the C–H bond has shown up solely after collecting spectra from different demineralized enamel zones.

2PEF images with their corresponding nonlinear optical spectra generated by sound enamel (1) and subsurface lesion (2) regions are shown in (Fig.2 A, B, C). The green pseudo-color was used to designate auto-fluorescence of enamel. The characteristic enamel rods structure is clearly observed in the high-resolution 2PEF images in (Fig.2 A, B). The intensity contrast among regions 1 and 2 reveals the importance of organic matrix in enamel. In region 1, enamel prism sheaths (white arrows) revealed high fluorescence, whereas no fluorescence was detected from the prisms themselves. These observations were entirely overturned in region 2.

Dental enamel emitted broad 2PEF spectra from 400 to 700 nm. Maximum 2PEF intensity was localized at 520 nm. Site-specific spectral profiles from sound enamel and lesion area vary slightly in terms of intensity as well as in the relatively strong shift of the carious enamel spectrum to the red (at about 650-750 nm) compared to the intact enamel spectrum (Fig.2 C).

Moreover, SHG peak at ~435 nm was exclusively collected from lesion zone of two specimens as depicted in (Fig.3).

Fig.4B describes the alteration in organic/mineral ratio at (2931/430 cm^{-1}) in the selected regions. The ratio of the two intensities was calculated by incorporating the area under the peaks to analyze the variation in organic matrix composition of affected and unaffected enamel. This difference was found to be statistically significant. Recorded spectra were employed in terms of intensity as illustrated in (Fig.4 A, C, D). The graphs combine the obtained PO_4^{3-} intensity at 960 cm^{-1} and 2PEF signal intensity at 520 & 675 nm; produced by region 1 & 2 respectively. A significant difference has noticed regarding the PO_4^{3-} intensity at 960 cm^{-1} released by the two regions (Fig.4A). Slight increases in the intensity of 2PEF signal at 520 nm generated by region 2 was detected as compared to region 1. Though, the statistical difference was not significant (Fig.4C). However, the red shift of the fluorescence at 675 nm differs significantly in terms of intensity after comparing the two spectra emanated by the two regions (Fig.4D).

DISCUSSION

Confocal Raman microscopy and multiphoton microscopy are non-invasive optical techniques which are potentially useful in detecting tiny changes in the chemical composition of enamel in vitro. To date there are no studies outside our research group that investigate and demonstrate the combined performance of these methods in caries detection.

The Raman spectrum acquired from a dental section shows eminent vibrational bands related to the tooth structure. Among the main distinguished Raman bands of tissues is the one at 960 cm^{1} which is assigned to ν_1 (PO_4^{3-}) symmetric stretching mode. Since the phosphate peak intensity is linearly proportional to its amount within the inorganic crystals; perceptible alterations in its intensity can refer to the changes in the degree of enamel mineralization [26,29,30]. In this study;

phosphate peak exhibits greater intensity in sound enamel, confirming its higher mineral content compared to the lesion zone as demonstrated by (Fig.1A, C) and (Fig. 4A).

The CH group was previously employed to investigate the effect of laser and radiotherapy treatment on chemical composition of dental hard tissues [31,32]. As far as we know, this is the first work that shows how to exploit the CH stretch band to evaluate the consequence of enamel subsurface lesion development with respect to its organic matrix. Likewise, the presented work tries to correlate the changes affecting the enamel organic and inorganic components stimulated by caries progression through the use of characteristic vibrational bands.

Raman band at 2931 cm^{-1} observed just after acquiring a set of spectra from different lesions (Fig. 1C); is related to the bending and stretching modes of CH group of lipids and proteins [33,34]. Accordingly, the observed alterations in mineral component of enamel at 960 cm^{-1} were accompanied by changes in the amount of organic matrix represented by the ratio of organic component at 2931 cm^{-1} to mineral at 430 cm^{-1}. Based on the Raman spectral maps; the higher the organic/mineral ratio in the outer part of enamel (looks alike red zone in Fig.1B); the lower is the intensity of mineral content in the same zone (blue area in Fig.1A). Earlier studies [35,36] invested the CH stretch band to inspect the distribution of organic components in an intact cross section of a human tooth. They localized a remarkable gradual compositional change through the enamel film, represented by increased organic contents of inner enamel nearby DEJ compared to the outer counterpart. Contrary to our findings where the organic/mineral ratio in the outer demineralized enamel was found to be significantly higher than that in the inner intact enamel layer (Fig. 4B). This distinguished deleterious effect induced by caries formation, could help in identifying caries lesion early enough.

In this work, the fluorescence of demineralized tooth surface was correlated to the variation in its chemical composition which has been detected through the use of Raman microscopy. By comparing 2PEF images with the structural motifs observed by confocal Raman imaging system; the morphological similarity of the acquired images is quite evident.

2PEF images (Fig.2A, B) were made in the region of sound and diseased enamel. In region 1, the main 2PEF contrast comes from the prism sheaths rich in organic matrix rather than from inside-prism spaces evenly filled with inorganic HA crystals. Whereas 2PEF emanates from inside the prisms in region 2; where destructive caries lesion has induced changes in the chemical structure of enamel as well as intense crystals abnormality [37,38]. In consonance with the attached calibration bars that set the upper and lower limits with respect to fluorescence intensity; carious areas depicted by the 2PEF images comprise some semi-filled (deep green) and completely filled (bright green) prisms that could be related to the level of demineralization and subsequent optical inhomogeneity. These results are in accordance with earlier results communicated by Chen [39].

The 2PEF of enamel is an inherent fluorescence issued by intrinsic fluorophores [10] that could arise from decomposition of organic components from larger, longer-chained molecules into smaller, shorter chained molecules. Hence, the emergence of CH band at 2931 cm^{-1} in carious enamel spectrum (Fig.1C) as well as the increased organic/mineral ratio in the carious enamel part (Fig.4B); can stand behind the fluorescence of diseased enamel.

The evident red shift of the fluorescence spectrum from carious enamel, compared to that from sound enamel in (Fig.2 C); is another indication of carious lesion formation [40,41]. Since there was an evident shift of the fluorescence (released by diseased enamel) to longer wavelengths, there was also a pronounced difference in the intensity of the fluorescence at 675nm (Fig. 4D). The red

shift is probably large enough to allow the construction of a relatively simple opto-electrical system for its detection. As expected from earlier research with other types of UV-sources [42,43]; it is likewise possible that the incident light in the red or near infrared region becomes applicable for the detection of carious lesions due to the even red shift of the fluorescence from the regions with enamel caries, compared to that from non-carious enamel [43]. The outcomes of this research are consistent with results reported in previous studies [44,45] where they concluded that fluorescence intensity increases with caries progression. Another study showed that undamaged tooth structure exhibits little or no fluorescence while damaged tissue exhibits fluorescence proportional to the degree of caries severity [46]. However, our results are discordant with other studies [47,48], where teeth were illuminated with a blue light of wavelength 488nm. In these researches; damaged enamel generally exhibited less fluorescence and appeared darker than the healthy tissues. The nature or type of fluorescence is dependent on the wavelength of the incident light. Unlike shorter wavelengths; the infrared light is less susceptible to scattering and absorption by enamel than visible light [18,49]. Therefore, changes in light absorption and scattering mode, could explain the discrepancy of the obtained results [50,51].

Hydroxyapatite crystals in enamel belong to the 6/m point group symmetry. Thus, no SHG is anticipated to arise from ideal HA crystals [52-54]. However, the SHG can arise from the external strains around the cracks and from WSL areas that induce breakage of the 6/m point group symmetry [39,55,56]. These studies are in agreement with our records demonstrated in (Fig.3).

IN CONCLUSION: The obtained results demonstrate a great potential for both techniques in imaging and elucidating the structure/feature relationship in dental tissues. Changes in 2PEF reflect changes in chemical composition of enamel; thereby simplifies quantification of subsurface lesions. Moreover, since non-invasive management of enamel subsurface lesions

represents an essential goal of modern dentistry, the obtained results reveal the fundamental role of organic matrix that must be taking into account while developing remineralizing dental products based on calcium phosphate salts. With the limitations of this study, further laboratory studies together with clinical research are consequently required to increase the knowledge on this subject.

ACKNOWLEDGEMENTS

The authors love to acknowledge the financial support of Iraqi government represented by Ministry of Higher Education and Scientific Research as well as the Labex Numev, convention ANR-10-LABX-20. Special thanks to Dr. Friedrich Menges (developer of Spekwin32 & Spectragryph) for his unconditional help and support.

AUTHOR CONTRIBUTIONS

Al-Obaidi R. contributed to conception, design, acquisition, analysis and interpretation of data, prepared figures 1–4 and drafted the manuscript. Salehi H., T. Cloitre contributed to acquisition, analysis and interpretation of data. Cuisinier F. J. G., C. Gergely. contributed to conception, design, interpretation of data. Jacquot B, Tassery H. contributed to conception. All authors reviewed the manuscript and gave final approval.

COMPETING FINANCIAL INTERESTS

Authors declare no competing financial and non-financial interests in relation to the work described.

REFERENCES

1 Brès, E., Voegel, J. C. & Frank, R. High-resolution electron microscopy of human enamel crystals. *Journal of microscopy* **160**, 183-201 (1990).

2 Curzon MEJ, F. J. *Chemical composition of enamel.* (1983).

3 Odutuga, A. & Prout, R. Lipid analysis of human enamel and dentine. *Archives of oral biology* **19**, 729-731 (1974).

4 Eastoe, J. Organic matrix of tooth enamel. *Nature* **187**, 411 (1960).

5 Cury, J. A. & Tenuta, L. M. A. Enamel remineralization: controlling the caries disease or treating early caries lesions? *Brazilian Oral Research* **23**, 23-30 (2009).

6 De Jong, E. d. J. *et al.* A new method for in vivo quantification of changes in initial enamel caries with laser fluorescence. *Caries research* **29**, 2-7 (1995).

7 Huminicki, A. *et al.* Determining the effect of calculus, hypocalcification, and stain on using optical coherence tomography and polarized Raman spectroscopy for detecting white spot lesions. *International journal of dentistry* **2010** (2010).

8 Slimani, A. *et al.* Confocal Raman mapping of collagen cross-link and crystallinity of human dentin-enamel junction. *J Biomed Opt* **22**, 1-8, doi:10.1117/1.JBO.22.8.086003 (2017).

9 Gibson, E. A., Masihzadeh, O., Lei, T. C., Ammar, D. A. & Kahook, M. Y. Multiphoton microscopy for ophthalmic imaging. *Journal of ophthalmology* **2011** (2011).

10 Stookey, G. K. Quantitative light fluorescence: a technology for early monitoring of the caries process. *Dental Clinics* **49**, 753-770 (2005).

11 Benedict, H. Note on fluorescence of teeth in ultraviolet rays. *Science* **67**, 442 (1928).

12 Benedict, H. The fluorescence of teeth as another method of attack on the problem of dental caries. *J Dent Res* **9**, 274-275 (1929).

13 Björkman, U. H., Sundström, F. & ten Bosch, J. J. Fluorescence in dissolved fractions of human enamel. *Acta Odontologica Scandinavica* **49**, 133-138 (1991).

14 Bachmann, L., Zezell, D. M., Ribeiro, A. d. C., Gomes, L. & Ito, A. S. Fluorescence spectroscopy of biological tissues—a review. *Applied Spectroscopy Reviews* **41**, 575-590 (2006).

15 Cloitre, T. *et al.* Multiphoton imaging of the dentine-enamel junction. *Journal of biophotonics* **6**, 330-337 (2013).

16 Zoumi, A., Yeh, A. & Tromberg, B. J. Imaging cells and extracellular matrix in vivo by using second-harmonic generation and two-photon excited fluorescence. *Proceedings of the National Academy of Sciences* **99**, 11014-11019 (2002).

17 Zipfel, W. R. *et al.* Live tissue intrinsic emission microscopy using multiphoton-excited native fluorescence and second harmonic generation. *Proceedings of the National Academy of Sciences* **100**, 7075-7080 (2003).

18 Denk, W., Strickler, J. H. & Webb, W. W. Two-photon laser scanning fluorescence microscopy. *Science* **248**, 73-76 (1990).

19 Zipfel, W. R., Williams, R. M. & Webb, W. W. Nonlinear magic: multiphoton microscopy in the biosciences. *Nature biotechnology* **21**, 1369 (2003).

20 Hall, A. & Girkin, J. A review of potential new diagnostic modalities for caries lesions. *Journal of dental research* **83**, 89-94 (2004).

21 Lin, P.-Y., Lyu, H.-C., Hsu, C.-Y. S., Chang, C.-S. & Kao, F.-J. Imaging carious dental tissues with multiphoton fluorescence lifetime imaging microscopy. *Biomedical optics express* **2**, 149-158 (2011).

22 Oheim, M., Michael, D. J., Geisbauer, M., Madsen, D. & Chow, R. H. Principles of two-photon excitation fluorescence microscopy and other nonlinear imaging approaches. *Advanced drug delivery reviews* **58**, 788-808 (2006).

23 So, P. T., Dong, C. Y., Masters, B. R. & Berland, K. M. Two-photon excitation fluorescence microscopy. *Annual review of biomedical engineering* **2**, 399-429 (2000).

24 Helmchen, F. & Denk, W. Deep tissue two-photon microscopy. *Nature methods* **2**, 932 (2005).

25 iPLESP. *BiostaTGV*, <https://marne.u707.jussieu.fr/biostatgv> (2000).

26 Al-Obaidi, R. *et al.* Chemical & Nano-mechanical Study of Artificial Human Enamel Subsurface Lesions. *Scientific reports* **8**, 4047 (2018).

27 Salehi, H. *et al.* Label-free detection of anticancer drug paclitaxel in living cells by confocal Raman microscopy. *Applied Physics Letters* **102**, 113701, doi:10.1063/1.4794871 (2013).

28 Reed, R. *et al.* Radiotherapy effect on nano-mechanical properties and chemical composition of enamel and dentine. *Archives of oral biology* **60**, 690-697 (2015).

29 Gilchrist, F., Santini, A., Harley, K. & Deery, C. The use of micro-Raman spectroscopy to differentiate between sound and eroded primary enamel. *International journal of paediatric dentistry* **17**, 274-280 (2007).

30 Hannig, C., Hamkens, A., Becker, K., Attin, R. & Attin, T. Erosive effects of different acids on bovine enamel: release of calcium and phosphate in vitro. *Archives of oral biology* **50**, 541-552 (2005).

31 Liu, Y. & Hsu, C.-Y. S. Laser-induced compositional changes on enamel: a FT-Raman study. *Journal of dentistry* **35**, 226-230 (2007).

32 Reed, R. *et al.* Radiotherapy effect on nano-mechanical properties and chemical composition of enamel and dentine. *Archives of oral biology* **60**, 690-697, doi:10.1016/j.archoralbio.2015.02.020 (2015).

33 Lopes, C. B. *et al.* The effect of the association of NIR laser therapy BMPs, and guided bone regeneration on tibial fractures treated with wire osteosynthesis: Raman spectroscopy study. *Journal of Photochemistry and Photobiology B: Biology* **89**, 125-130 (2007).

34 Pinheiro, A. L. *et al.* Raman spectroscopy validation of DIAGNOdent-assisted fluorescence readings on tibial fractures treated with laser phototherapy, BMPs, guided bone regeneration, and miniplates. *Photomedicine and laser surgery* **28**, S-89-S-97 (2010).

35 He, L.-H. & Swain, M. V. Enamel—A functionally graded natural coating. *Journal of dentistry* **37**, 596-603 (2009).

36 Wentrup-Byrne, E., Armstrong, C. A., Armstrong, R. S. & Collins, B. M. Fourier transform Raman microscopic mapping of the molecular components in a human tooth. *Journal of Raman Spectroscopy* **28**, 151-158 (1997).

37 Huang, T. T., Jones, A. S., He, L. H., Darendeliler, M. A. & Swain, M. V. Characterisation of enamel white spot lesions using X-ray micro-tomography. *Journal of dentistry* **35**, 737-743 (2007).

38 Amjad, Z., Koutsoukos, P. & Nancollas, G. The mineralization of enamel surfaces. A constant composition kinetics study. *Journal of dental research* **60**, 1783-1792 (1981).

39 Chen, S.-Y., Hsu, C.-Y. S. & Sun, C.-K. Epi-third and second harmonic generation microscopic imaging of abnormal enamel. *Optics express* **16**, 11670-11679 (2008).

40 Sundström, F., Fredriksson, K., Montan, S., Hafström-Björkman, U. & Ström, J. Laser-induced fluorescence from sound and carious tooth substance: spectroscopic studies. *Swed Dent J* **9**, 71-80 (1985).

41 Slimani, A. *et al.* Multiphoton Microscopy for Caries Detection with ICDAS Classification. *Caries research* **52**, 359-366 (2018).

42 Bjelkhagen, H. Early detection of enamel caries by the luminescence excited by visible laser light. *Swed Dent J.* **6**, 1-7 (1982).

43 Booij, M. & Ten Bosch, J. A fluorescent compound in bovine dental enamel matrix compared with synthetic dityrosine. *Archives of oral biology* **27**, 417-421 (1982).
44 Mendes, F. M., Pinheiro, S. L. & Bengtson, A. L. Effect of alteration in organic material of the occlusal caries on DIAGNOdent readings. *Brazilian Oral Research* **18**, 141-144 (2004).
45 Yokoyama, E., Kakino, S. & Matsuura, Y. Raman imaging of carious lesions using a hollow optical fiber probe. *Applied Optics* **47**, 4227-4230 (2008).
46 Lussi, A., Hibst, R. & Paulus, R. DIAGNOdent: an optical method for caries detection. *Journal of dental research* **83**, 80-83 (2004).
47 Alfano, R. & Yao, S. Human teeth with and without dental caries studied by visible luminescent spectroscopy. *Journal of dental research* **60**, 120-122 (1981).
48 Ando, M., Van Der Veen, M. H., Schemehorn, B. R. & Stookey, G. K. Comparative study to quantify demineralized enamel in deciduous and permanent teeth using laser–and light–induced fluorescence techniques. *Caries research* **35**, 464-470 (2001).
49 Lin, S.-J. *et al.* Evaluating cutaneous photoaging by use of multiphoton fluorescence and second-harmonic generation microscopy. *Optics letters* **30**, 2275-2277 (2005).
50 Pretty, I. & Ellwood, R. The caries continuum: opportunities to detect, treat and monitor the re-mineralization of early caries lesions. *Journal of dentistry* **41**, S12-S21 (2013).
51 Ten Bosch, J. Light scattering and related methods in caries diagnosis. *Early Detection of Dental Caries I*, 81-90 (1996).
52 Boyd, R. (New York: Academic Press, 1992).
53 Jiang, W. & Cao, W. Second harmonic generation of shear waves in crystals. *ieee transactions on ultrasonics, ferroelectrics, and frequency control* **51**, 153-162 (2004).
54 Lyubchanskii, I. *et al.* Second-harmonic generation from realistic film–substrate interfaces: the effects of strain. *Applied Physics Letters* **76**, 1848-1850 (2000).
55 Popowics, T., Rensberger, J. & Herring, S. Enamel microstructure and microstrain in the fracture of human and pig molar cusps. *Archives of oral biology* **49**, 595-605 (2004).
56 Ichim, I., Li, Q., Li, W., Swain, M. & Kieser, J. Modelling of fracture behaviour in biomaterials. *Biomaterials* **28**, 1317-1326 (2007).

Figure 1. (**A**) Raman phosphate map built from phosphate peak intensity at 960 cm^{-1}. (**B**) Image constructed from organic to mineral ratio at (2931/430 cm^{-1}). Individual Look Up Tables (LUT) on both sides. Region 1: Sound enamel, Region 2: Lesion area, R: Resin. (**C**) Corresponding Raman spectra generated by region 1, 2 respectively.

Figure 2. (**A & B**) 2PEF signal images; where region 1 belongs to sound enamel while region 2 belongs to lesion area. Subjective calibration bars on both sides. White arrows refer to enamel prism sheathes. Double ended black arrows delineate enamel rods. (**C**) Corresponding nonlinear

optical spectra generated by region 1(red line-sound enamel), 2 (blue line-lesion area) respectively. IR: Infrared excitation laser.

Figure 3. Nonlinear optical spectra generated by lesion zone (region 2). SHG peak at ~435 nm is evident, arising from broken 6/m point group symmetry due to the external strains in subsurface lesion area.

Figure 4. Raman spectra applied with reference to the peak intensity to show: (**A**) Variation in PO_4^{3-} intensity at 960 cm^{-1} & (**B**) Alteration in the ratio of two intensities at (2931/430 cm^{-1}) between sound and carious enamel. Nonlinear optical spectra measured by MPM, were employed in respect to 2PEF intensity at: (**C**) 520 nm and (**D**) at 675 nm to demonstrate the difference between healthy and carious enamel in terms of intrinsic fluorescence. Asterisk (*) recurrently indicates a significant difference ($p < 0.05$) between the two zones. Horizontal bar indicates no significant difference ($p > 0.05$) among the groups linked by it.

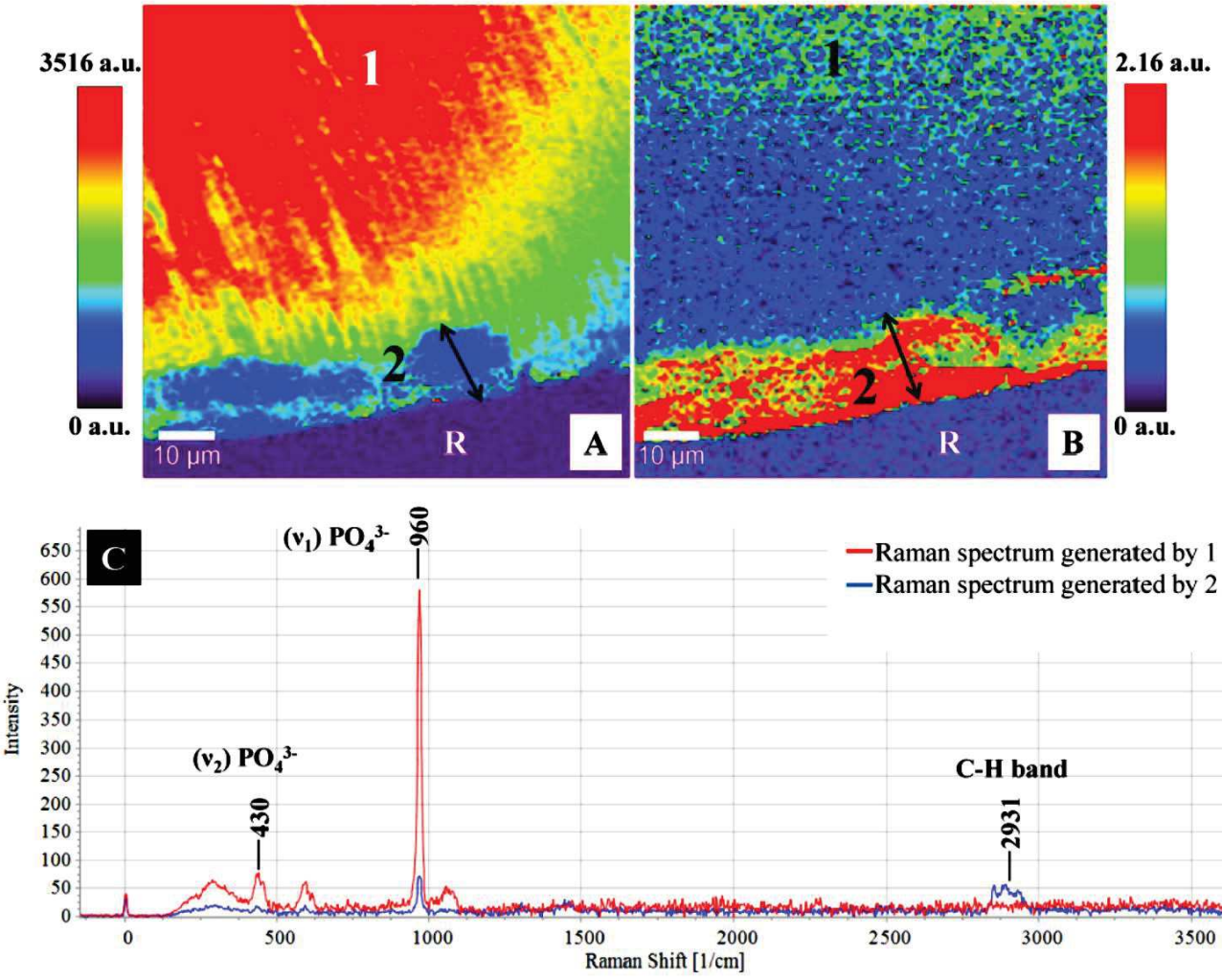
3516 a.u.
0 a.u.
1
2
10 µm
R
A
2.16 a.u.
0 a.u.
1
2
10 µm
R
B
C
(v1) PO4 3-
960
(v2) PO4 3-
430
C-H band
2931
Raman spectrum generated by 1
Raman spectrum generated by 2
Intensity
Raman Shift [1/cm]
0
50
100
150
200
250
300
350
400
450
500
550
600
650
0
500
1000
1500
2000
2500
3000
3500

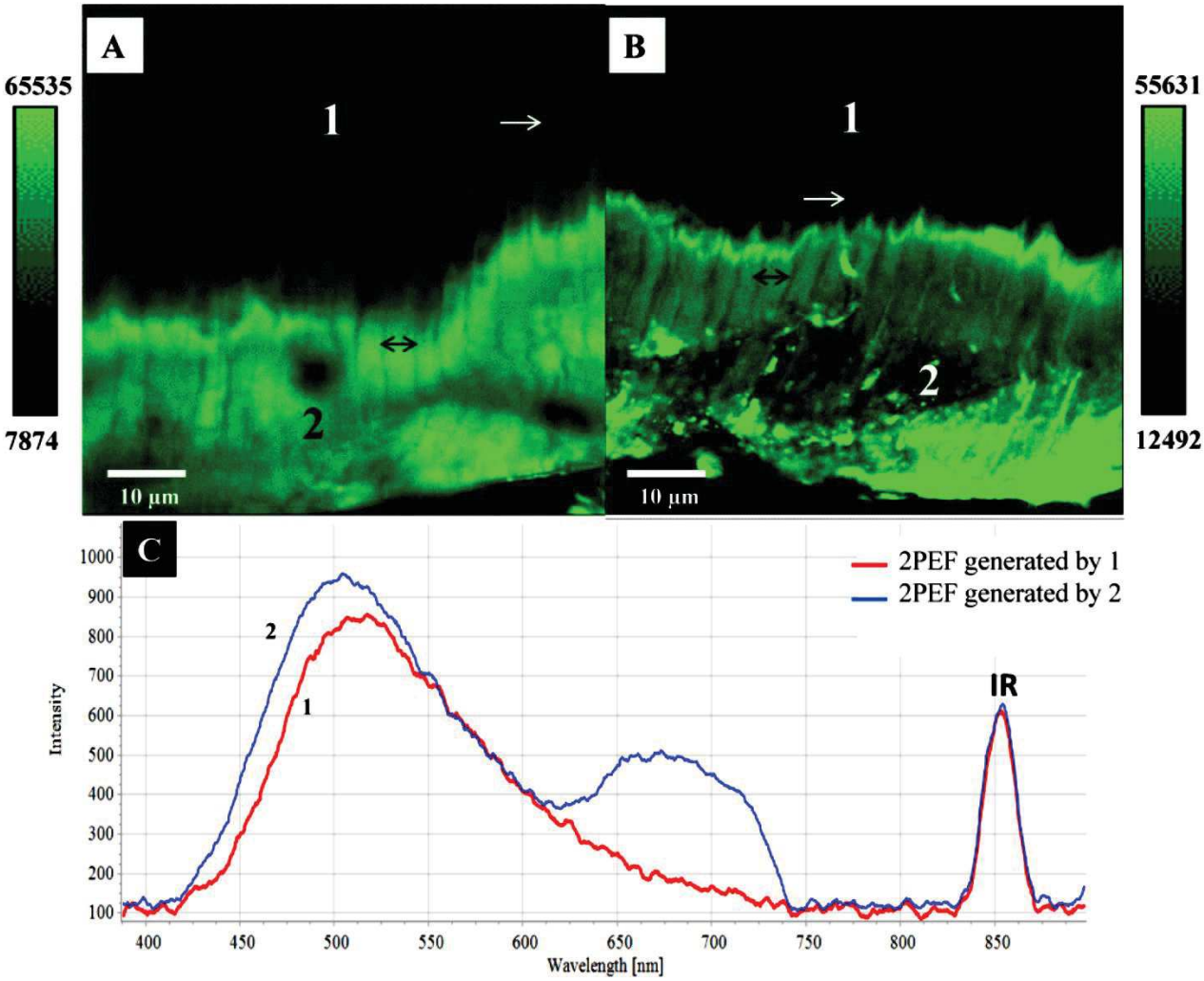
A
B
C
65535
7874
55631
12492
1
2
10 µm
2PEF generated by 1
2PEF generated by 2
IR
Intensity
Wavelength [nm]

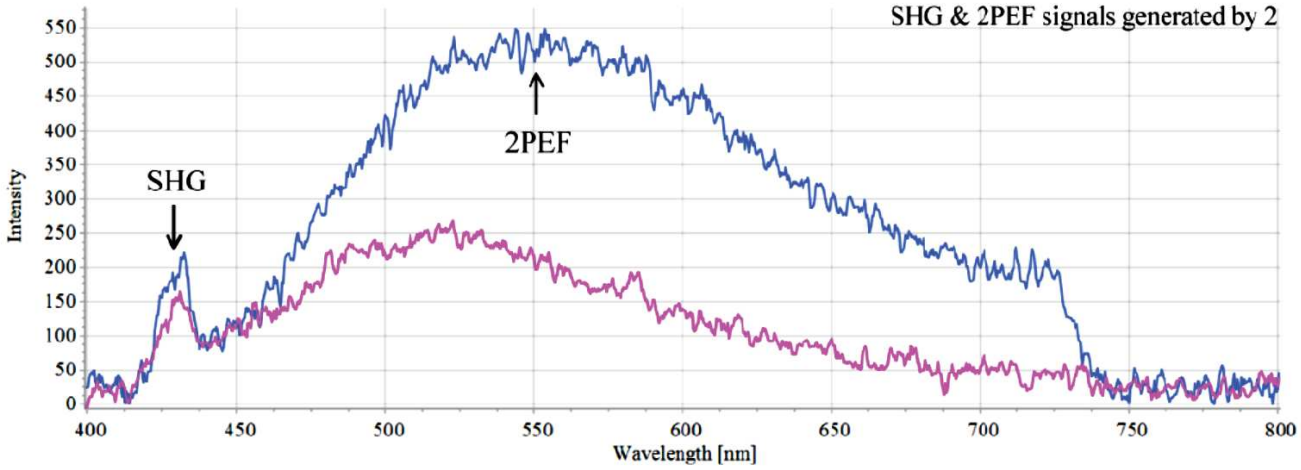
SHG & 2PEF signals generated by 2
SHG
2PEF
Intensity
Wavelength [nm]
0
50
100
150
200
250
300
350
400
450
500
550
400
450
500
550
600
650
700
750
800

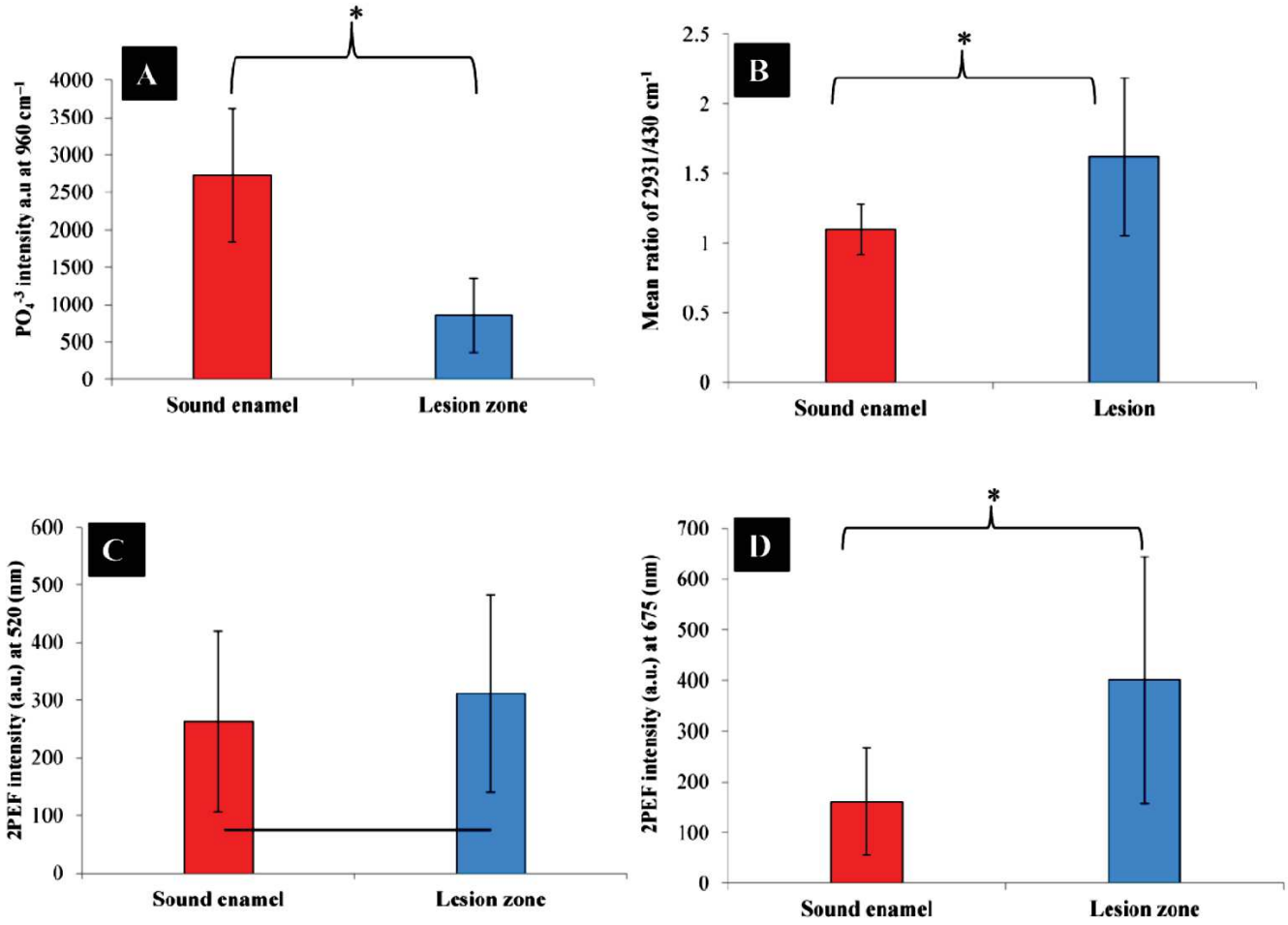
A
*
PO_4^{-3} intensity a.u at 960 cm^{-1}
4000
3500
3000
2500
2000
1500
1000
500
0
Sound enamel
Lesion zone
B
*
Mean ratio of 2931/430 cm^{-1}
2.5
2
1.5
1
0.5
0
Sound enamel
Lesion
C
2PEF intensity (a.u.) at 520 (nm)
600
500
400
300
200
100
0
Sound enamel
Lesion zone
D
*
2PEF intensity (a.u.) at 675 (nm)
700
600
500
400
300
200
100
0
Sound enamel
Lesion zone